Durability of Rubber Components under Multiaxial Cyclic Stresses

Federico Coren

School of Mechanical Engineering

Thesis submitted for examination for the degree of Master of Science in Technology.
Espoo 27.11.2017

Thesis Supervisor :

Ass.Prof. Heikki Remes

Thesis advisor:

Dipl.-Ing. Andreas Dutzler

Aalto University
School of Engineering

AALTO UNIVERSITY
SCHOOL OF ENGINEERING

ABSTRACT OF THE
MASTER'S THESIS

Author: Federico Coren

Title: Durability of Rubber Components
under Multiaxial Cyclic Stresses

Date: 27.11.2017 Language: English Number of pages: 6+94

Department of Solid Mechanics

Professorship: Fatigue of materials

Supervisor: Ass.Prof. Heikki Remes

Advisor: Dipl.-Ing. Andreas Dutzler

An accurate understanding of the fatigue behaviour of structural components through their working life, is a key factor for a light-weight and optimal design. Fatigue life has to take into consideration a series of parameters spacing from material properties, to working condition to the nature of the cyclic loads. This work consist in the development of a technique able to determine fatigue life of rubber components as well as the location and direction of the cracks.

An hyper-elastic, third-order, five-parameter, phenomenological material model has been selected and multiple components have been simulated under variable cyclic multi-axial loading.Several fatigue indicators and damage accumulation models have been taken into account. Eventually Cauchy rotated stresses have been chosen as fatigue indicator, coupled with Palgrem-Miner damage accumulation rule calculated in different spacial directions using critical-plane method. The Cauchy rotated stresses have been selected in order to be able to implement Haigh diagram data from existing literature. Furthermore the use of this tensor enables the determination of the location and orientation of critical planes referred to the un-deformed configuration. A custom equivalent stress method has been implemented in order to take into account mean stress sensitivity deriving from phenomena like strain induced crystallization.

The developed method has been tested against literature as well as experimental data in order the evaluate its quality. Correct calculation of the co-rotated Cauchy tensor has been verified against a uni-axially loaded specimen subjected to a rotation in the reference system. A diabolo specimen has been simulated under torsional loading in order to verify the correct location and orientation of cracks. Correct interpolation of multi-axial stress states deriving from multiple external loads have been verified against results from a FEM solver. Lastly a component from literature has been tested using different load signals, and the data from fatigue life, crack location and crack orientation have been gathered.

The procedure proved to be successful in the prediction of the location and orientation of cracks referred to the un-deformed configuration. Furthermore a precise fatigue life estimation of components under different load signals has been achieved. The procedure is highly customizable depending on fatigue and material properties of the specimen analysed. This procedure has proven to be a successful predictor tool for fatigue life estimation of multi-axially, cyclic loaded rubber components.

Keywords: Rubber,Durability,Fatigue,Multiaxial Loading

Thanks

I want to thank my tutor Andreas Dutzler for the great support received and my supervisor Heikki Remes for the support he provided me.

A special thank to my family for the love, support, and constant encouragement I have gotten over the years and throughout my whole studies.

A thanks also to all the wonderful people I met during my studies for all the opportunities they gave me.

Otaniemi, 27.11.2017

Federico Coren

Symbols and abbreviations

Symbols

W	Strain energy density
$\mathbf{F}$	Deformation gradient Tensor
$\mathbf{C}$	Right Green-Cauchy deformation tensor
$\mathbf{B}$	Left Green-Cauchy deformation tensor
$\mathbf{R}$	Rotation tensor
$\mathbf{E}$	Lagrangian strain
$\mathbf{P}$	1^{st} Piola Kirchhoff stress tensor
$\mathbf{S}$	2^{st} Piola Kirchhoff stress tensor
$\boldsymbol{\sigma}$	Cauchy stress
J	Determinant of $\mathbf{F}$
B	Bulk Modulus
W_c	Cracking energy density
θ	crack orientation angle
D	Damage $0 \leq D \leq 1$
N_f	Number of Cycles

Operators

$\nabla \hat{A}$	gradient of function $\hat{A}$
$\nabla \times \mathbf{A}$	curl of vector $\mathbf{A}$
$\dfrac{\mathrm{d}}{\mathrm{d}t}$	derivative with respect to variable t
$\dfrac{\partial}{\partial t}$	partial derivative with respect to variable t
$\sum_i$	sum over index i
$\mathbf{A} \cdot \mathbf{B}$	dot product of tensors $\mathbf{A}$ and $\mathbf{B}$
$\mathbf{A} \times \mathbf{B}$	vectorial product of tensors $\mathbf{A}$ and $\mathbf{B}$
$\mathbf{A} \otimes \mathbf{B}$	cross product of tensors $\mathbf{A}$ and $\mathbf{B}$

Abbreviations

CB	Carbon Black
NR	Natural Rubber
CS	Carbon Steel
UV	Ultra Violet radiation
w% w	Mass fraction of a component into the bulk.

Contents

Abstract ii

Contents v

1 Introduction 1
- 1.1 Rubber . . . 1
- 1.2 State of the Art . . . 1
- 1.3 Scope of the Thesis . . . 3

2 Material Behaviour of Elastomers 4
- 2.1 Elastomer and rubber components . . . 4
- 2.2 Stress-strain relation . . . 8
- 2.3 Viscoplasticity . . . 10
- 2.4 Mullin Effect . . . 11
- 2.5 Temperature Dependency . . . 12
- 2.6 Strain induced crystallization . . . 13

3 Constitutive Equations 14
- 3.1 Hyperelasticity theory . . . 14
- 3.2 Stress-Strain relations . . . 14
- 3.3 Third Order Deformation . . . 15

4 Fatigue Behaviour of Rubber 17
- 4.1 Influence of material properties . . . 18
- 4.2 Influence of surface finish . . . 21
- 4.3 Environmental conditions . . . 21
- 4.4 Stress Levels . . . 22

5 Fatigue Life Modelling 23
- 5.1 Stretches . . . 24
- 5.2 Stresses . . . 25
- 5.3 Stresses from continuum damage mechanics . . . 25
- 5.4 Energy based criteria . . . 28
  - 5.4.1 Strain Energy Density . . . 28
  - 5.4.2 Cracking Energy Density . . . 28
- 5.5 Configurational Mechanics . . . 31

6 Damage accumulation theory 32
- 6.1 Continuum damage mechanics . . . 32
- 6.2 Palgrem-Miner linear damage accumulation . . . 33

7 Mean stress sensitivity 36

8 Critical plane method 38

9 Cycle counting **41**
9.1 Cycle counting techniques . . . 43
9.1.1 Rainflow counting . . . 43
9.1.2 Markov-Matrix . . . 45
9.1.3 Range Pair Method or Reservoir counting . . . 46
9.2 Level Crossing . . . 46
9.3 Peak Counting Method . . . 47
9.3.1 Signal Filtering . . . 48

10 Work procedure description **50**
10.1 Cauchy rotated in reference configuration . . . 50
10.2 Haigh diagram creation . . . 52
10.2.1 Haigh diagram using interpolating polynomial surface . . . 52
10.2.2 Haigh diagram using interpolating planes . . . 53
10.3 Mean stress sensitivity Correction . . . 56
10.4 Haigh Diagram Testing . . . 57
10.5 Multiaxial Load Signals . . . 57

11 Method implementation **60**

12 Model Validation **64**
12.1 Single-Element Cube . . . 65
12.2 Eight Block Cube . . . 70
12.3 Diabolo Test n.1 . . . 72
12.4 Diabolo Test n. 2 . . . 78
12.4.1 Material properties . . . 78
12.4.2 Element type . . . 78
12.4.3 Signal for diabolo test . . . 82
12.4.4 Life estimation . . . 84

13 Discussion and Conclusions **85**

List of Figures **87**

Bibliography **91**

1 Introduction

1.1 Rubber

Rubber has a long application history in many engineering fields. Thanks to its nature, rubber can withstand elongations many time its lengths, returning to almost the same initial dimension. From aerospace, to car industry, its sealing and damping properties have come to use in thousands of different applications. When used as dampers, the work principle consist in imposing great deformation to bulks of rubber. The effect is dual: it works as springs as well as a damper. As a matter of fact the micro-structure consist in long polymeric chains cross-linked together [39]. Any external load results in the internal movement of such chains, and the sub-sequential relative movement of the chains leads to a dissipation of energy. This is a valuable property when the designer goal is to limit the stresses and vibration transmitted between different structures.

Estimation of fatigue of rubber has becoming more and more important due to the need of correctly designing rubber based components. The need to optimize the whole life-cycle of engineered specimen has pushed towards the study of the nature and entity of the damage due to multi-axial loads. Knowing the exact service life allows to deploy longer inspection time-intervals and through the proper dimensioning of the components, the material can be allocated in the zones where it is more stressed.

1.2 State of the Art

Life influencing factor in rubber materials can be divided in four main categories: 1) material properties, 2) surface properties, 3) working conditions and 4) geometrical properties. Material properties derive from the base material composition as well as on the presence of possible impurities deriving from both the manufacturing and processing of the base material[14, 17, 26]. Surface conditions also are closely related to the manufacturing processes such as composition of mould detacher, curing agents and anti-oxidizers. Working conditions are determined by the specific application the component is supposed to endure, and mostly consist in the environment temperature, environment chemical composition[3, 31] and load frequency, intensity and mean level. The geometrical properties have a direct effect in the load distribution inside the components and are one of the main challenges in fatigue design of rubber components. Since most of the properties above regard the production processes, this work has focused on the load distributions inside the rubber components and their relation with fatigue life.

Constitutive models describing the behaviour of rubber materials must take into account a series of phenomena such as hyperplastic behaviours, cycle softening [11], creep and strain dependent viscoelastic storage modulus. In order to get an accurate material description, a hyperplastic model has been selected. Since the material studied presented strong strain induced crystallization [36, 22], some stress-compensation techniques for tackling with mean stress sensitivity deriving from this phenomena have been developed.

In fact a procedure has been develop that allows for a mean stress correction based on experimental data. The Haigh diagram is parametrically described as a combination of logarithmic planes that are tuned to fit onto experimental data. The fitted Haigh diagram is then used to calculate equivalent stresses for any given R value. Due to the nature of the procedure, materials with extremely different mean stress sensitivity can be modelled.

Fatigue life for rubber components follows a power law, where the cycles to failure are related with a fatigue estimator. Among the possible ones, the most used are max principal stresses, strains, strain energy density, cracking energy density, and J integral (Eshelby stress tensor)[5]. During the work life of a component, two different damage phenomena can be found. The first regards the crack nucleation: the life associated with this damage can be described through a Wöhler relation. The second describes crack growths, but since it usually regards less than 10% of the component life, it can be neglected in fatigue design. As a matter of fact the crack propagation regime is usually associated with a deterioration of the mechanical properties below acceptable levels.

From literature, the indicators with the highest fatigue prediction capabilities are principal stresses and cracking energy density[13, 6]. The latest has been deemed as not suitable for design purpose since the parameters needed to determine such quantity are extremely challenging. Among damage accumulation methods two have usually been deployed, namely Palmgren-Miner linear accumulation damage and Continuum damage mechanics [4]. Whereas the latest allows to take into consideration load sequence effects and a precise description of damage due to crack formation and crack propagation, the parameters governing such models were deemed not feasible for design purposes. Furthermore the typical components' load history, consisting of millions of cycles, would have made the associated calculations too long, so linear damage accumulation is the most widely adopted solution for design purposes.

One of the most common practise adopted in industry is to gather data from the real world and to slightly modify the designs if failures are seen. This conservative and somehow un-efficient practise is quite expensive and time demanding. As a matter of fact relying on implementation of designs that might not be optimised can result in working life way shorter then expected. Furthermore this technique lack a predictability power when new designs must be implemented. On the other hand extremely refinate models exist, where crack nucleation and growth can be successfully described [4, 5, 6, 13, 37]. The proposed method in such works do apply well only on highly controlled test environment where it is possible to determine a series of parameters regulating these models. Nevertheless the derivation of such parameters is painstaking [30] and they are usually highly dependent from the composition of the rubber mixture [34, 18, 17]. Such data can be almost impossible to be determined in Industrial application, where many times the only information available on the rubber mixture is the Macro Mechanics properties. For this reason such models cannot be easily implemented in an industrial world.

Some commercial software such as FEMFAT [1] and MSC.Fatigue [2] do have the

possibility to perform multiaxial fatigue analysis, but having been designed for metal material lack some of the features that have been developed in this procedure. Namely the rubber mean stress sensitivity and the rotation of the stress tensors is not possible. On top of that the procedure developed during this work is able to automatically retrieve the stress states obtained from the combination of multiple external loads. The possibility to simulate multiaxial load conditions ensure the ability to represent the complexity of real world stress states.

1.3 Scope of the Thesis

There is no available method today to perform an accurate fatigue life estimation of elastomer components in industrial application. Current industrial design practice involve either a process of trials and error or the use of software that have been designed primarely for metal components.[1, 2]. Laboratories practices involves the use of extremely complicated models, whose practical application is hampered by the presence of parameters that are hard to be determined. For this reason this work aims at developing a procedure that can predict with enough confidence the fatigue life of rubber components, but considering at the same time the need have a reliable, effective and time-efficient design procedure, thus reducing the gap between laboratories and industrial procedures. Compared to existing techniques this work is one of the first able to cope with fatigue of multiaxially loaded rubber specimen.

The model accuracy will be verified with experimental data derived from literature work as well as by real world component given by Siemens Mobility (Graz). The fatigue design method will consist in the developing of a procedure able to cope with large strains of the component, to take into account the mean stress sensitivity present and to determine the fatigue life of the component as well as the crack location and crack orientation. The model will be able to interpolate multiaxial stress states deriving from up to three different external loads. The model will be limited in the description of the crack nucleation only since it describes the majority of the fatigue life scenarios. This choice is also backed up by the fact that crack propagation regime is usually associated with a deterioration of the mechanical properties below acceptable levels for industrial application. This work focuses on long fatigue life ($N_{cycles} > 10^4$) and this is related to long signal loads. In order to avoid simulating with FEM the whole load history, some technique must be deployed in order to decrease the simulation time. Note that a multi-axial stress states might also develop from mono-axially loaded specimen if geometry features or material constitution allow it, so it is important to understand how different signals might interfere each other to give a specific stress state. The possibility of describing dynamically the change of the mechanical and fatigue properties as well as the capability of describing load sequence effects of the rubber has been discarded. This allows to develop a time-efficient analysis method suitable for rubber components and industry application. Models describing load sequence effect and dynamic change of rubber properties are way too complex and computational heavy to be used in any real world scenario.

2 Material Behaviour of Elastomers

2.1 Elastomer and rubber components

Elastomer are a family of material made up by polymers presenting viscoelasticity properties and very weak inter-molecular forces. They usually present low Young modulus and the capability to sustain large strains without incurring in permanent deformation. Monomers composition is usually based upon hydrogen, carbon, silicon or oxygen. Their structure is amorphous, existing above glass transition temperature. Due to the length of the polymeric chains and the few cross-links, a great segmental motion is possible. Their application space from sealant, to adhesive to soft molded parts. As a matter of fact the ability to be greatly deformed and the capability of some elastomers to be phobic towards specific solvents, makes them ideal to be used as sealant components. The peculiar micro-structure allows them to dissipate mechanical energy in form of heat due to friction and entropy. This phenomena can be described as entropic elasticity ([16]). In particular stretching a sample results in the widening of the polymeric ends, and this causes an overall increase in the order of the system, thus leading to a decrease in the configuration entropy. To compensate such decrease the material heats up, and if a proper heat exchange mechanism can take place, the component will dissipate thermal energy with the environment. Due to the possibility of being moulded in a great variety of shapes, their ability to bond with metal while curing, and their damping properties, elastomer are widely used in many industrial application. From Automotive to Railway to Aeronautical industry, their field of application is wide.

Elastomer in industry usually consist in Natural Rubber, and for this reason this work will focus on them. Natural rubber is a thermoplast consisting in long chains of Natural Polyisopropene (cis-1,4 Polyisopropene). The polymerization process consist in the creation of long chains, like the one in fig 2. Typical chain molecular weight are around 10^5 *up to* 10^6 Dalton.

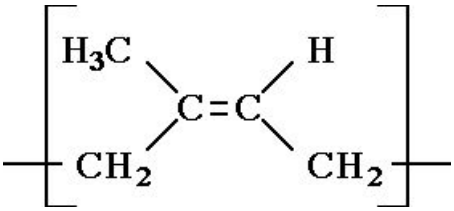

Figure 1: cis-1,4 Polyisopropene, the monomer at the base of the structure of the Natural rubber polymeric chain in fig:2 source [39]

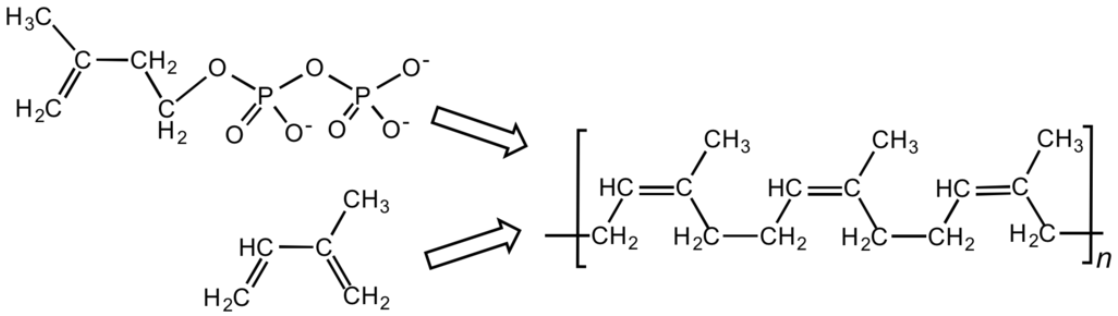

Figure 2: Polymerization principle and final polymer structure. source [39]

Due to the natural origin of the rubber, the presence of impurity is non negligible. Minerals absorbed by the plant are transferred to the rubber, and impurities deriving from the manufacture locations can be found in the rubber matrix [18]. In order to tackle degradation due to environment contaminants such as Oxygen, Ozone, UV and other chemicals, many addictive are incorporated in the mass of rubber prior to final manufacturing.[18] This addictive space form accelerators of the curing process, to mould detacher to mechanical properties enhances.
Radical scavenger of low molecular weight are added to the mixture when high temperature application are required [3]. Other addictive are added to the mixture in order to improve long term durability and Zinc oxides are normally added to act as polymerization catalysts. In order to improve the dispersion of the various fillers, strearic acids are used. Black Carbon is normally added to improve mechanical properties specifically the strength and stiffness[32]. On top of that rubber might be aided with the presence of waxes on its surface, that acting as a physical barrier reduce the amount of contaminants entering the component.
All of these addiction to the base material might be a source of problems when the particle size of the fillers is big enough to become a crack initiator. As a matter of fact, aggregates of Carbon Black particles have been observed to become the preferred location to crack initiation, due to their action of stress concentrator.[32, 22]

The biggest commercial source of natural rubber consist in cultivation of ***Havea brasiliensis*** even if other sources exist.

Figure 3: Havea Brasilianis. source [39]

The bark of the tree (fig: 3) is incided and the Latex collected. Due to this manifacturing process almost 6 percent in weight is composed by other particles: lipids (1.5–3% w/w), proteins and polypeptides (2% w/w), carbohydrates (0.4% w/w) and minerals (0.2% w/w).[30]

Rubber components are usually manufactured through mould injection, compression mould or transfer moulding. Rubber Injection Mould (fig:4)consist in forcing a uncured and preheated mass into a metallic mold. Here curing process happens and the components can be then extracted. Compression molding (fig:4)consist in the shaping of a preform thought the aid of metallic forms. This is an ideal process where the geometry of the rubber components are not too complicated. Transfer molding (fig:4)differs from compression one only in the placement of the raw material, this time at the top of it.

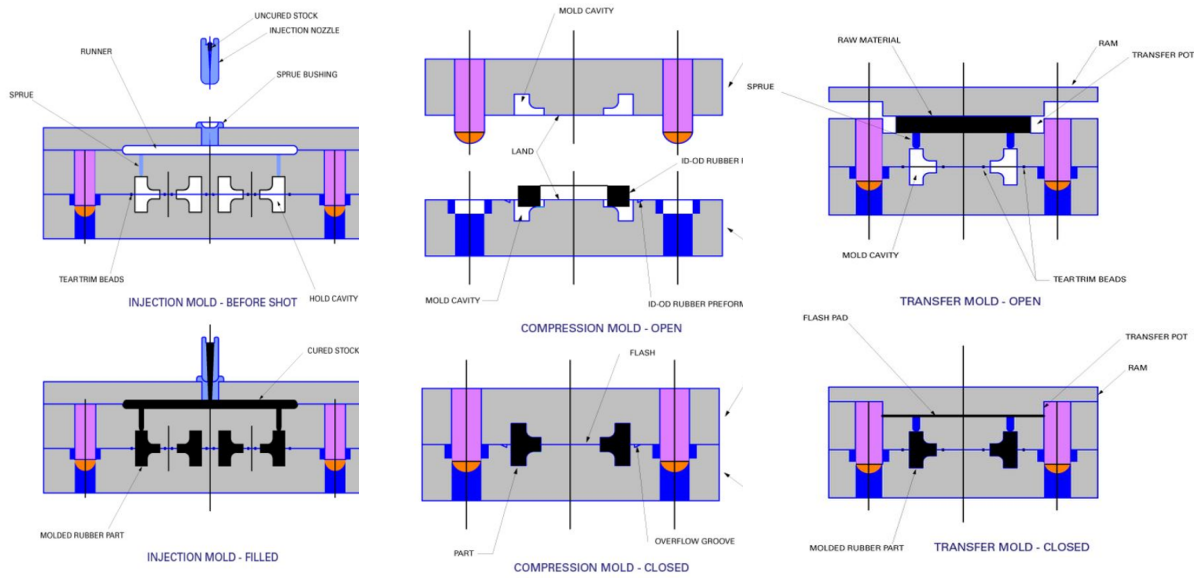

(a) (b) (c)

Figure 4: Figure 4: Injection Molding (a), Compression Molding (b) and Transfer Molding (c)

The production process is of great importance concerning fatigue life. Some of the greater problems derive from the initial mixture of the raw material and from the mould environment. Aggregate from uneven mixing of rubber with mechanical enhances such as Carbon Black particles might result in crack precursor when their size exceed the 30-40 μ m. [23]. As a matter of fact the stress gradient on the interface surface of such particles might be high enough to create the correct condition for a crack to nucleate and develop.

Surface condition deriving from the moulding process poses also a great influence on the life. On the mold surface there are usually some detached substances, like waxes, that prevent the rubber to bond with the metallic surface while curing. This wax layer determines the surface roughness, and to higher smoothness level correspond longer service life. Surface imperfection as small as 1 mm are considered to be an initial stage of a crack, thus shifting the component from a regime of crack nucleation to a way shorter regime of crack propagation.

2.2 Stress-strain relation

Elastomer possess a peculiar material behaviour, that cannot be fully described via a simple elastic relation (fig:5). Characteristic of the material is a very high capacity of reversibly retaining several hundred percent of strain. Elastomers are generally considered to be incompressible materials. The polymeric structure,consisting of monomeric chains cross-linked together, allow the material to behave like a solid. At the same time the covalent bonds allow the overall structure to be heavily deformed, thus acting like a liquid. On top of that the elastomers present a highly packed atomic structure, resulting in a great resistance to change the volume. Furthermore, like liquid, polymer chain can greatly move in respect one to another, resulting in an ease to change shape. Stress strain curve obtained from experiment data shows a non linear progression up to failure point. The curve usually presents one or two turning points during an extension cycle. Qualitatively a stress-strain shown in fig: 5.

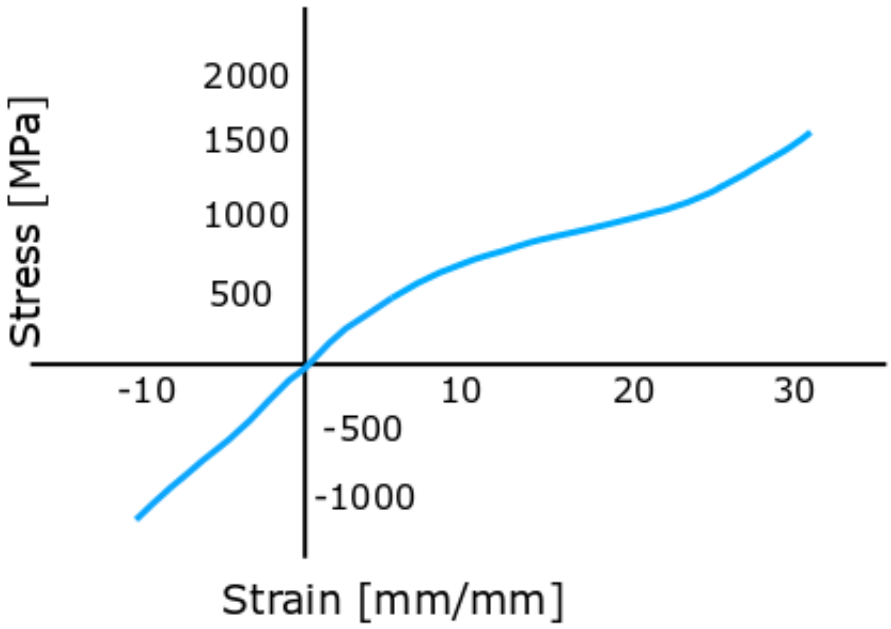

Figure 5: Example of measured stress strain curve.

To model material behaviour the most success full models are Hyper-elastic ones, where the stress-strain relation is derived form a definition of strain energy density function. Several models are available (fig:7) and a comparison made by [21] (fig:6)reports principal advantages and drawbacks of each. After some evaluation (tab:6), the model adopted in this work has been a 3rd order, 5 Parameters Phenomenological method (Mooney Rivlin 5 param in fig 7) , that will be further discussed in following sections. The choice for this method is its ability to correctly predict the stress-strain relation and to be relatively stable.

Material Model		Strenghts	Weakeness	Evaluation
Arruda Boyce		Physical base, stable only two parameters	Limited phisical description,can represent ´´ up turn ´´ only	Limited
Marlow		Correctly predicts measurement results	Not parametrizable, rarely commercially implemented	Limited
Ogden	1. Order		Not sufficient for proper phisical description	Unsatifactory
	2. Order	From second order on, it describe with enough accuracy the profile of the stress strain curve	Numerical instability arises for some materials	Unsatisfactory
	3. Order			
	4. Order			
	5. Order			
	6. Order		Numerical instability due to too high order	
Poly-nomial	1. Order Mooney Rivlin	Classic Literature Method	Numerical instability arises for some materials	Unsatisfactory
	2. Order Mooney Rivlin			
Reduced Polynomial	1. Order Neo Hooke	One parameter only, stable most of the times. Classic literature model	The ´´up turn´´ cannot be modelled	**Satisfactory**
	2. Order		Not better results then Neo Hooke, although of higher grade	Unsatisfactory
	3. Order Yeoh	Correct prediction of stress-strain relations, classic material model	Not innerly numerically stable	**Satisfactory**
	4. Order		Numerical instability arises for some materials	Unsatisfactory
	5. Order	Correct prediction of stress-strain relations	Not better compared to Yeoth, despite the higher grade	Unsatisfactory
	6. Order			Unsatisfactory
Van der Waals		Correct prediction of stress-strain relations, physical base	rarely commercially implemented	Limited

Figure 6: Comparison of constituive models.

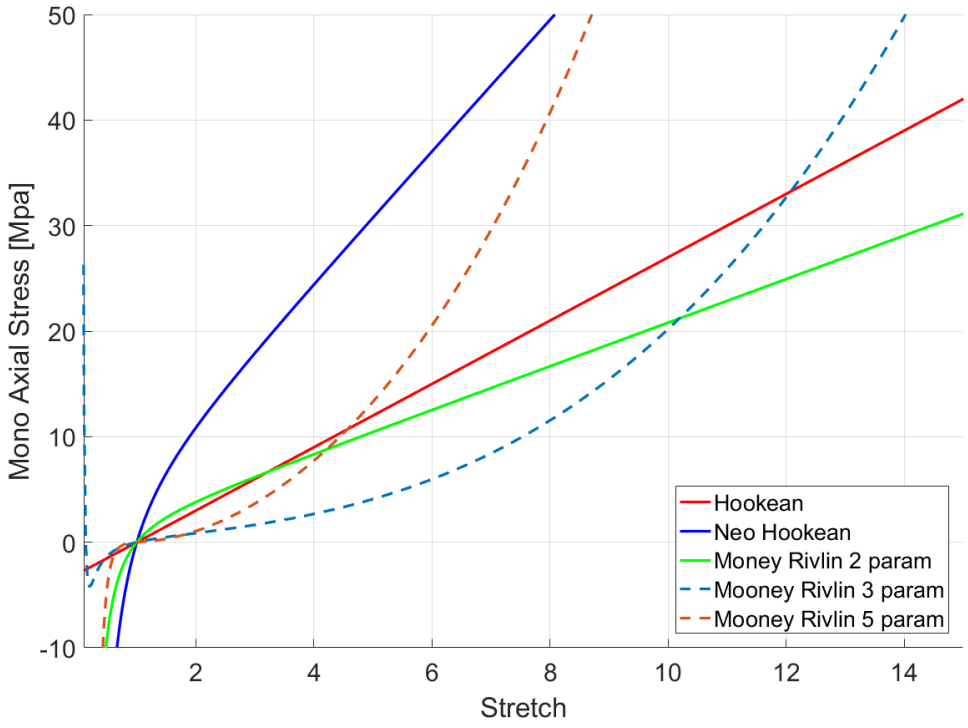

Figure 7: Example of different constitutive models

2.3 Viscoplasticity

Cyclic deformation of elastomers leads to energy dissipation in form of heat due to two different phenomena. The first one is linked to the relative movement and interaction of the polymeric chains with the filler material and themselves, thus leading to a energy loss due to friction. The second phenomena relates with configuration entropy [16]. As a matter of fact as the elastomer is stretched, the tendency of the fibres will be to aligned in an orderly fashion. This will lead to a decrease in the local entropy that will be compensated via an increase of the rubber temperature.(fig:8) A difference in the temperature between the rubber and the surrounding will lead to a dissipative heat flux.Due to this phenomena, the rubber will exhibit an Hysteric behaviour depicted in fig:9).

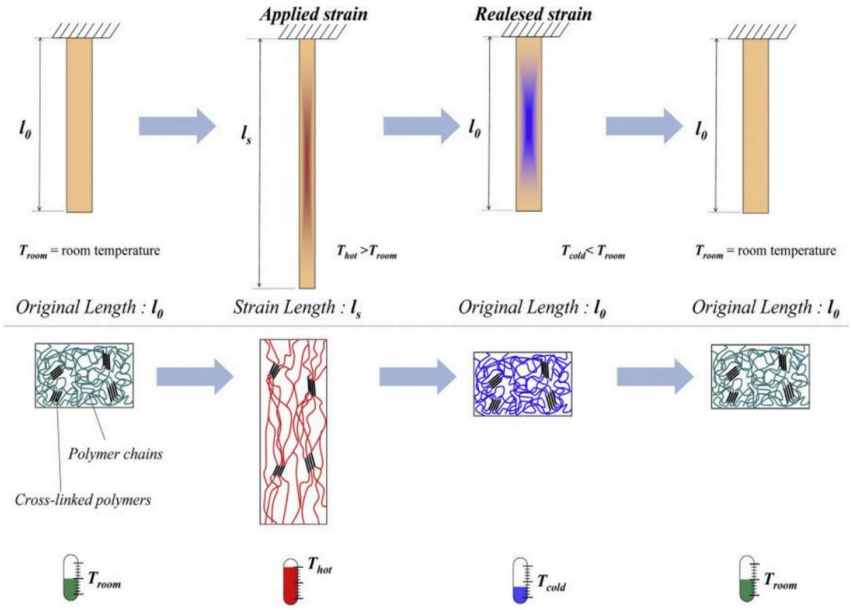

Figure 8: Depiction of temperature increase due to straining of rubber. Source [39]

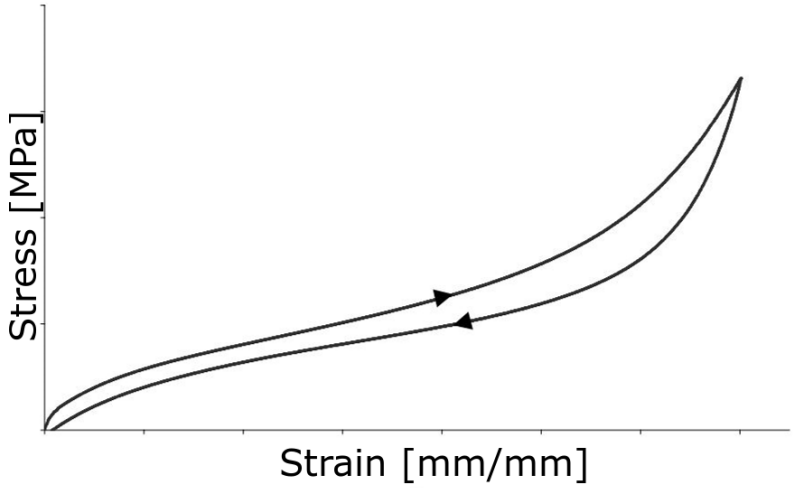

Figure 9: Hysteresis behaviour during a loading-unloading cycle. Source [24]

The pronounced damping properties of elastomer is due to this large hysteresis. Elastomer material exhibit a frequency dependent behaviour under mechanical stresses. Under cyclic loading, elastomer exhibit a dependence of the viscoelastic storage modulus on the amplitude of the applied stress. Over approximately 20 % elongation, the storage modulus approaches a lower bound. This property is called Payne effect and it is dependent from filler content. It can furthermore be linked with a breaking of weak bonds at microscopical level. The models used in fatigue design are nevertheless not able to include such effect, so its contribution will be excluded in this work.

2.4 Mullin Effect

During the first cyclic loads, most of the rubber components will be subject to a degradation of the mechanical properties in the form of a cyclic softening as seen in fig: 10. This effect goes under the name of Mullinś effect. The entity of such relaxation depends from the magnitude of the loads. After an amount of loads around 10^2 cycles the effect will not be noticeable anymore. [11] Mullins effect has a great influence in the material characterization, and for this reason standard procedure require an initial amount of pre-stretches before measuring mechanical properties. Mullins effect are in close connection with the filler's nature and size [26]

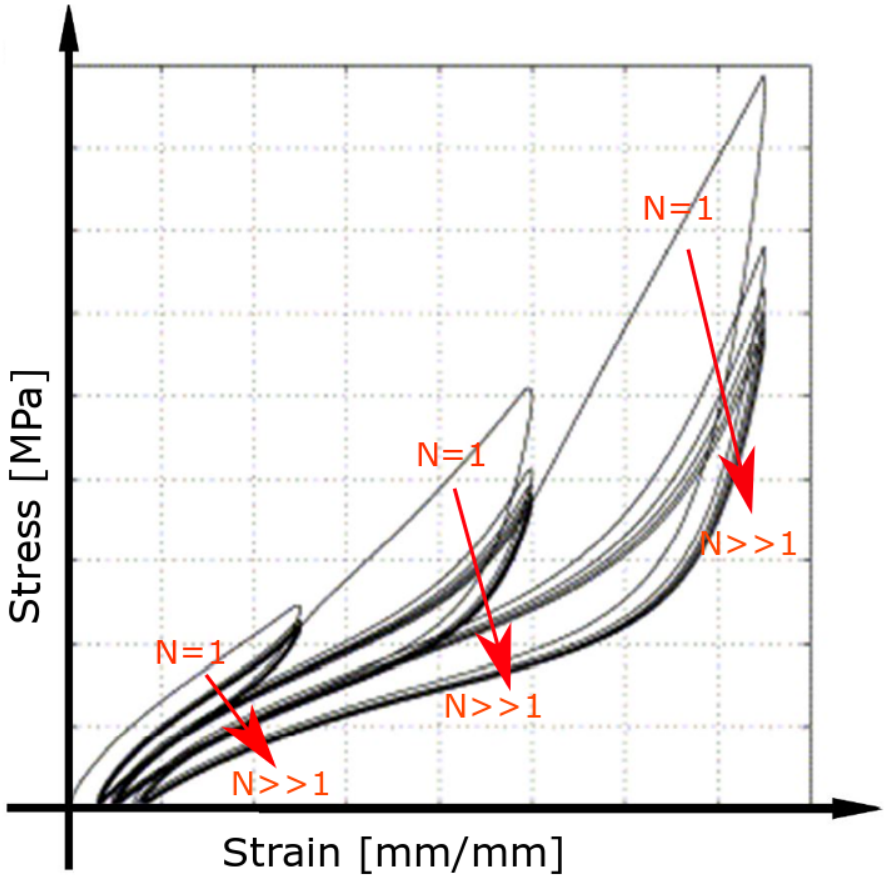

Figure 10: mullins effect during showed for different strain level. Source [21]

2.5 Temperature Dependency

The mechanical properties of rubber are dependent from temperature. Below the glass transition temperature, the elastomer will crystallize and become brittle. Glass transition temperature for Natural rubber are usually around $-70°$ Celsius. With increase in temperature two phenomena will occur. At room temperatures they will exhibit a negative thermal expansion with temperature increase. This can be easily explained by referring to image 8, as a matter of fact the increase of thermal energy will allow a more intricate configuration of the polymer chain, thus reducing the occupied volume.

2.6 Strain induced crystallization

Elastomers subjected to strains over 200 exhibit a behaviour called strain induced crystallization.(fig:11) This phenomena is based upon a local crystallization of the polymer chain due to stretching. This event is reversible and the crystallized part returns to an amorphous conditions upon relaxing[36] .

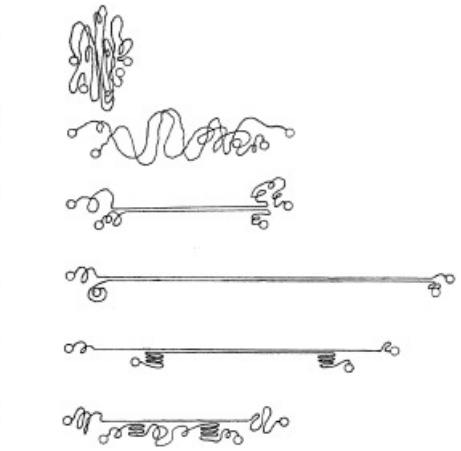

Figure 11: Effect of the strain induced crystallization on the Polymeric chains. Source [29]

This phenomena is of great interest in rubber since it can lead to an increase of the fatigue life. As a matter of fact, crack tip are interested to a zone of high stresses and strains. The formation of a crystallized area at the crack tip acts as a crack-propagator preventer. This phenomena is at the base of the peculiar shape of Haigh diagrams, where for R values greater than 0 the fatigue life increases.

3 Constitutive Equations

3.1 Hyperelasticity theory

Rubber materials, due to their peculiar mechanical behaviour, need to be described through advanced material models, usually referred to *Hyperelastic Materials* or *Green Elastic Materials.* Hyperelastic models are successfully used in application on non-linearly elastic, isotropic, non compressible materials, and these models are special cases of Cauchy materials. The stress state at each point is univocally determined by the present state of deformation compared to an arbitrary initial one. In this work, the initial state will also be referred to the reference configuration, and the deformed one also to the spatial (current) configuration. In the constitutive equation of a Cauchy material, the stress state does not depend upon the deformation path to which a material is subjected, nor on the deformation rate to reach a certain configuration. Moreover volume forces (body forces) and inertial forces, do not affect material properties.
Special case of Cauchy materials are the Hyperelastic or Green elastic ones. This class of constitutive model derive the stress-strain relations through a function known as strain energy density.
Strain energy density is a scalar valued function that associates the *Right Cauchy-Green deformation tensor* to the strain energy density release.

$$W = \hat{W}(\mathbf{C}) \tag{1}$$

3.2 Stress-Strain relations

Due to its molecular nature, for solicited elastomer is easier to change shape rather then changing volume. As a matter of fact shear modulus is much smaller when compared to the bulk one. The stress strain relation can be described through the use of the $1st\ Piola - Kirckhoff$ stress tensor and the $Deformation\ Gradient$ $\mathbf{F}$, but in order to obtain them the hydrostatic pressure must be derived. In order to do so it is important to start from the Bulk modulus definition for a nearly incompressible material. The Bulk Modulus is described as the ratio in change of pressure over the fractional volume compression and for elastomer is very high.

$$B = \frac{\Delta P}{\Delta V / V} \tag{2}$$

For incompressible materials, $J := det\mathbf{F} = 1$. Where $\mathbf{F}$ is the two point *Deformation Gradient Tensor*. In order to maintain the incompressibility throughout the equations, the strain energy function can be described as

$$W = W(\mathbf{F}) - p(J - I) \tag{3}$$

The hydrostatic pressure p functions as a Lagrange multiplier, used to enforce the incompressibility constraint. Under this hypothesis the *1st Piola-Kirchhoff* stress is given by:

$$\mathbf{P} = -p\ J\ \mathbf{F}^{-\mathbf{T}} + \frac{\partial W}{\partial \mathbf{F}} = -p\ \mathbf{F}^{-\mathbf{T}} + F\ \cdot \frac{\partial W}{\partial \mathbf{E}} = -p\ \mathbf{F}^{-\mathbf{T}} + 2\mathbf{F} \cdot \frac{\partial W}{\partial \mathbf{C}} \tag{4}$$

Where $\mathbf{E}$ is the *Lagrangian Strain*, $\mathbf{C}$ is the *Right Cauchy-Green* deformation tensor. Any stress tensor can be derived from the previous expression. Since in for fatigue prediction Cauchy and rotated Cauchy stresses are important, we report the definition of Cauchy stress:

$$\boldsymbol{\sigma} = \mathbf{P}\ \cdot \mathbf{F}^{\mathbf{T}} = \ -p\ I + \frac{\partial W}{\partial \mathbf{F}} \cdot \mathbf{F}^{\mathbf{T}} = \ -p\ I + \mathbf{F} \cdot \frac{\partial W}{\partial \mathbf{E}} \cdot \mathbf{F}^{\mathbf{T}} = \ -p\ I + 2\mathbf{F} \cdot \frac{\partial W}{\partial \mathbf{C}} \cdot \mathbf{F}^{\mathbf{T}} \tag{5}$$

3.3 Third Order Deformation

The model used in this work for describing the material properties is an invariant based, Third Order Deformation model with 5 describing parameters. Phenomenological model refers to the fact that the physical description of the material behaviour is not based upon a theoretical physical description, whereas is backed only by relations inferred through the empirical observation of certain phenomena. For this reason the 5 describing parameters ensure that the function describing the stress/strain relation passes through the measured stress/strain points. These parameters are obtained using a least square method for the parametrized function over the measured experimental data. In particular the strain energy density is here described as a linear combination of the two invariants $\lambda_1,\ \lambda_2$ of the *Left Cauchy-Green deformation tensor* $\mathbf{B}$. Strain invariants are derived from the following relation:

$$J = \ \lambda_1\lambda_2\lambda_3 \tag{6}$$

The five parameter models is chosen since it can successfully describe the upturn in the stress strain curve as seen in picture 5. This leads to the parametrization of $\mathbf{W}$ in the following way

$$\begin{aligned} W_5 =& C_{10}\left(I_1-1\right)+C_{01}\left(I_2-1\right)+C_{20}\left(I_1-1\right)^2+C_{01}\left(I_2-1\right)^2 \\ &+C_{11}\left(I_1-1\right)\left(I_2-1\right)+\frac{1}{d}\left(J-1\right)^2 \end{aligned} \tag{7}$$

With this definition of strain energy density, the uni-axial stresses are given as:

$$\begin{aligned} \mathbf{S} =& 2C_{10}\left(\lambda-\frac{1}{\lambda}\right)+2C_{10}\left(\lambda-\frac{1}{\lambda^3}\right)+6C_{11}\left(\lambda^2-\lambda-1+\frac{1}{\lambda^2}+\frac{1}{\lambda^3}-\frac{1}{\lambda^4}\right) \\ &+4C_{20}\lambda\left(\lambda-\frac{1}{\lambda^3}\right)\left(\lambda^2-\frac{2}{\lambda}-3\right)+4C_{02}\lambda\left(2\lambda-\frac{1}{\lambda^2}-3\right)\left(1-\frac{1}{\lambda^3}\right) \end{aligned} \tag{8}$$

Stability criterion are met for

$$\frac{\partial\sigma_{\mathbf{ij}}}{\partial\epsilon_{ij}}\geq 0 \quad \text{and} \quad \partial\sigma_{ij}\partial\epsilon_{ij}\geq 0 \tag{9}$$

Equation 9 refers to the monotony of the strain-stress curve for any given stress state. The monotonic trend can be seen in fig: 12. In particular the monotony of the function assures that the force applied to the specimen always increases. As a matter of fact a negative value of the derivative of the stress in regards of the strain would suggest that a negative force applied to the specimen would result in a positive elongation, and this effect would be not physically viable. The derivation of all the parameters described in 9 is obtained through an optimization fitting process. Experimental data are gathered and the parameters are usually optimized with a least square method.

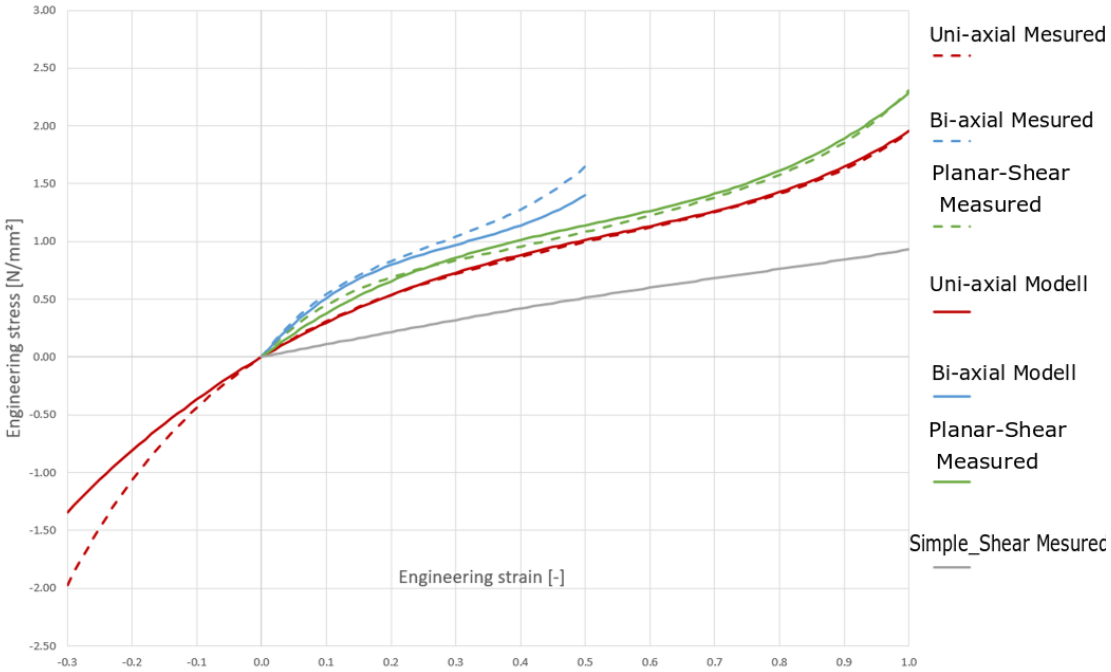

Figure 12: Comparison between measured data and Model prediction on Stress-Strain relation.

4 Fatigue Behaviour of Rubber

Fatigue life of Rubber can be divided in three different stages:

1. **Crack nucleation**. This represent from 80% to 90% percent of the component life up to complete failure. In this stage the cyclic loads starts creating some micro crackign, usually around rubber defects, that might in a second stage grow to cracks. This part of fatigue life is well described by Wholer life relations.[32]
2. **Crack growth**. This phenomena occurs when a single crack develops enough to start being noticeable. Once a micro-crack becomes big enough to promoted to crack (usually has to be bigger then 1 mm) the crack growth becomes somehow fast. In this stage the crack growth related to the cyclic stress levels is governated by an exponential law similar to the Paris one. [15]
3. **Component failure**. The failure of a component might be defined in several ways. Underling them all is the assumption that a failed component is not longer able to perform the task it was designed for.

Fatigue in rubber is a quite challenging phenomena to tackle with. As a matter of fact many parameters have a great influence on the overall life of components:

- **material properties** deriving from manufacturing of the raw materials as well as being influenced by the producing processes.
  - Fillers
  - Curing accelerators (ZnO_x, *stearic acid,...*)
  - Detacher Residuals from manufacturing processes (SiO_2, $CaCO_3$,...)
  - Anti-Degradants (*Antioxidants, UV shielders,...*)
  - Mixing residuals (*Carbon Black aggregates, Zinc Oxide aggregates,...*
- **Surface condition**
- **Working conditions**
  - Temperature
  - Load frequency
  - Load Level
  - Chemical environment
  - UV exposure
- **Component geometry** for the distribution of stresses inside the components.

Many of the previous parameters are closely related with production and service parameters that should be analysed case by case when putting a component into service. Since this work is intended to serve as a tool for understanding the fatigue life deriving from solicitation, the main focus will be on the geometrical properties of the components and how they affect the stress state at various locations.
The following section will briefly analyse the different influencing factor in order to get a complete overview of the topic.

4.1 Influence of material properties

Rubber is composed primarily by polymeric chains cross-linked by covalent atomic bonds. Nevertheless due to the natural origin of most of the rubber used in industry, a non indifferent part of it is composed by impurities. These consist manly of lipids (1.5–3% w/w), proteins and polypeptides (2% w/w), carbohydrates (0.4% w/w) and minerals (0.2% w/w).[30]. Also natural fibers contaminants as well as carbon-based inclusion are known to exist in the specimen.[32]. Such impurities are important in determining mechanical properties of rubber as well as they have a great influence on fatigue life.

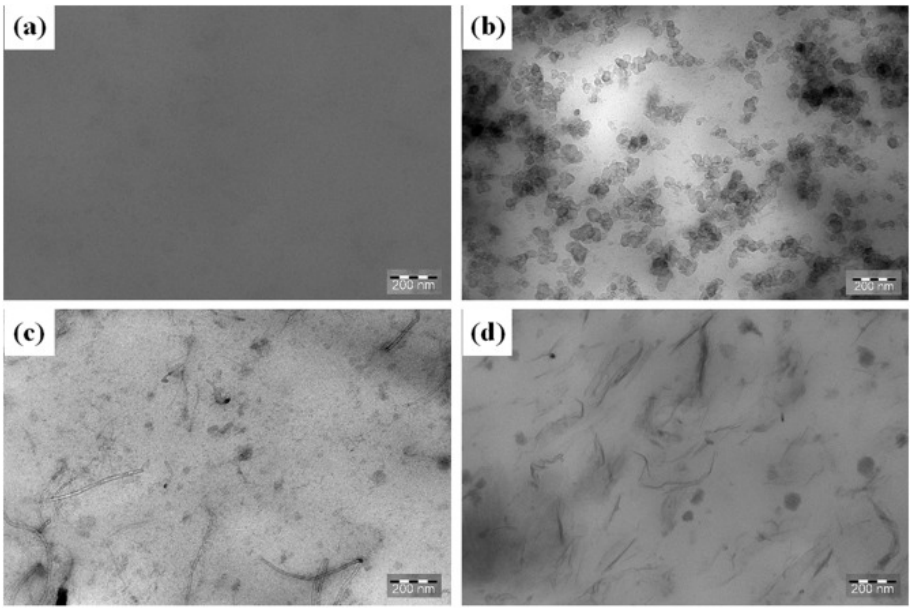

Figure 13: TEM micrographs of composites: (a) NR-0; (b) CB-10.7; (c) CNTs-1.2; (d) GO-1.6. Source: [12]

Apart from natural impurities, natural rubber is often mixed with mineral compounds such as Carbon Black, Silica Oxide and Zircon Oxides, (fig:13) in order to improve mechanical properties[14][32]. Other mineral-based filler such as Si_2 *and* $CaCO_3$ are added to the mixture to improve processability. Fillers might have beneficial properties in increasing fracture toughness and fatigue life, especially with the increase of the CB content.[14]. The presence of Carbon Filler has been observed to produce the highest strain amplification level and area at the crack tip. This leads to the optimal dissipation of input energy, thus

improving fracture and fatigue performances.[12]. Carbon Black fillers is an inexpensive material obtained as a by product from combustion of hydrocarbons (eg. from power plants).
Many other fillers have been investigated, but choosing the wrong one might result in a detrimental effect. As an example Natural rubber filled with Carbon Nanotubes (CNTs) exhibit a much higher hysteresis loss compared with CB that results in weakened fatigue resistance. Some other fillers, like planar Graphene oxide, play a very limited rove in fatigue and crack growth prevention. [12]. Uneven mixing of the raw material might result in worse fatigue properties. It has been observed by that black carbon aggregate with size over $200 - 400\mu m$ might act as crack precursor (fig:14)[9][23].

The two failure mechanism at microscopic level as indicated by[32] are:

- **Rubber de-cohesion**: is a phenomena that happens at rigid inclusion location (e.g. SiO_2, $CaCO_3$), and consist in the particle surface getting clear of the rubber. This then induce an extreme local deformation that, over cyclic loading, can lead to the tearing of the rubber material. These kind of rigid inclusion present a clear interface with the rubber matrix.

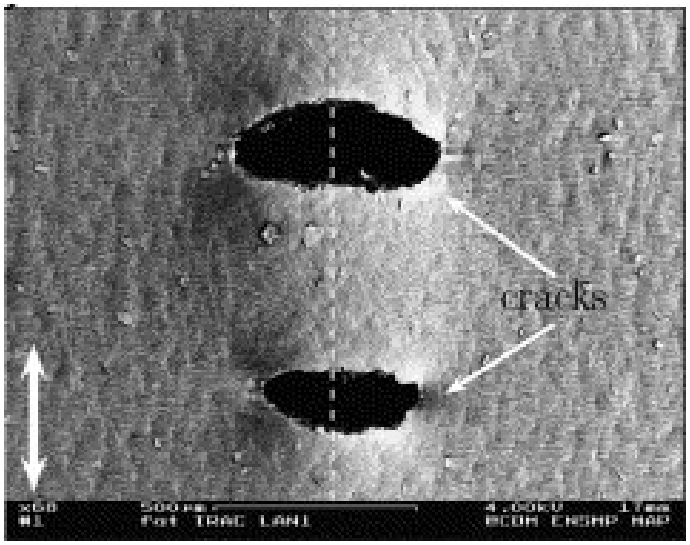

Figure 14: Images of cracks due to decohesion processes in a specimen deformed state Source: [32]

- **Rubber cavitation**: is a phenomena occurring at agglomerate location (e.g. Carbon black and ZnO_2)(fig:16,15) that do not present a clear interface with the rubber matrix. These are consequence of non homogeneous mixing processes, but can hardly be avoided. Cavitation consist in the spontaneous void nucleation under a certain stress-state.

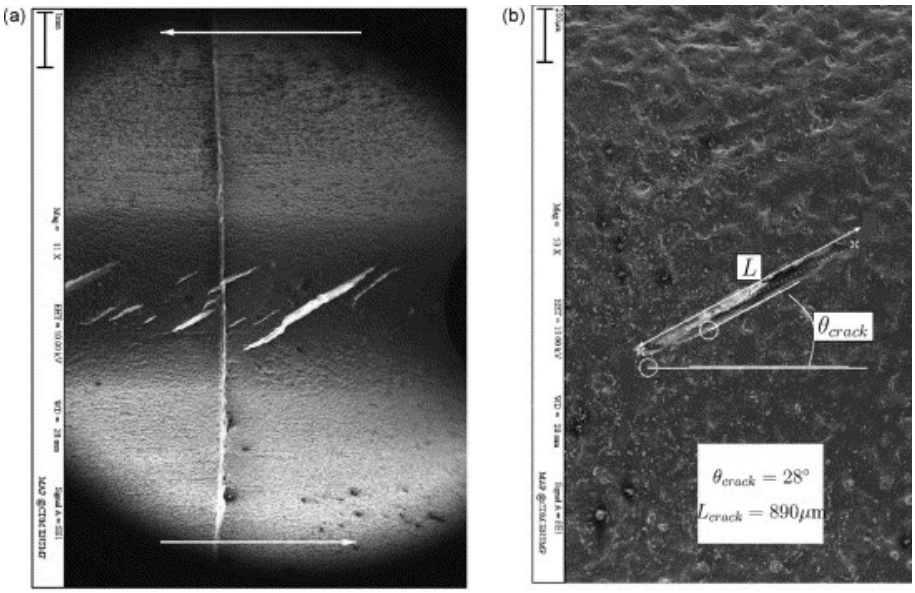

Figure 15: Images of cracks in a specimen deformed state Source: [32]

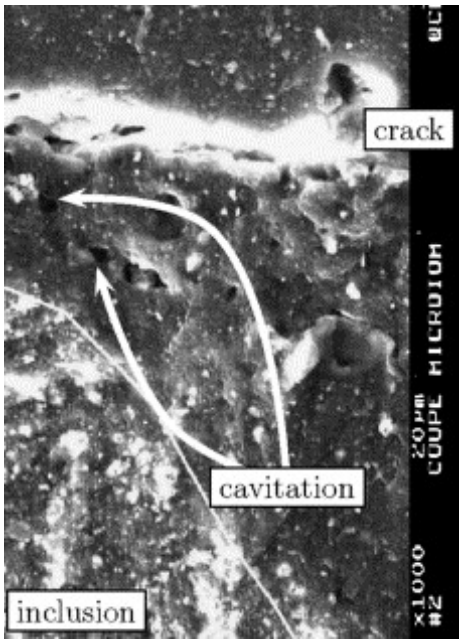

Figure 16: Images of Micro and Macroscopic craks inside a specimen Source: [9]

4.2 Influence of surface finish

Surface finish plays a great role in the fatigue life of rubber components. Most of the components are created when a raw mass is heated and shaped against a mold. In order to avoid the adhesion between the rubber and the mold, some detacher agents, like gypsum ($Mg_3Si_4O_{10}(OH)_2$) can be used. Also this compond can create agglomerates detrimental to fatigue life, sine they represent the perfect location for a crack to develop. (fig:17)[9, 19]

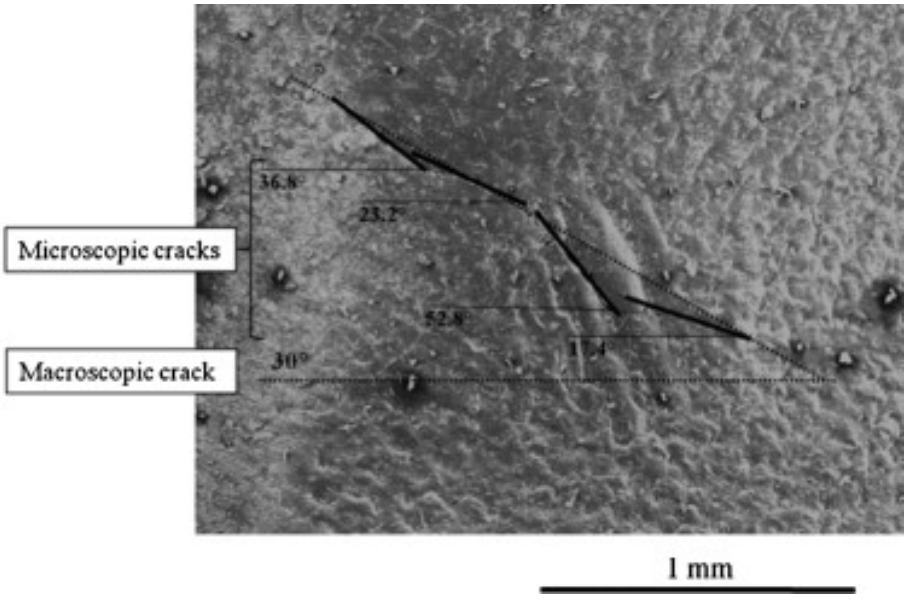

Figure 17: Images of cracks in a specimen deformed state Source: [9]

The progressive cooling of big components can also results in the presence of stresses located under the skin of the component at a distance approximately $200 - 400\mu m$ from the surface. This is due to the low conductivity of the rubber that in a cooling process can allows the formation of very steep temperature gradients.

4.3 Environmental conditions

Working conditions are described by the following parameters

- **Temperature**: Temperature has a great influence on the mechanical and fatigue properties of rubber. Temperatures below glass transition temperature will render the rubber brittle and decrease significantly fatigue life. Higher temperatures will initially increase the elastic coefficient, thus changing the stress state. Even higher temperatures will increase the reactivity of the rubber with the atmospheric oxygen until burning event occurrence.
- **Chemical Environment**. Presence of solvents, Oxygen O_2 and Ozone O_3 will induce a deterioration of the mechanical properties of the rubber. [31]. The degraded surfaces will start presenting cracks and crevices, and the surface properties such as wettability and hardness will also change [31].

- **Ultra-Violet radiation**. Radiation on spectra more energetic then the visible one, will also contribute to the material degeneration. [31]

4.4 Stress Levels

Due to the very nature of fatigue, higher stressess level will result in shorter service life. On top of that the load frequency is important in determining the temperature at wich the component will work. As a matter of fact the energy converted into heat thanks to hysteretic processes tends to accumulate inside the component, since its flow is hampered by a very low thermal conductivity.The increase in the operating temperature due to self heat properties is detrimental to fatigue life.[40]

5 Fatigue Life Modelling

The components analysed in during this work are usually considered to fail after a certain stiffness quantity is lost (20%). For this reason the specimen will pass most of their working life under a stage of crack nucleation. Since the crack growth is happening only during a very limited amount of service life, this fatigue phenomena will be left out. On top of that the models describing crack growth in rubber materials are governed by a great amount of parameters, which determination is everything but simple. Since this work aims at developing a procedure useful in practical application, the fatigue crack-growth models were deemed infeasible to be applied.
Fatigue life under crack nucleation can be easily described as a power-law, where the fatigue life is related to a suitable fatigue indicator.(fig:18)

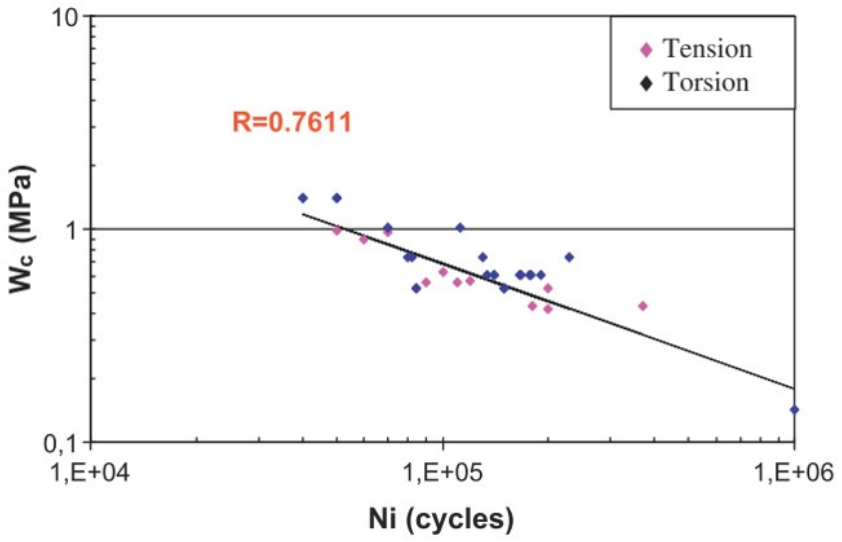

Figure 18: A generic Wöhler line, where **W** is a generic fatigue life indicator

From literature several life indicators have been studied:

- **Stretches based criteria**
- **Stress based criteria**
- **Energy based criteria**
- **Configurational Mechanics**

5.1 Stretches

The use of principal stretches has been adopted in order to predict fatigue life in many works [8], [20] [40]. The advantages of using such indicator reside in the possibility of easily measure them through direct measurement techniques such strain gauges or Digital Image Correlation processes.
They successfully predict the direction of the crack propagation, but fail to predict fatigue life if used on multiaxially loaded specimen. In the figure 19 is possible to observe as this method presents a too big scatter of data, thus failing to unify experimental multiaxial fatigue data. [6]. Furthermore since the hydrostatic stress seems to be a very good indicator, the strain tensor is not able to predict fatigue life since it does not effect the hydrostatic component of the stress.[7]

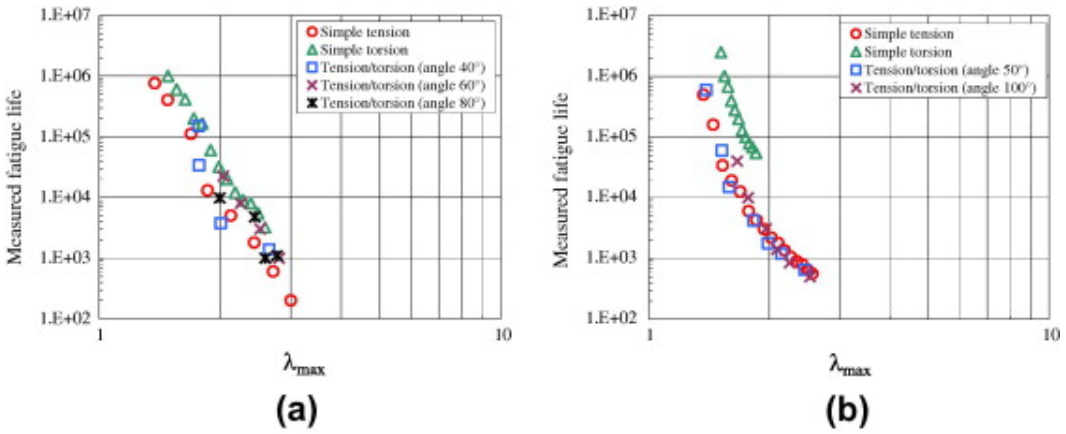

Figure 19: Wöhler curves created using the maximum principal stretch. They clearly show a disagreement in the life estimation, thus defining the principal stretch as not a suitable fatigue life indicator. **a** and **b** refer to different experimental setups. Source[6]

5.2 Stresses

Principal stress direction can also be used as fatigue indicator.(fig:20) In particular Cauchy stresses criteria have shown as the crack direction is perpendicular to the direction of the highest principal Chauchy stress. This method has proven to be excellent in unifying experimental data from multiaxial experiments[6].
Stress criteria are suitable for rubbers exhibiting strain induced crystallization as well[6]. During a load sequence, the maximum stress components endured by a material is given by:

$$\phi = \frac{1}{2} \max_{t=t_0,t_c} [\sigma(t)] \tag{10}$$

Where t_c refers to the final time of the time interval analysed.

This criteria unifies experimental data from different load conditions as possible to be seen in fig:(20)

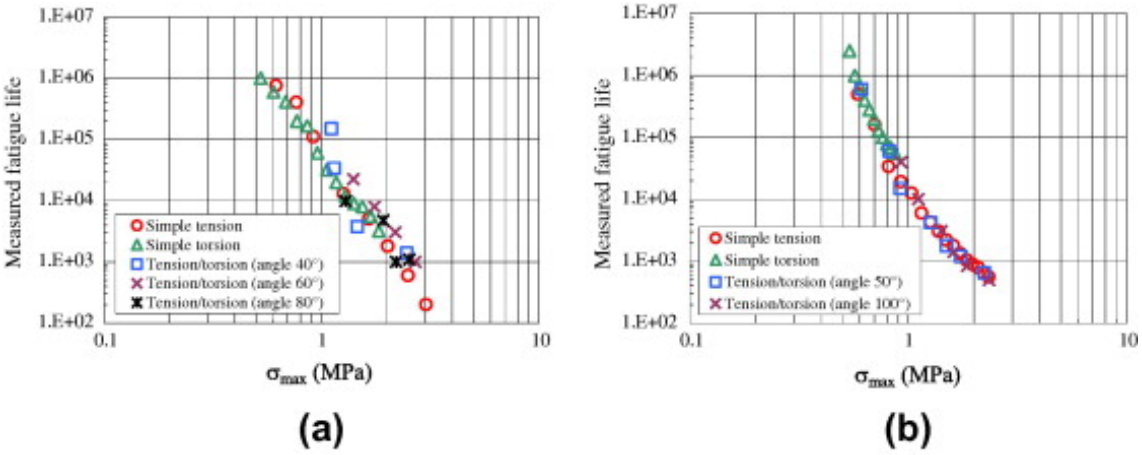

Figure 20: Wöhler curves created using the maximum principal Cauchy stress. **a** and **b** refer to different experimental setups. Source[6]

5.3 Stresses from continuum damage mechanics

It is possible to formulate a stress indicator based on continuum damage mechanics that copes with multiaxial loading.[5]. Continuum damage mechanics is a theory that takes into account the initiation and propagation of cracks through a specimen. The principal assumption is that the presence of these microcraks and defects decrease the net section of the specimen, determining an increase of the load transfer to the material elements. Using the Second Piola-Kirchoff stress tensor, the effective principal stresses relate with the following relation:

$$\mathbf{S}_{eff} = \frac{\mathbf{S}}{(1-D)} \tag{11}$$

Where D is a damage parameter assuming values between 1 (fracture) and 0 (virgin material). Furthermore it is a parameter evolving from the net section decrease. Damage kinetic can be described as :

$$\dot{\mathbf{D}} = -\frac{\partial \varphi *}{\partial y} \tag{12}$$

Where y is the damage strain energy release rate and $\partial\varphi*$ is the dissipation potential

$$\varphi* = \frac{A}{a+1}\left(\frac{-y}{A}\right)^{a+1} \tag{13}$$

Where A and a are fitting parameters that need to be obtained experimentally. For the next series of derivation, the use of any Strain energy density is possible. Following the decription of [5] the Ogden formulation of Strain Energy Density is deployed.

$$\mathbf{W} = \sum_{i=1}^{n} \frac{\mu_i}{\alpha_i}(\lambda_1^{\alpha_i} + \lambda_2^{\alpha_i} + \lambda_3^{\alpha_i} - 3) + \frac{9}{2}K(\mathbf{J}^{\frac{1}{3}} - 1)^2 \tag{14}$$

where K is the Bulk modulus, **J** is the Jacobian (=1 for incompressible materials), μ_i *and* α_i are material parameters, $\mu = \sum \mu_i$ is the shear modulus.

Damage strain energy release rate is

$$-y = \frac{\partial \mathbf{W}}{\partial D} \tag{15}$$

The damage strain energy release rate can be written differently since the W is a function of the effective principal stresses $\mathbf{S_{eff}}$.

$$-y = \frac{\partial \mathbf{W}(\mathbf{S_{eff}})}{\partial D} \tag{16}$$

Differentiating 11 with respect to D damage variable,

$$\frac{\partial \lambda_i(\mathbf{S}_{eff})}{\partial D} = \frac{\mathbf{S}_{eff}}{(1-D)\frac{\partial \mathbf{S}_{eff}}{\partial \lambda_i}} \; with \; 1 \leq i \leq 3 \tag{17}$$

Using 14,15,17 the damage strain energy release rate becomes

$$-y = \frac{\mathbf{S}_{eff}}{1-D} \tag{18}$$

Where eventually $\mathbf{S}_{eff}$ can be defined with the following parameters

$$\begin{aligned} \mathbf{S}_{eff} &= \sum_{i=1}^{3} \frac{\partial \mathbf{W}}{\partial \lambda_i} \\ &= \sum_{i=1}^{3} \frac{(\sum_{j=1}^{n}\ \mu_j \lambda_i^{-2} + p\lambda_i^{-2})(\sum_{j=1}^{n}\ \mu_j \lambda_i^{\alpha_j - 1})}{(\sum_{j=1}^{n}\ \mu_j(\alpha_j - 2)\lambda_i^{\alpha_j - 3} + \frac{\partial p}{\partial \lambda_i}\lambda^{-2} - 2p\lambda_i^{-3})} \end{aligned} \tag{19}$$

The life expectation prediction using this indicator has poven to be effective [6]. The figure21 shows how life of two different specimen geometry under different load cases are successful.

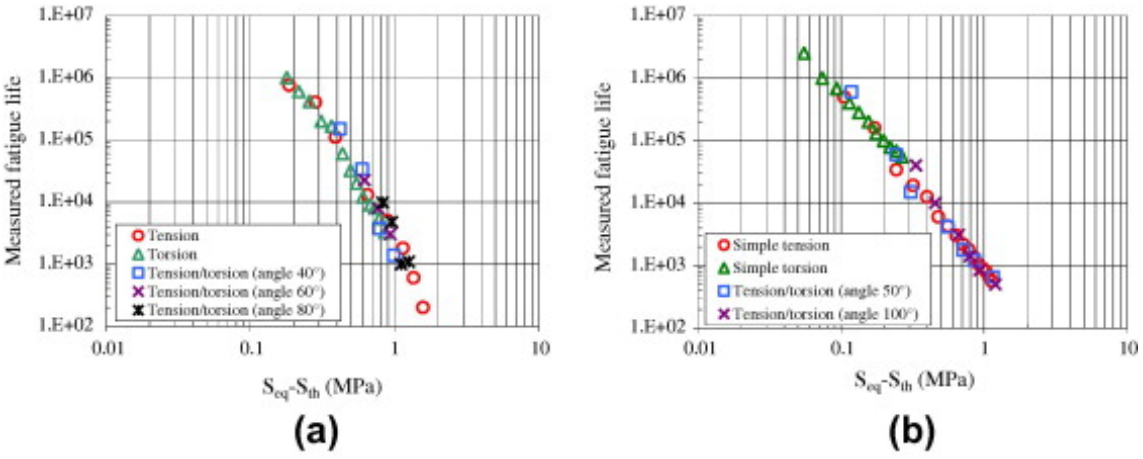

Figure 21: Wöhler curves created using the continuum damage mechanics. **a** and **b** refer to different experimental setups. Source[6]

The drawback from using such predictor is the high number of parameters that need to be defined in order to correctly describe $\mathbf{S}_{eff}$, as well as the correct determination of a $\mathbf{S}_{tresh}$. This value is correspond to the stress values below which no crack nucleate. The determination of such value is purely empirical, adding further complexity to an already complex model.
The great number of parameters needed to correctly implement such technique, coadiuvated by the great parameter sensitivity of this model, has deemed it as not feasible for industrial

application. On top of that the parameter of $\mathbf{S}_{eff}$ changes continuously with every cycle. Such property enables the model to take into account load history of the signal, but on the other hand require the simulation of every single cycle, thus making it not a feasible damage calculation technique for long and complicated load signals.
Furthermore the need to accurately describe the loss of section due to the damage accumulation would result in the need of having a FEM model with and extraordinary fine mesh. This would result in an increase of computational requirements that is not suitable for application on large specimen.

5.4 Energy based criteria

5.4.1 Strain Energy Density

One of the proposed fatigue indicator is the Strain Energy Density.(fig:22) Since rubber material are successfully described by hyperelastic constitutive models, the strain energy function is already defined. Nevertheless this quantity does not successfully describe fatigue life as described by [6].Specifically they are not able to cope neither with mono-axial nor multiaxial loading of specimens.
Moreover being the strain energy density a scalar entity, it does not provide useful information on the direction of the crack propagation.

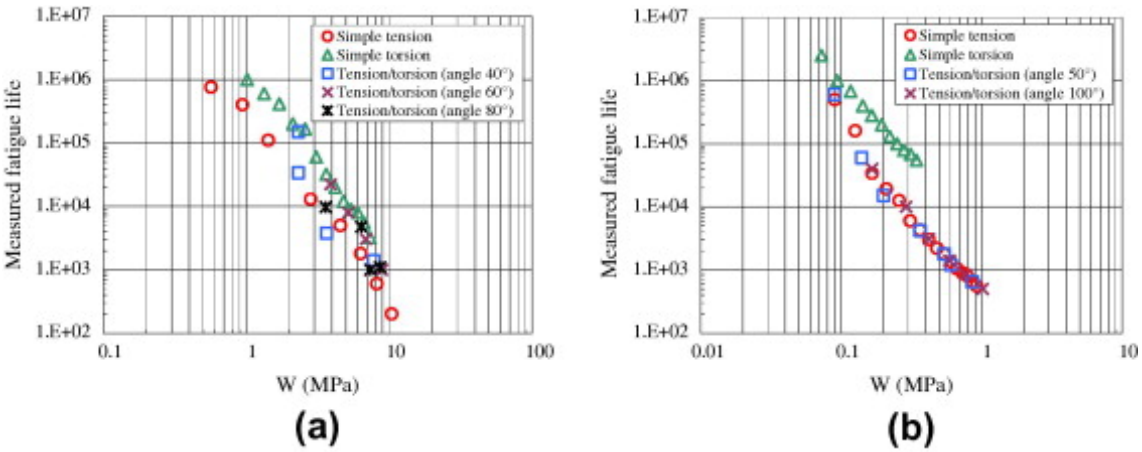

Figure 22: Wöhler curves created using strain energy density indicator. **a** and **b** refer to different experimental setups. Source[6]

5.4.2 Cracking Energy Density

Cracking energy density is a theory that modifies the strain energy density tensor through a critical-plane based approach. In this case the assumption underliyng this theory is that only a certain part of the strain energy density is available for crack growth. This quantity is defined as $\mathbf{W}_c$. Once this quantity is defined, for a certain load cycle, there is the need to find a material plane that maximize such quantity. The plane that succeed in doing so is designed as the critical plane, and it will nbe the location of the crack growth. More

specifically, let $\mathbf{r}$ be the normal direction of a given material plane. Under the infinitesimal strain framework, lets consider an incrementt of cracking energy density. This quantity is defined as the dot product between the Cauchy traction vector $\boldsymbol{\sigma}\ \mathbf{r}$ and a strain increment $d\epsilon$ in the $\mathbf{r}$-direction.[6]:

$$dW_c = (\boldsymbol{\sigma}\boldsymbol{r})(d\epsilon\mathbf{r}) \tag{20}$$

Extending eq. 20 to the Finite strain framework,

$$dW_c = \frac{1}{\mathbf{R}_\theta^T\mathbf{C}^{-1}\mathbf{R}_\theta}\ \mathbf{R}_\theta^T\mathbf{S}d\mathbf{E}(\mathbf{F}^T\mathbf{F})^{-1}\mathbf{R}_\theta = \frac{\mathbf{R}_\theta^T\mathbf{S}d\mathbf{E}\mathbf{C}^{-1}\mathbf{R}_\theta}{\mathbf{R}_\theta^T\mathbf{C}^{-1}\mathbf{R}_\theta} \tag{21}$$

Where $\mathbf{R}_\theta = (\cos\theta, \sin\theta)$ with θ crack orientation angle referring to the material configuration.

The use of this quantity can lead to correct prediction of life endurance.(fig:23) The outcomes of such results are highly dependent from the material parameters. In particular in the following images it can be seen as the presence of a correctly scaled $\mathbf{S}_th$ (threshold value for nucleation) determines the success or failure of the theory.(fig:24)

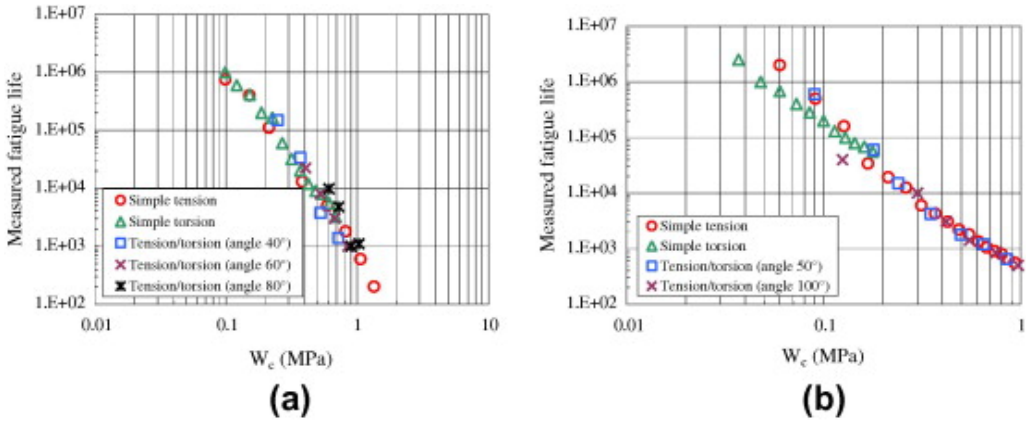

Figure 23: Wöhler curves created using continuum damage model. Note that the prediction not able to unify all experimental data. **a** and **b** refer to different experimental setups.Source[6]

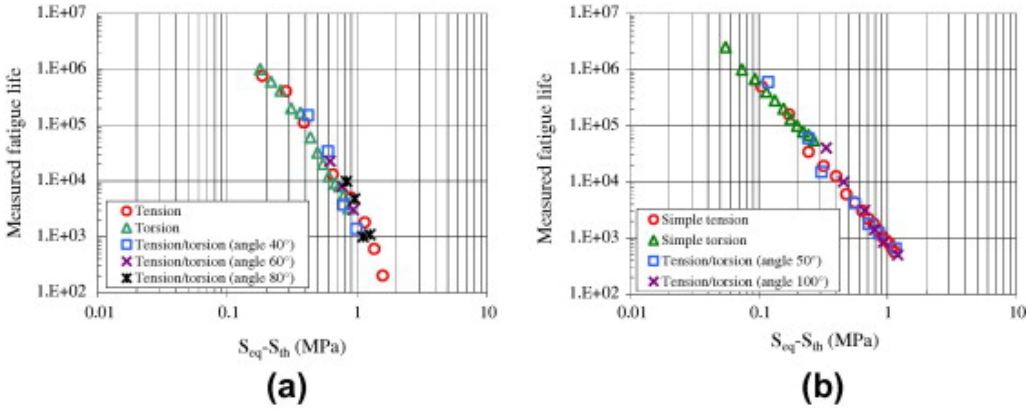

Figure 24: Wöhler curves created using continuum damage mechanics, where the introduction of a threshold value for the effective stress S_{eff} allows the model to successfully predict fatigue life. **a** and **b** refer to different experimental setups Source[6]

The need of a series of parameter used in the correct implementation of such procedure, deemed it as not feasible to be adopted in this work. As a matter of fact the governing parameters for the Cracking energy density are hard to define and require a further series of mechanical testing. Due also to the great sensitivity of such model to the parameters choice, it has been not taken into consideration in this work as a feasible fatigue indicator.

5.5 Configurational Mechanics

The configurationa mechanics model has been initially proposed by [38]. The foundation of such theory is based on the assumption of the existence of an intrinsic defect located into the rubber specimen. In order to extend this theory to multiaxiality, the critical plane method developed by [38] was adapted in recent works by [28]. This has been done on the principle that a material tends to reduce its potential energy b:

$$b^* = |min[(b_i)_{i=1,2,3}, 0]| \tag{22}$$

For $b^* \neq 0$ the propagation of the crack will develop on the first principal direction of the configurational stress defined as:

$$\mathbf{b} = W\mathbf{I} - \mathbf{CS} \tag{23}$$

where W is the strain energy density, $\mathbf{I}$ the identity tensor, $\mathbf{C}$ the right Cauchy-Green tensor and $\mathbf{S}$ the second Piola Kirchhoff stress tensor. Since the eigenvalues of $\mathbf{b}$ are the same ones as $\mathbf{C}$ and $\mathbf{S}$, the criterion in eq. 22 can be re-written as

$$b^* = S_{max}\lambda^2_{max} - W \tag{24}$$

With S_{max} *and* λ_{max} the maximum components of the two respective tensors. Since this model uses the stretch tensor (that proved to be un-effective 5.1) if fails as well at giving satisfactory fatigue life.(fig:25)

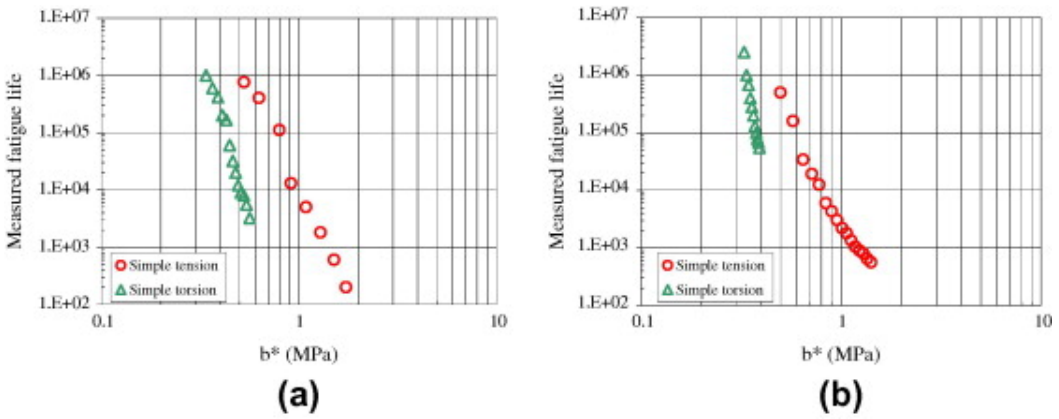

Figure 25: Wöhler curves created using configurational mechanics. Such technique does not allow a satisfactory fatigue life prediction. **a** and **b** refer to different experimental setups. Source[6]

6 Damage accumulation theory

The need for accounting the progressive damage deriving from the stress history, has led to the formulation of several damage accumulation theories. The three most used ones are the Linear damage accumulation one (Plagrem Miner rule), a modified version of it and one based upon the Continuum damage Mechanics theory [5]. Due to the very complex nature of the fatigue problem, where the fatigue life is extraordinarily sensitive material and fatigue parameters, the use of complicated damage accumulation method may not result in any tangible advantage. The implementation of sophisticated models rises the computational effort and require the determination of several more parameters that might not be easy to determine. For this reason the Linear damage accumulation method has been commonly used for fatigue design purposes.

In the following section a description of all three methods is presented, with particular care on the description of the pros and cons of every method.

6.1 Continuum damage mechanics

Using the continuum damage mechanics (5.3), it is possible to define both a fatigue life criterion as well as a damage accumulation method. As a matter of fact the damage accumulation can be derived from the description of how the damage parameter **D** evolves through the cycle history.[5]. For a given step, the increment of D_i is given by:

$$D_i = 1 - \left[(1 - D_{i-1})^{1-a} - (1 + a)\left(\frac{\mathbf{S}_eq}{A}\right)^a N_i\right]^{\frac{1}{1+a}} \tag{25}$$

Where S_{eq} is the effective stress acting at a certain time step i. D_0 is the damage level for time=0 and D_f is the damage after a certain cycle. A and a are fitting parameters to be experimentally determined. Given a series of n signal blocks of given amplitude, fatigue life $N_f = N_n$ can be derived from

$$\int_{D_0}^{D_f} (1 - D)^a \, dD \; = \sum_{i=0}^{n-1} \int_{N_i}^{N_f} \left(\frac{S_{eq(i+1)}}{A}\right)^a \, dN \tag{26}$$

This model parameters depend on the material ones plus the two damage parameters. Furthermore equation 25 can be re-written in order to show that this is a linear cumulative law:

$$(1 - D_{i-1})^{1+a} - (D_i - 1)^{1+a} = \frac{N_i}{N_{fi}} \tag{27}$$

Noting again that the value of D evolves from 0 till 1 (complete failure), the relation 27 is behaving similarly to a Palgrem-Miner cumulative damage. The parameters needed to describe the previous relation(a and A) must be determined with some axial loading

experiment, thus increasing the workload needed to apply such technique [6]

Strong point of this method is the capability of taking into consideration the sequence effect of the cyclic loading. This is extremely useful if the material present a strong load sequence sensitivity. On the other hand such technique burdens the analyser with a huge amount of calculations, since analysis must be performed to determine the stress state for each cycle. Such peculiarity deems this technique as infeasible for long signals or big models, since the computational load would be staggering.

Under the proper condition, this method presents some of the highest accuracy in predicting fatigue life, as possible to be seen in fig:26.

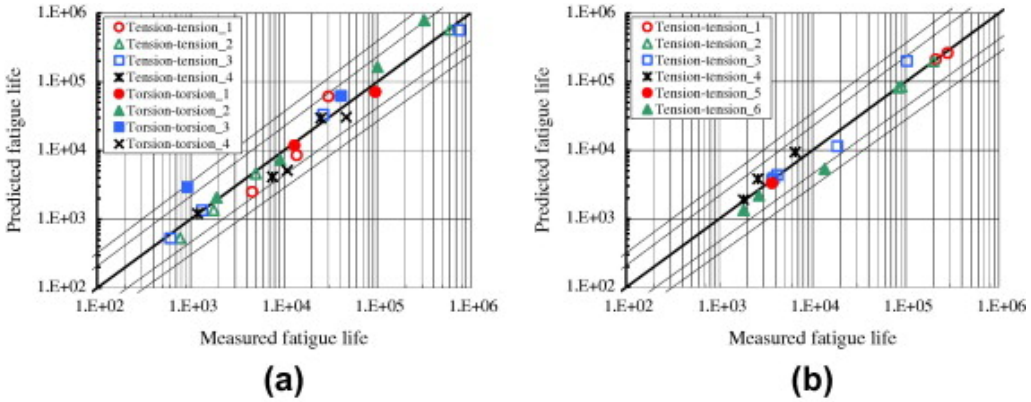

Figure 26: Comparison of predicted life vs measured fatigue life using continuum mechanics tecniques. **a** and **b** refer to different experimental setups. Source[6]

6.2 Palgrem-Miner linear damage accumulation

Palgrem-Miner damage accumulation theory, is one of the most widely adopted techniques to calculate damage accumulation. Its effectiveness resides in the simplicity of this model. If on one hand it does not consider load sequence effects, and its linearly summing up the damage deriving from each cycle, on the other hand, most of the time the data available to the designer on the load history or on working conditions would not anyway be enough to use some more refined model.
This rule is based on the principle that the damage D can be expressed in the following form:

$$D_i = \frac{N_i}{N_f} \tag{28}$$

Where D is the damage induced by N_i cycles of a load that would require N_f cycles at constant amplitude to bring the component to failure.

For expressing the total damage, it suffices to sum the partial damages:

$$D = \sum_{i=1}^{n} D_i = \sum_{i=1}^{n} \frac{N_i}{N_f} \tag{29}$$

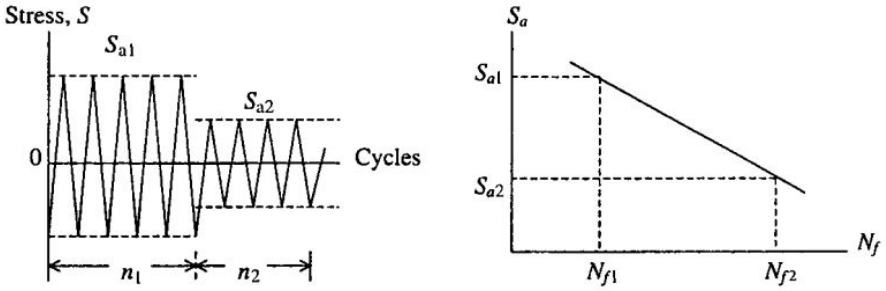

Figure 27: Stresses S and corresponding fatigue life N. Source [29]

For $D = 1$ the component will be subjected to failure. The following image shows life predicted vs measured for two samples subjected to different external stresses conditions.

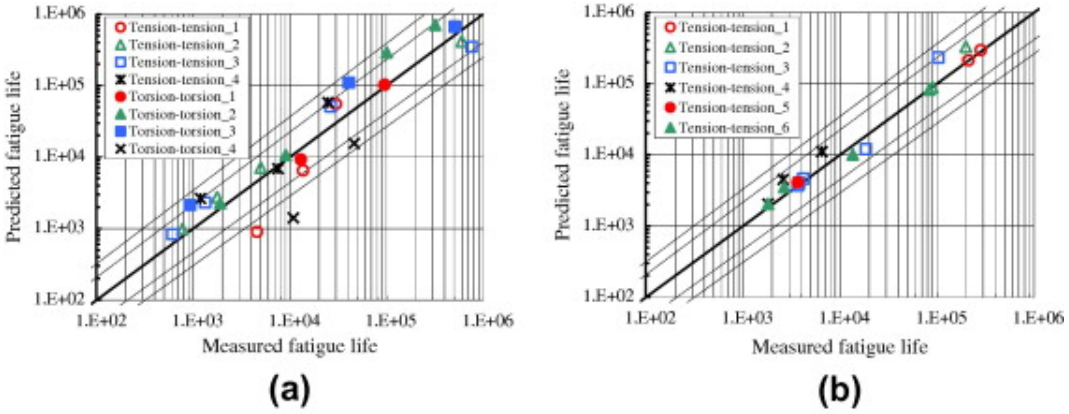

Figure 28: Comparison of predicted life vs measured fatigue life using Palgrem-Miner linear accumulation damage. **a** and **b** refer to different experimental setups.Source[6]

Modified Palgrem-Miner

In order to tackle the non-linear nature of damage in rubber components, [5] has proposed a non-linear parameter to the classical Palgrem-Miner relation in the form of:

$$D = \sum_{i=1}^{n} D_i = \sum_{i=1}^{n} \left(\frac{N_i}{N_f} \right)^{\beta} \tag{30}$$

With the proper choice of the β fatigue parameter is possible to get a better agreement between the predicted and measured fatigue life. Weak point of this technique is the need to determine a further empirical parameter in order to make life prediction. As a matter of fact the β parameter has so far no physically understood meaning.

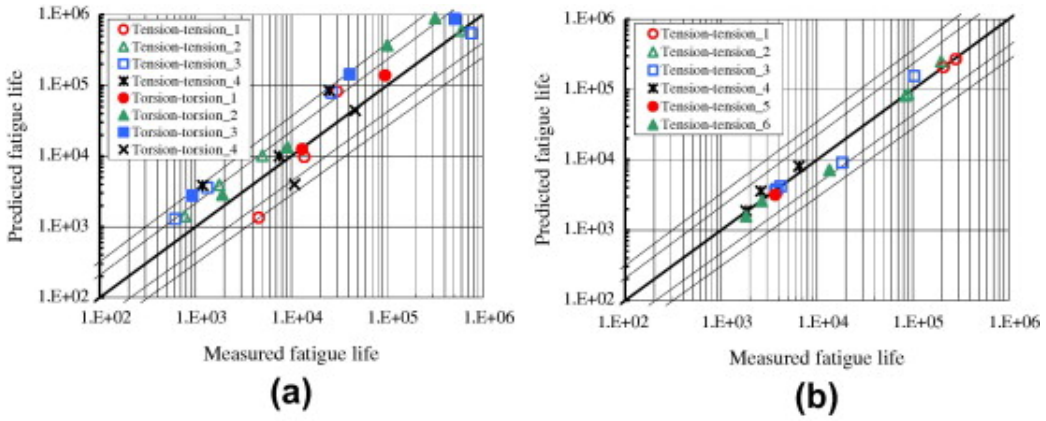

Figure 29: Comparison of predicted life vs measured fatigue life using Palgrem-Miner modified accumulation damage. **a** and **b** refer to different experimental setups. Source[6]

7 Mean stress sensitivity

Mean stress levels affect the fatigue life of components.

Mean stress is defined as

$$R = \frac{\sigma_{min}}{\sigma_{max}} \tag{31}$$

Extreme mean stresses can be high enough to be greater then the maximal stress that the material can bear, thus leading to complete component failure. On the other opposite, also negative mean stresses can be higher than the maximum allowable compressing stress. In between this extremes lies a zone where some peculiar behaviour might appear. For most of material, compressive mean stresses increase fatigue life. Crack nucleation and propagation are related to the values of tensional stress, that lead to a de-cohesion of the material. For this reason a compressive mean stress, reduces the tensile stress at the crack tip, thus slowing down the damage process. On the other hand a positive mean stress applied on the component will raise the value of the tensile stresses also at the crack tip, thus accelerating the failure process.

Natural rubber as well as carbon filled synthetic rubber present a peculiarity property of increasing fatigue life for increasing mean stresses level. This phenomena is due to the capability of such polymers to crystallize under strain. For a detail description refer to chapter 2.6.
The relation between mean stresses and stress amplitude can be easily visualized through a Haigh Diagram.(fig:30)

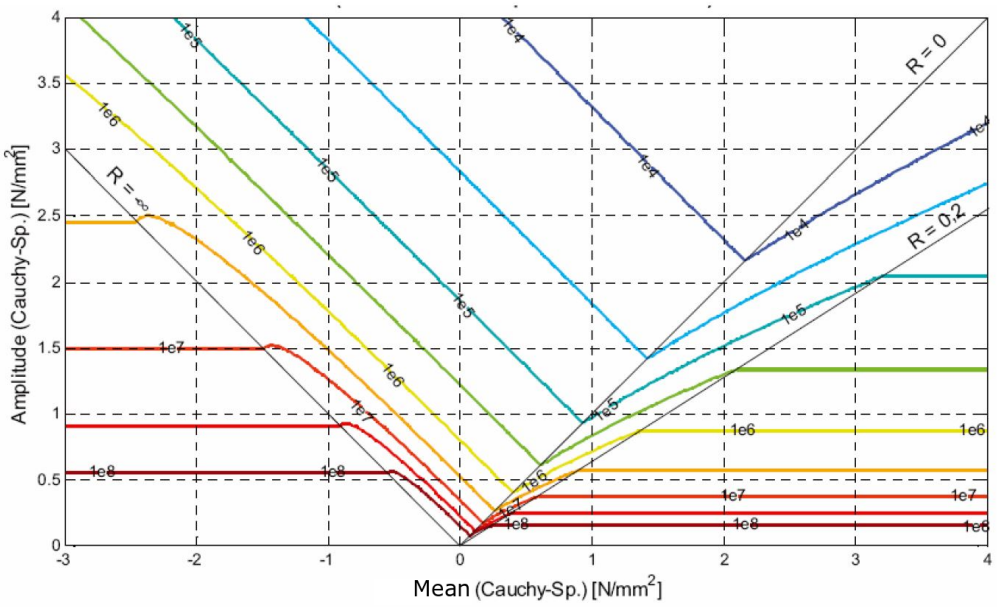

Figure 30: Haigh Diagram for Natural Rubber with Shore Hardness 60A. Source[21]

In the figure 30 is possible to observe the representation of a Scalar field, where for coordinates there are the mean stresses (Mittelwert) and Cauchy stress amplitude. The data represented are the iso life lines, representing the life for different combinations of mean stress and amplitude. The figure 31 gives a graphical representation of the data field obtained from [24].

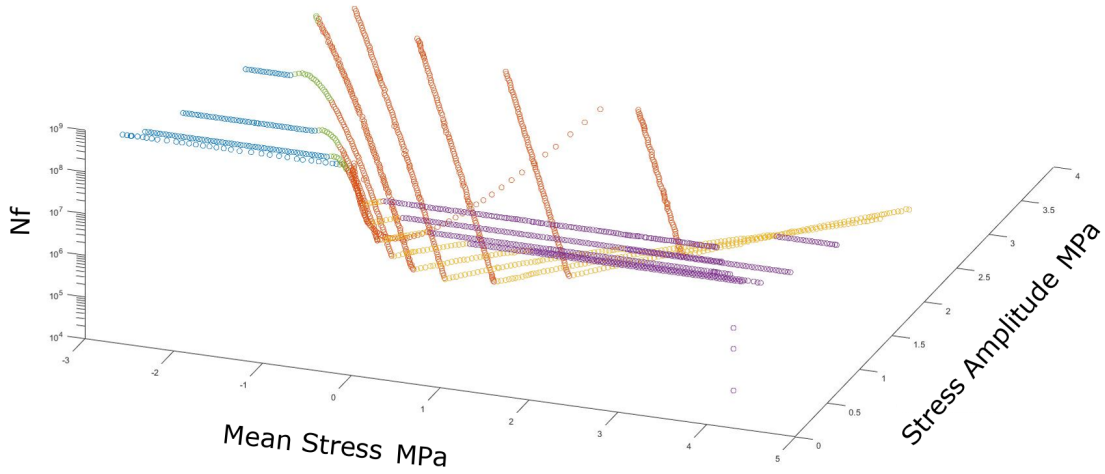

Figure 31: Data points used to determine the Haigh Diagram, view from side. The height of the point is in accordance with life value.

Following any given line from left to right is possible to be seen as with the increase of the mean stress the stress amplitude tolerable by the component decrease until reaching a value or R=0 where due to the strain crystallization process, the allowable stresses increase, to flatter out after R=0.2.

8 Critical plane method

Critical plane methods have been developed on the observation that crack growth develops along preferential directions. Depending on the material is possible to use an indicator of the location and direction of the crack preferred developing plane. In particular for rubber materials it has been observed that cracks are growing perpendicularly to the maximum Cauchy stress[13].

Critical planes method based on strain definition have also been proposed, but they lack the ability to predict failure direction [13]. The idea behind is that during a cycle the stress levels vary in different direction, but only the direction of the maximum stress is designed to receive a damage.

This method calculates the stresses over a certain amount of direction, selects the most stresses direction and calculates the damage for the specific direction.(fig:32) The damage data is stored and when the element plane should be subjected to a subsequent damaging stress, the damage will be summed to the value of the existing one.

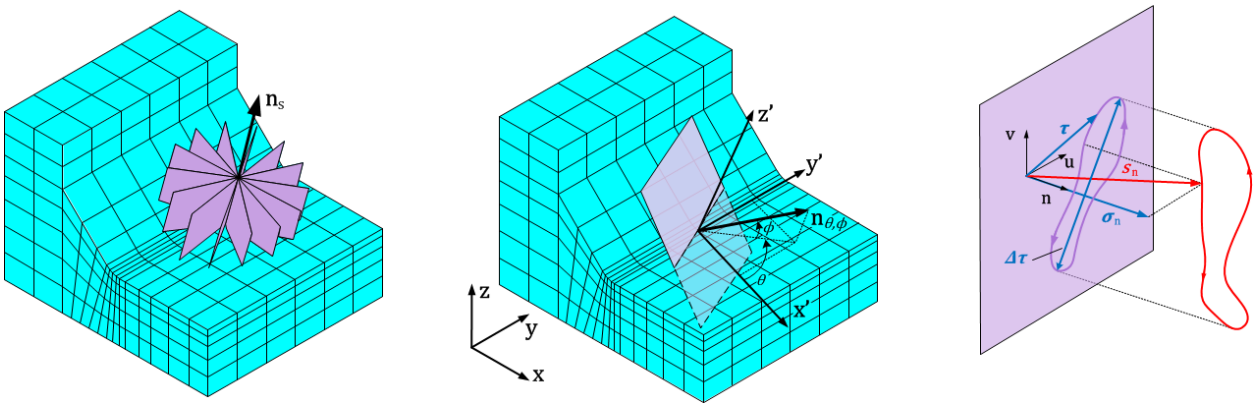

Figure 32: Critical plane method. In the fist image is possible to see the plane directions and the normal axe of the plane sheaf. Second picture shows the parameters defining plane directions and components. Picture to the right shows how a stress tensor has different components along a path into space. Source [27]

In a Formal way [7], let's consider a stress variable T, and a generic plane Δ described as normal to a versor $\mathbf{n}$. This versor can be described in the cartesian coordinate system with two angles ϕ *and* θ.
Projecting the stress tensor with the versor leads to:

$$\mathbf{T} = \boldsymbol{\sigma} \cdot \mathbf{n}$$

Modules and coordinate of the normal stress tensor $\mathbf{N}$ is obtained by projecting $\mathbf{T}$ in the $\mathbf{n}$ direction as follows:

$$N = \mathbf{n} \cdot \mathbf{T} = \mathbf{n} \cdot \boldsymbol{\sigma} \cdot \mathbf{n}$$
$$\mathbf{N} = (\mathbf{n} \cdot \mathbf{T}) \cdot \mathbf{n}$$

Amplitude and mean value for normal stress referred to a generic plane follows the dependence

$$N_a = \frac{1}{2}\left(max(\mathbf{n} \cdot \sigma \cdot \mathbf{n}) - min(\mathbf{n} \cdot \sigma \cdot \mathbf{n})\right)$$
$$N_m = \frac{1}{2}\left(max(\mathbf{n} \cdot \sigma \cdot \mathbf{n}) + min(\mathbf{n} \cdot \sigma \cdot \mathbf{n})\right)$$

In the procedure the following calculations are done: Firstly a rotation matrix is established, describing the direction cosines for referred to the material coordinate system. This matrix is identified as A.

$$A = \begin{bmatrix}\mathbf{n} & \mathbf{u} & \mathbf{v}\end{bmatrix} = \begin{bmatrix} a_{11} & a_{12} & a_{13} \\ a_{21} & a_{22} & a_{23} \\ a_{31} & a_{32} & a_{33} \end{bmatrix}$$

Normal stress σ_n for the search plane can be determined from the generic stress tensor and the rotation matrix (eq. 8)

$$\sigma_n = \sigma_x a_{11}^2 + \sigma_y a_{12}^2 + \sigma_z a_{13}^2 + 2(\tau_{xy} a_{11} a_{12} + \tau_{xz} a_{11} a_{13} + \tau_{yz} a_{13} a_{12})$$

Cycle counting technique are used for the variable amplitude loading to resolve the amplitude of the stress.

Shear component for the search plane are defined through:

$$\begin{aligned}\tau_u = {} & \sigma_x a_{11} a_{21} + \sigma_y a_{11} a_{22} + \sigma_z a_{13} a_{23} + \tau_{xy}(a_{11} a_{22} + a_{12} a_{21}) + \tau_{yz}(a_{12} a_{23} + a_{13} a_{22}) + \\ & + \ \tau_{zx}(a_{13} a_{31} + a_{11} a_{33}) \\ \tau_v = {} & \sigma_x a_{11} a_{21} + \sigma_y a_{11} a_{22} + \sigma_z a_{13} a_{23} + \tau_{xy}(a_{11} a_{22} + a_{12} a_{21}) + \tau_{yz}(a_{12} a_{23} + a_{13} a_{22}) + \\ & + \ \tau_{zx}(a_{13} a_{31} + a_{11} a_{33})\end{aligned}$$

In this work the number of planes considered was set to 36 in order to limit the calculation time. Moreover the crack initiate mostly on the surface, so the plane method will only search over a sheaf of planes proper to the outbound normal of an element.

A problem that arises derive from the convectional number of planes taken into consideration. As a matter of fact the stress is projected to the closest accumulation plane. If the

stress is not laying on the same plane as the nearest plane, the stress will be projected on it and thus it will be smaller then the original. The natural way of tackling such problem would be to have a very high number of search planes, but the calculation time increases linearly with the amount of planes.

9 Cycle counting

Load signals (fig:33) refers to measure of quantity such as displacements, forces, elongations,etc. that might affect a specimen. They must be recorded and then associated with some technique to the fatigue life of the component.

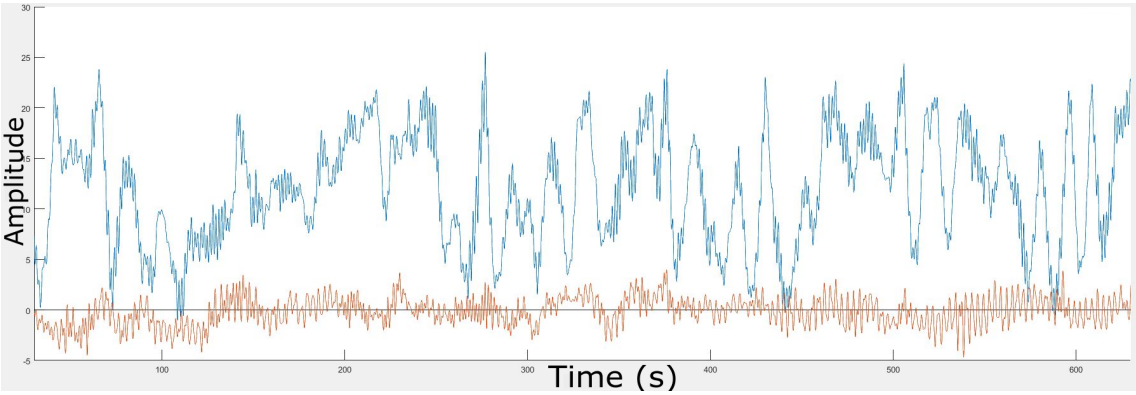

Figure 33: Example of a Load signal

For components working under specific conditions, it is possible to extrapolate a 'characteristic' load history. Once this is defined, it is possible to simulate it on the component and to estimate the damage associated. Following a linear damage accumulation model, it is then possible to understand the life fraction that this specific cycles series will cause, and to get a estimation on the whole fatigue life. One example might derive from the use of a typical signal for a train carriage travelling every day between two cities. As a matter of fact it is expected that the load signal affecting the train components, given same track average speed, will be very similar day by day.

Once a signal is analysed, the information about the solicitation amplitude and mean are stored in a more convenient way. With only the loss of the load sequence information it is possible to make a further simplification hypothesis in order to decrease computational time. This hypothesis consist in the quantization of the signal values. In this way it is possible to run a finite quantity of simulation process, and to gather the associated stress states.(fig:34) As a matter of fact signal amplitudes close one each other will create similar stress states into the specimen. By averaging the signal over a limited amount of levels, amplitude data higher than the average will be compensated by the ones that are lower. In fact for small amplitude variations it is possible to consider the stress increments as linear with the load increase. For short signal loads problems might arise from phenomena called sequence effect (fig:36). This phenomena consist in the occurrence of different fatigue life for a signal whose components are applied in different orders. On long signals this phenomenon can be ignored.

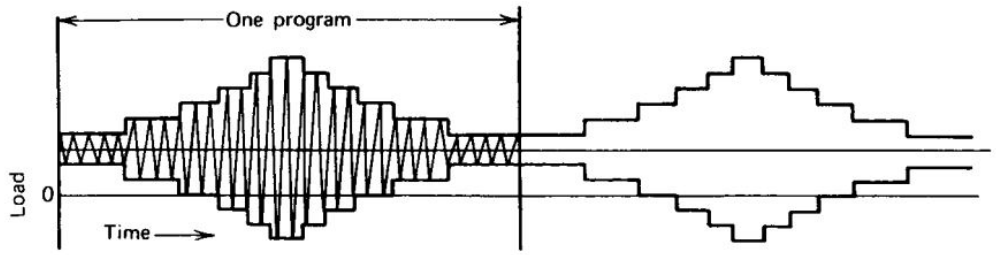

Figure 34: Example of signal block that can be repeated through time. Source [29]

In order to have a signal that would resemble the properties of the measured one, it is also possible to randomly rearrange the sequence of the transformed signals' blocks.(fig:35) This is a useful procedure when testing procedure must be done on some physical component. In fact this procedure will inhibit if not eliminate life estimation discrepancies due to load sequence effect.[29]

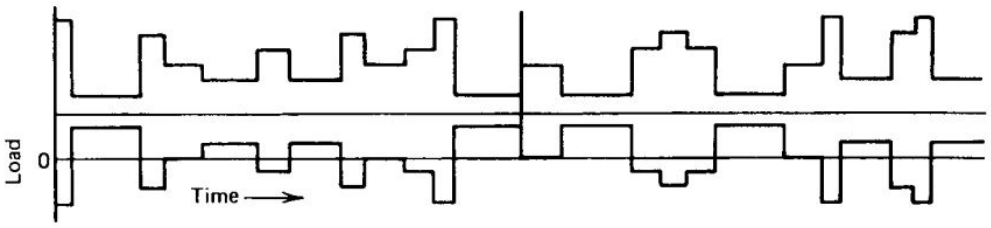

Figure 35: Example of signal block with random block sequence. Source [29]

It has been observed in the years that different load sequence produces different life outcomes[29]. Sequence effect exist both at early fatigue stages (micro-craking) and in later stages (crack propagation). Many service histories on the other hand present are such that sequence effects elide one each other. This phenomena is seen especially for long multi-axial fatigue loads where the load signal is not constantly repeating. [29]

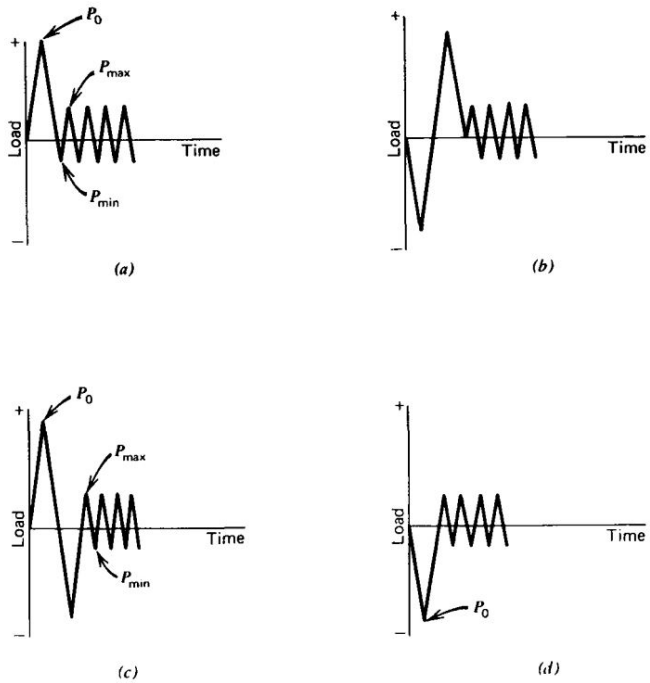

Figure 36: Examples of different sequences of the same load. Depending on the material properties they might influence the fatigue life of the component . Source [29]

9.1 Cycle counting techniques

Signal analysis techniques aim at condensing the information from a signal in a form useful to the fatigue calculation. Many different techniques have been implemented throughout the history of fatigue analysis, nevertheless the most important ones are the ones able to represent mean load and load amplitude, since this two parameters are of great importance in determining fatigue life.

9.1.1 Rainflow counting

This is one of the most diffused and implemented cycle counting method, which results are the same as for the reservoir method. With the load time plotted such that the time is the vertical axis, simulating rain pouring down a pagoda's roof, the lines go horizontally from a reversal to a succeeding range. Peaks and valley of the signal represent the roof of the pagoda. The calculation method consists of the following steps as described by [29] and depicted in figure 37 and 38.

1. The history must be rearranged in order to start either with the highest peak or the lowest valley

2. Starting from the highest peak go down until the reversal. The rain-flow process continue unless either the magnitude of the following peak is equal or larger than the peak from which is initiated or a previous rain-flow is encountered.

3. Repeat the same procedure for the next reversal and continue these steps to the end

4. Repeat the procedure for all the ranges and parts of a range that were not used in previous steps.

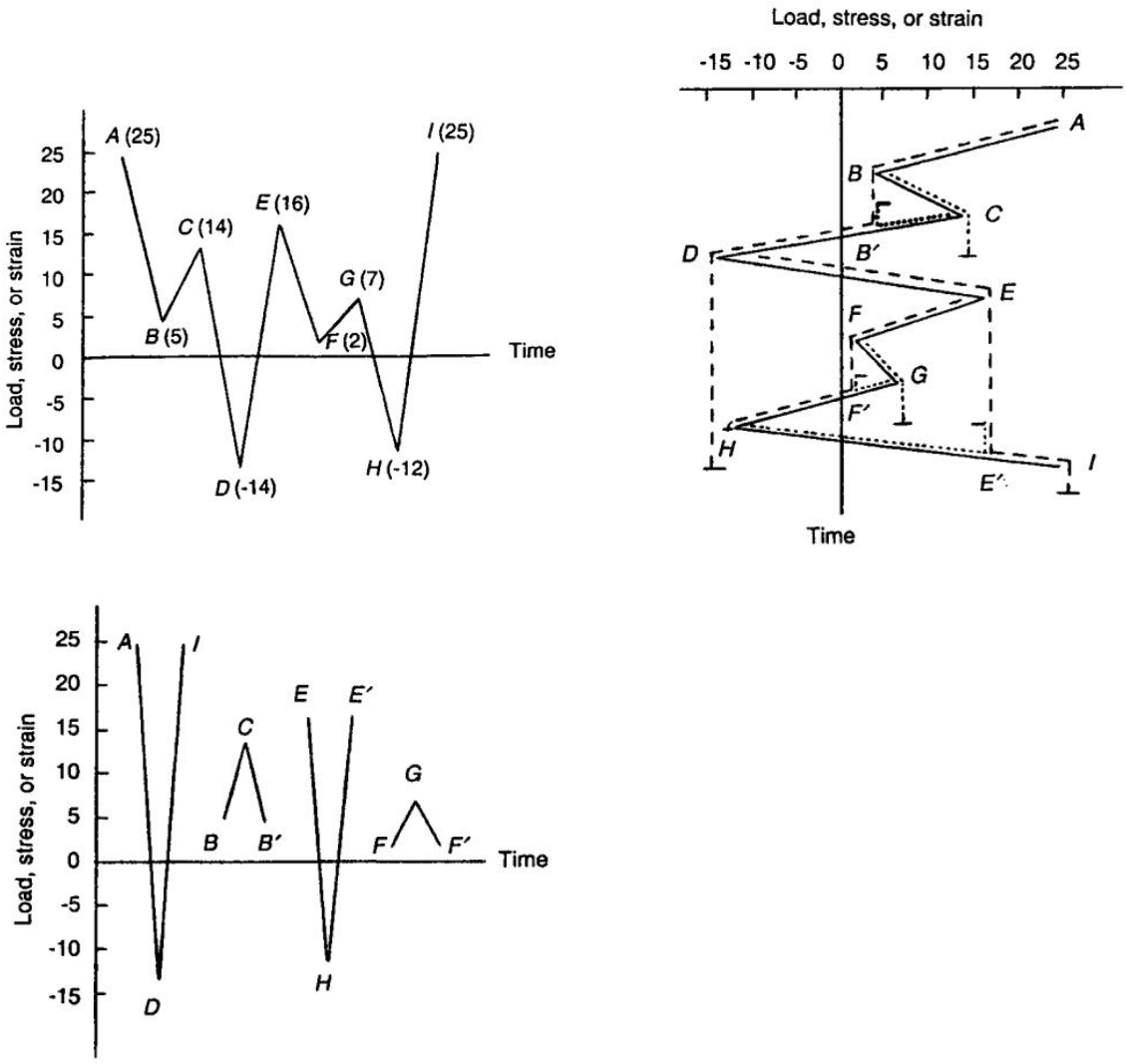

Figure 37: Left Top: load stress signal. Right Top: rainflow counting illustration. Left Bottom: Resulting count. Source [29]

Cycle	Maximum	Minimum	Range	Mean
A–D–I	25	−14	39	5.5
B–C–B′	14	5	9	9.5
E–H–E′	16	−12	28	2
F–G–F′	7	2	5	4.5

Figure 38: Result of the previous Rain-Flow counting .Source [29]

9.1.2 Markov-Matrix

A graphical way to represent signals after rainflow counting is represented by Markov Matrix (fig: 39). The plot consist in a vectorial field where the height of the columns is proportionate to the number of occurrence of a certain cycle. On the axis there are mean and amplitude of the signal.

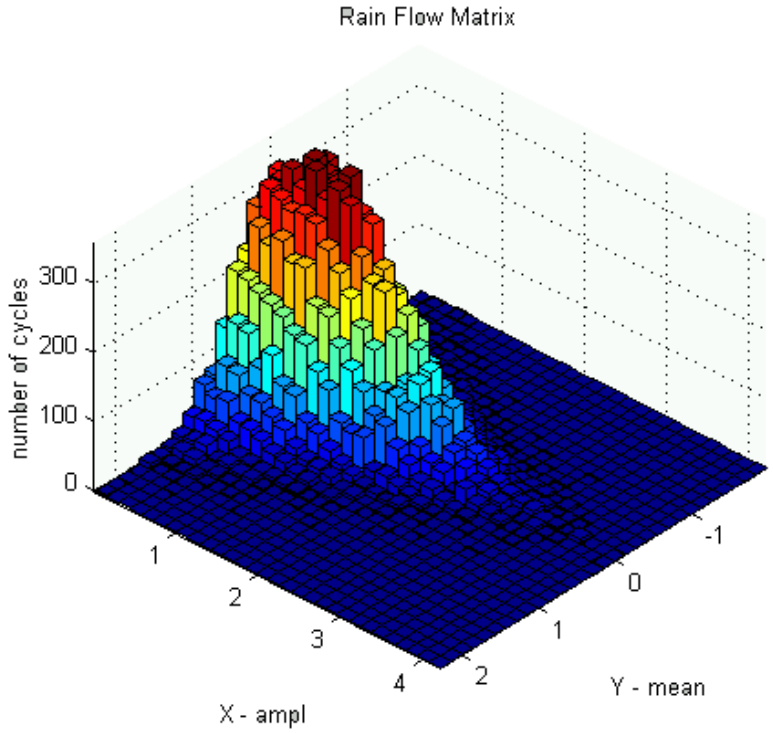

Figure 39: Result of the previous Rain-Flow counting .Source [29]

9.1.3 Range Pair Method or Reservoir counting

This method consist in the initial count of cycles containing small ranges. Their reversal points are then removed from the original signal.(40) The counting procedure produces the same data as the rainflow method, and is one of the most used counting method adopted today.

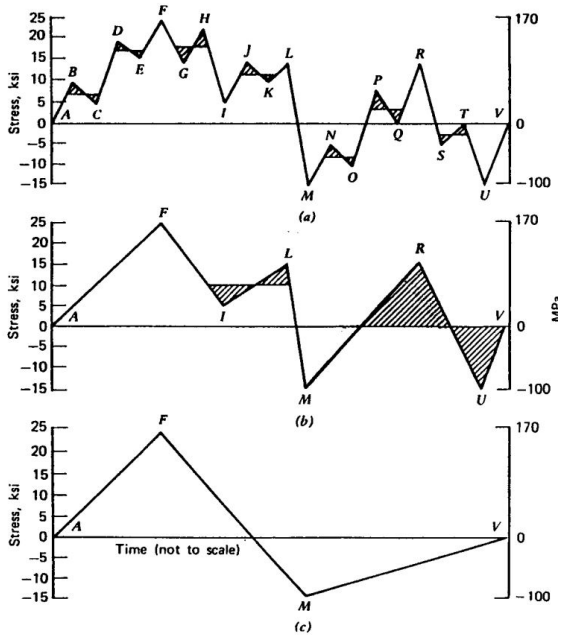

Figure 40: Range pair counting. In step (a) the smaller cycles are counted and eliminated from the signal. Increasing with cycle size as in (b). In (c) there is the last cycle left by the method.Source [29]

9.2 Level Crossing

Level crossing consist in the counting on how many times a certain signal crosses some pre-defined levels. After the counting is performed, an equivalent signal can be created. This starts with the creation of the most fatigue-damaging cycles when the largest possible cycle is obtained form the recorder list. This is followed by the second largest possible.(fig: 41) This process is iterated until all the values of the count have been used. This method cannot be used when load sequence effect has to be taken into consideration.

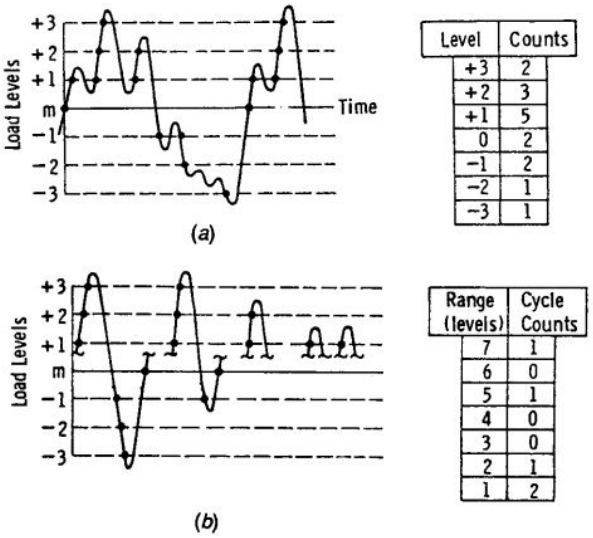

Figure 41: Level Crossing Method.Source [29]

9.3 Peak Counting Method

This method consist in simply counting the number of occurrence of peaks present in a given load history. The equivalent signal is then recreated starting from the biggest amplitude achievable, continuing to move to the smaller values until no more peaks are available.(fig: 42)As for the Level crossing method, load sequence effect is lost in the signal transformation.

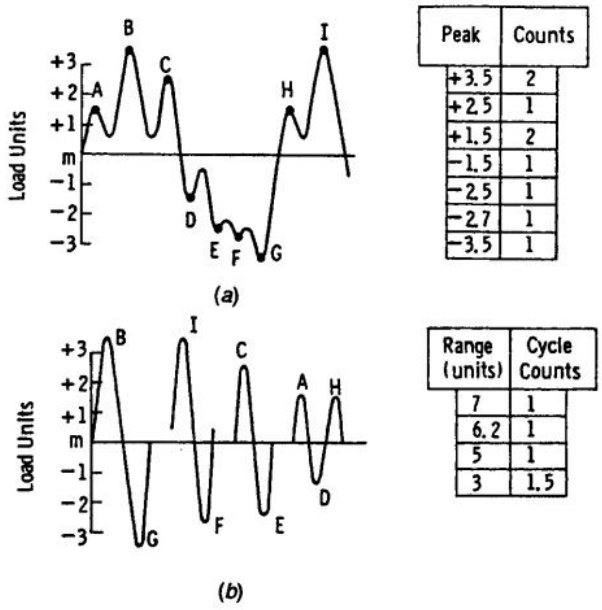

Figure 42: peak counting method. Source [29]

9.3.1 Signal Filtering

In order to decrease the amount of data present in a signal without affecting too much the quality of the information carried by it, it is possible to filter away some low influencing components. As a matter of fact since the fatigue is dependent to a fatigue indicator by a power law, the effect of a signal component is exponentially depended from its magnitude. For this reason signals whose amplitude components are below certain level will only minimally influence fatigue life. (fig: 43)
Racetrack (or race track) method are based on the filtering of all the cycles whose amplitude is lower then a certain threshold. The reference amplitude is represented by the highest amplitude inside the signal.

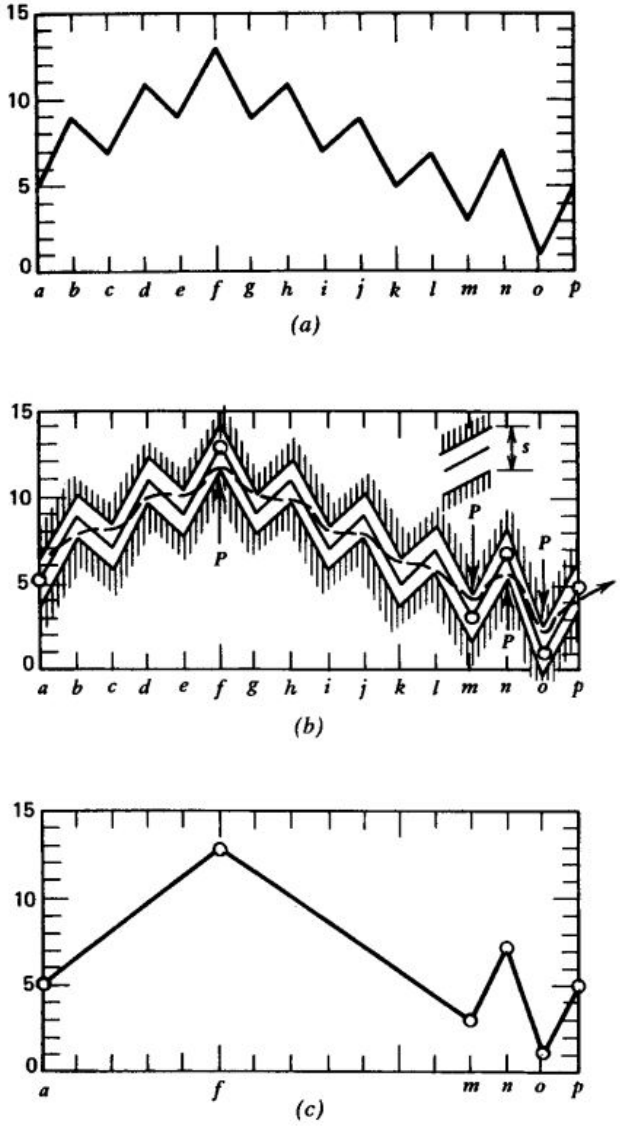

Figure 43: Racetrack filtering. This technique allows smoothing of the signal in order to exclude small amplitude cycles, whose effect is negligible. Source [29]

In fig: 44 is brought an example of a filtering that has been performed on a signal used on some components.

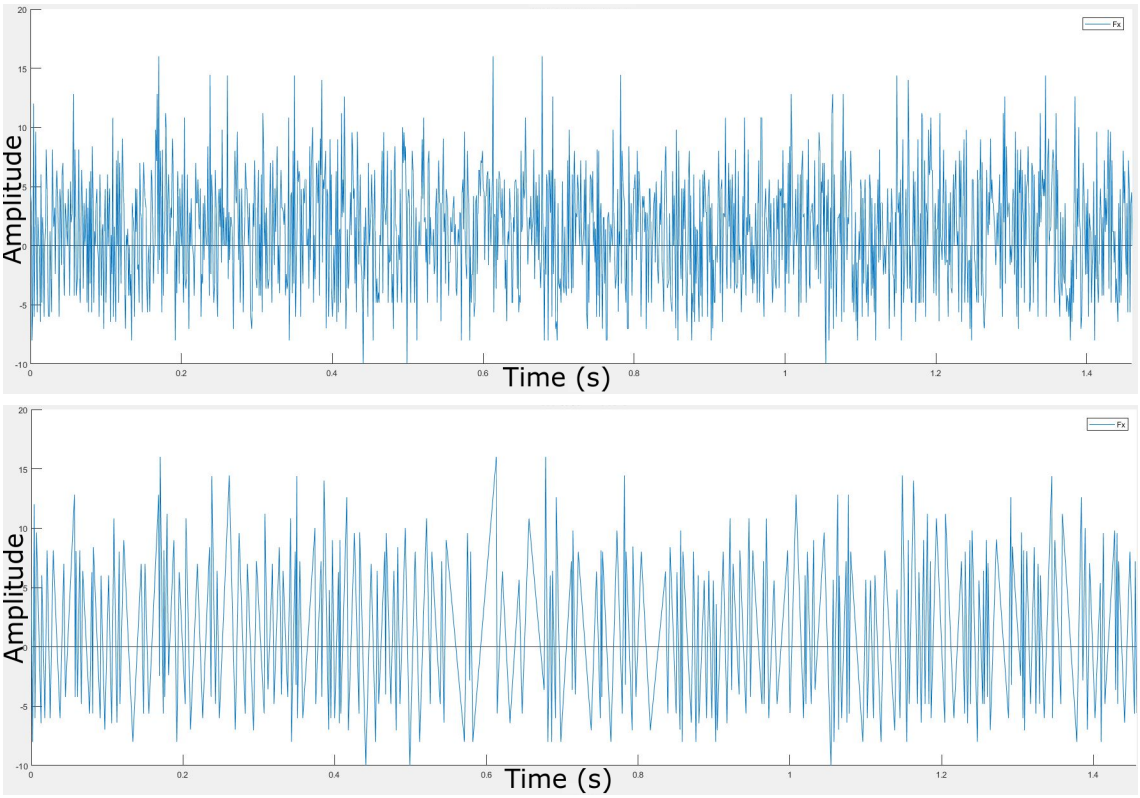

Figure 44: Original signal and signal filtered with a 40% racetrack filter. It is possible to see how in the filtered signal all the small cycle components have been eliminated.

10 Work procedure description

The fatigue procedure used in this work has been created with the help of existing literature and methods.[27]. The further formulation is done in order to create a suitable method for analysing rubber components. Having the original procedure being written for Metallic material, a series of radical changes have been applied.

10.1 Cauchy rotated in reference configuration

Due to the very nature of the Hyperelastic material models, the stresses and strains referred to the *Reference* and the *Material* system differs greatly. Cauchy stresses, some of the most reliable and used fatigue predictor (5.2), refer to the deformed configuration. For this reason it is not intuitive to understand the correct location of failure and crack orientation in the un-deformed configuration. (fig:45)

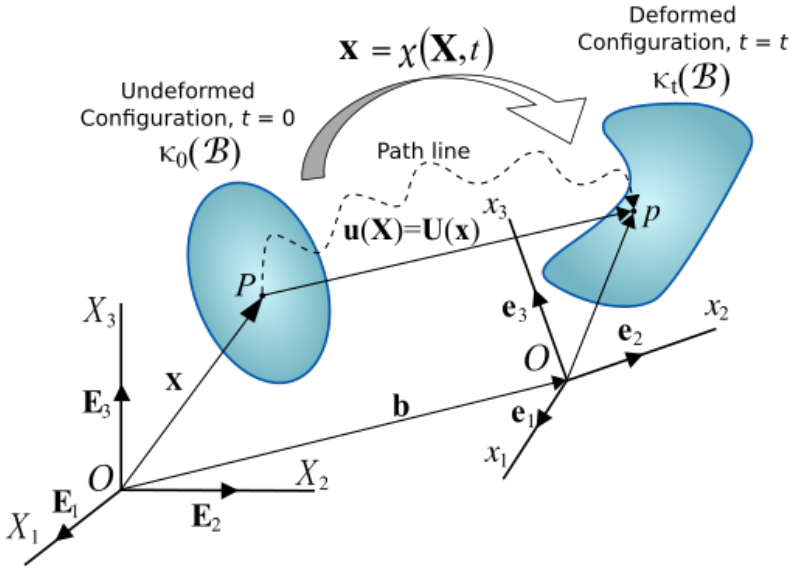

Figure 45: Deformation process of a body. The un-deformed configuration (*Reference* or *Material*)is represented with Capital letters. The deformed configuration (*Spatial* or *Current*) is represented by small letters. Source [39]

For this reason a rotation of the Cauchy stresses has been performed using the rotation tensor derived from the polar decomposition of the *Deformation Gradient*. Such approach has also been performed by [40][5][33]. This procedure is derived starting from the definition of the Cauchy stress through the deformation gradient

$$\mathbf{S} = \frac{1}{J} \cdot \mathbf{F}\ \mathbf{S}\mathbf{F}^T = \sum_{\alpha=1}^{3} \sigma_{\alpha\alpha} \cdot \mathbf{n}_\alpha \mathbf{n}_\alpha^T \tag{32}$$

Where n_α represent any direction in the space considered and $\sigma_{\alpha\alpha}$ are the normal stress components in the n_{th} direction.Written in vectorial notation,

$$\sigma_{\alpha\alpha} = \mathbf{n}_\alpha^T \cdot \boldsymbol{\sigma} \cdot \mathbf{n}_\alpha \tag{33}$$

The following derivation aims at finding suitable definition of n_α.

$$N_\alpha = \frac{\mathbf{F}\mathbf{n}_\alpha}{|\mathbf{F}\mathbf{n}_\alpha|} \tag{34}$$

Starting from this relation:

$$\mathbf{F}\mathbf{N}_\alpha = \lambda\ \mathbf{N}_\alpha \tag{35}$$

where $\lambda_\alpha = |\mathbf{F}\ \mathbf{n}_\alpha|$ are the stretches in the α direction.

$$\mathbf{R}\mathbf{U}\mathbf{N}_\alpha = \lambda_\alpha \mathbf{N}_\alpha \tag{36}$$

where $\mathbf{R}$ is the rotational component derived from the polar decomposition of the deformation tensor.$\mathbf{U}$ is on the other hand the *deviatoric* component derived from the polar decomposition of the deformation tensor. This tensor in three dimensional space is represented with a diagonal matrix, which elements will be constitute by the values of stretches along the direction of the material system. Since these values coincide with the λ s of the left side of eq 36, it is possible to rewrite eq 36 as follows:

$$\boldsymbol{R}\ \mathbf{U} N_\alpha = \lambda_\alpha\ N_\alpha \tag{37}$$

Inserting the definition for the normal vector of eq 37 in the equation 35, the Cauchy stresses referred to the reference configuration can be written as

$$\sigma_{\alpha\alpha} = (\mathbf{R}\mathbf{n}_\alpha)^T\, \sigma\, (\mathbf{R}\mathbf{n}_\alpha) \tag{38}$$

Calculating the transpose of the first left term, the previous expression becomes

$$\boldsymbol{\sigma}_{\alpha\alpha} = \mathbf{n}_\alpha^T\ \mathbf{R}^T\ \boldsymbol{\sigma}\ \mathbf{R}\ \mathbf{n}_\alpha \tag{39}$$

Where

$$\mathbf{R}^T\ \boldsymbol{\sigma}\ \mathbf{R}\ = \boldsymbol{\sigma}_{corotated}$$

This results shows that for getting the Cauchy stresses expressed in the reference configuration, it is necessary to rotate the stress tensor with the appropriate rotational matrix. Following this procedure is possible to obtain fatigue life calculation equal to the one using the Cauchy stresses, with the advantage of being able to identify crack direction referred to the undeformed configuration.

10.2 Haigh diagram creation

In order to create a procedure able to cope with data coming from different experiments (fig:47,31), a procedure has been developed that takes as parameter the data coming from experiments and uses them to modify the stresses following this order.

10.2.1 Haigh diagram using interpolating polynomial surface

An option to create a Haigh diagram is to use a polynomial interpolant surface in order to approximate the Haigh function. This has been performed as shown in fig 46.

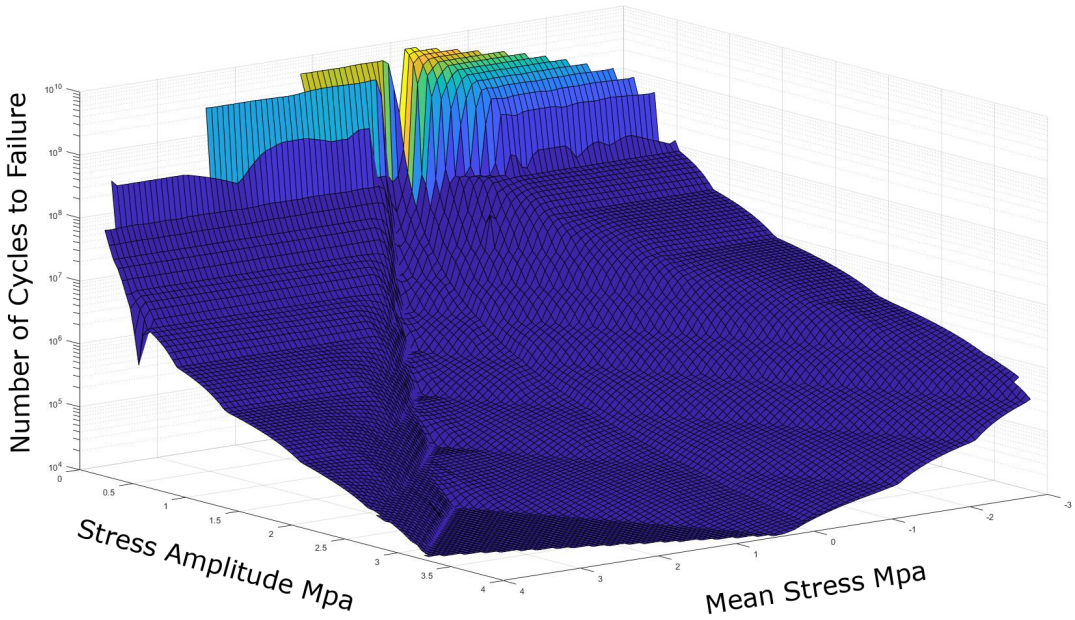

Figure 46: Interpolation made using a surface interpolation. In order to achieve a sufficient surface smoothness a very high number of data points are needed. Most of the times it is unlikely to dispose of such data quantity.

The option of using a linear surface interpolation as seen in fig:46 has been deemed not feasible since for reaching a smooth surface, the number of points required is too high. The use of just some dozen points for the creation of this surface will in fact result in peaks and irregularities that do not well represent the physical behaviour of the rubber.

10.2.2 Haigh diagram using interpolating planes

In order to represent an Haigh Diagram based on a smaller number of points, the following procedure has been implemented using plane approximants:

1. The data file containing triplets with mean stresses, stress amplitude and corresponding fatigue life are given as input-parameter. The life associated to a point in the map is transformed using a logarithm.(fig:47) This is done in order to be able to fit planes on the data given. As a matter of fact, since life data are well described by a logaritmic law, by changing the domain of the life to a logaritmic one, is possible to use a linear relation between amplitude and mean stress and fatigue life.

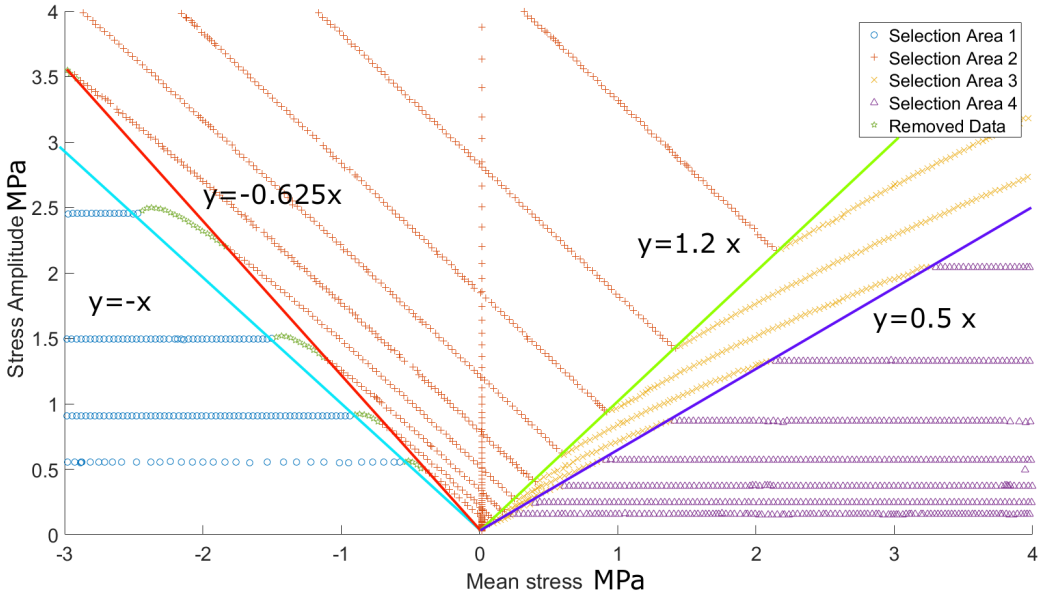

Figure 47: Data points used to determine the Haigh Diagram.Top view. Different points colour refers to different interpolation section. X axis contains the mean stress, y axis the amplitude stress.

2. The Haigh diagram area is divided in 5 sections as seen in fig:47. The dividing lines used to define five different areas are set to be lines passing by (0,0) and using the following angular coefficients: -0.625, -1, 1.2 , 0.5. These cohefficient are used for a Rubber of Shore Hardness 60. Depending from the material properties, other dividing lines can be used.The zones are defined using the following selection criteria:

   - Selection area n1: This refers to a zone where the fatigue life is not affected by the mean stress. Although this description does not correspond to the real one, no material data are available for the zone, so it is safer to assume no mean stress influence.

$$\left\{ amplitude + mean \leq 0 \right. \tag{40}$$

- Selection area n2: This zone is defined as

$$\begin{cases} amplitude - |mean| \geq 0 \\ amplitude + 1.2 * mean \geq 0 \end{cases}$$

- Selection area n3: This zone is defined as

$$\begin{cases} amplitude - mean \leq 0 \\ amplitude - 0.625 * mean \geq 0 \end{cases}$$

- Selection area n4: Also this refers to a zone where the fatigue life is not affected by the mean stress. Although this description does not correspond to the real one, no material data are available for the zone, so it is safer to assume no mean stress influence.

$$\begin{cases} amplitude - 0.625 * mean \geq 0 \end{cases}$$

- Selection area n5: This zone is removed from the data set. As a matter of fact the data here are due to previous interpolation processes made by [24] and do not correspond to reality. Specifically the data in this zone would suggest an decrease of fatigue life with a decrease of mean value for compressive stressees, and this is not observed in reality.

$$\begin{cases} amplitude + mean \leq 0 \end{cases}$$

3. After the data is selected by belonging region, a plane fitting procedure is performed. This procedure consist in fitting four different planes using the existing data.(with the possibility of customizing the number of planes in case different fatigue behaviours would request it). Specifically there are two zones where the fatigue life does not depend any more from the value of the mean stress (between R=-∞ going counter-clockwise and from R=0 going clockwise).The real behaviour of the rubber in these zones might also differ from the representation used in this work, but no test data are for such amplitude-mean stress conditions.

   The choice of using simple plane for interpolating the logarithmic life has been preferred over higher order interpolation in order to avoid un-physical behaviour at the connecting zones (R=-∞). As a matter of fact, observing the Haigh diagram obtained by [21], it is possible to see an abrupt change in the derivative of the lines associated with the iso-life lines, that would suggest a decrease of life for values of R approaching value of - ∞. This phenomena is not known to happen.

   On the other hand the use of plane approximation allow to a very time and computational resource efficient calculation, and the error associated with the approximation has been evaluated as comparable to the one deriving from the use of higher order approximation.

The planes on the zones 1 and 4 are created on the outbound values of the planes describing the inner sections. In this way it is possible to have a better continuity of the interpolating surface. (fig:48)

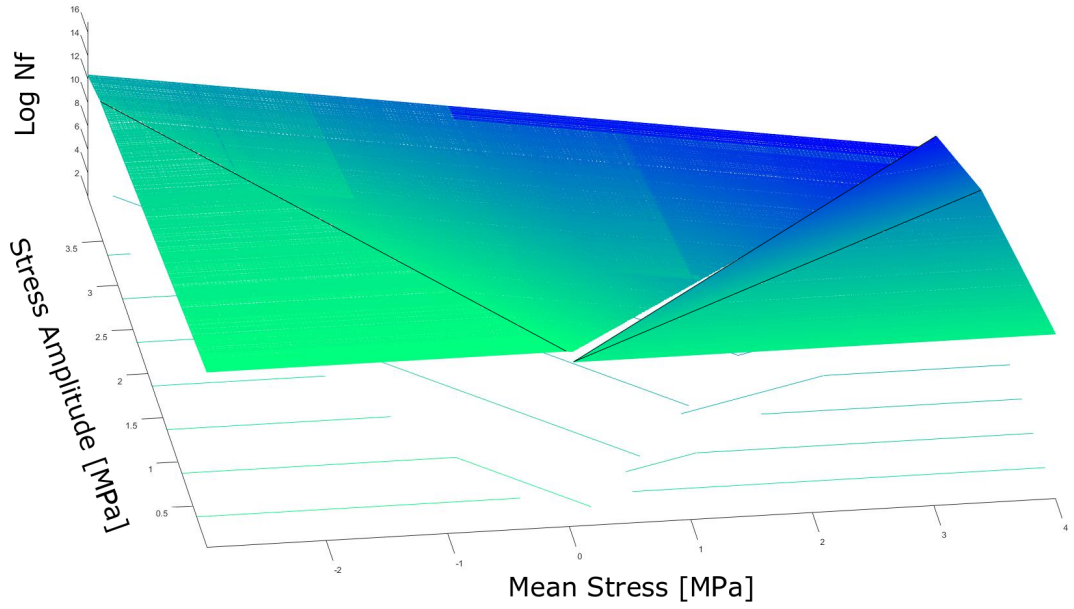

Figure 48: Representation of the interpolation planes.

Manual corrections

In order to reduce discontinuity between the two central fitting planes, is possible to manually intervene on the steepness and elevation of the singular planes. The external plane on the other hand develop from the boundary values of the central ones, thus not creating any hole in the surface.(fig:49)

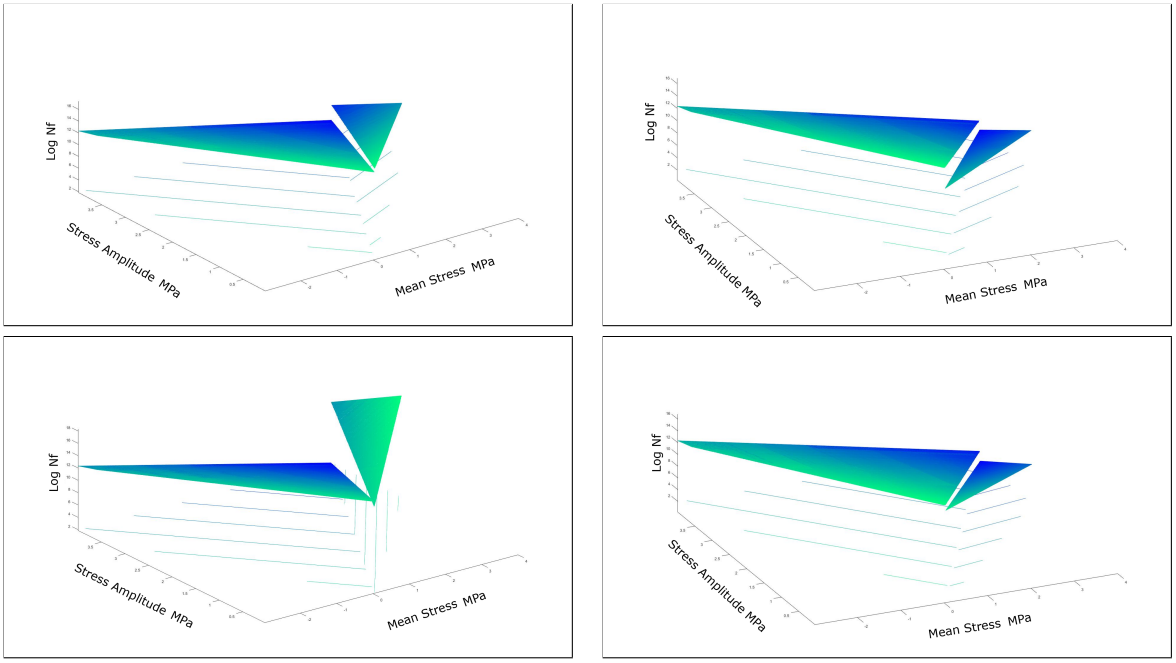

Figure 49: In in this image is shown how the parameters can be changed to manually modify slope and height of interpolating surfaces

10.3 Mean stress sensitivity Correction

After the Haigh diagram has been created, the following procedure is used in order to create an equivalent stress value for a fully reversed cycle.

- The stress signal contains mean stress and amplitude, is given as input to the procedure. For every coordinates couple, the maximum life is calculated.
- The values of the Wöhler curve for fully reversed loading (R=-1) is extrapolated from the existing data.
- The value of the life associated with a point on the map, is used to find the equivalent stress that would allow the same life for a fully reversed cycle
- The data with the equivalent allowable stresses is given as an input

10.4 Haigh Diagram Testing

Since no data were avaiable on the statistical aspects of the haigh diagram from [24], it has been assumed that the data refers to a 50% probability failure. Different assumptions would lead to different Haigh data.
The effectiveness of this method and its correct implementation has been tested against a custom made signal containing means and amplitude stresses, and the results (table 6)have been compared to the Haigh diagram of figure 30.

Original Amplitude	Mean	Equivalent amplitude
1.0	1.0	1.70
1.0	2.0	1.47
1.0	-2.0	0.41
1.7	0.0	1.69
1.7	-2.0	0.70
1.7	-3.0	0.70
2.0	1.7	3.19
2.0	2.5	3.07
2.0	2.4	3.13

Table 1: Signal processing through Haigh Diagram for accounting of mean stress sensitivity

10.5 Multiaxial Load Signals

The aim of this work is to develop an analysis procedure able to predict fatigue life of working parts. Many fatigue work focused on mono-axially loaded components. Such configuration allow for ease of testing and part simulation but is somehow not representative of real world components. As a matter of fact component that are subjected to loads during working conditions are usually subjected to multi-axial loading. This loading configuration will induce multi-axial stress states inside the material, even thouhg for complex geometries multi-axial stress states might arise also from mono-axial loading.

In order to analyze more than one signal at the time, it is important to get the signals value at every turning point of each signal. Such process is exemplified in the following image 50, where some sinusoidal loads are subjected to an extremization process and then to a rain-flow counting. The extremization process clears the signal from any point that is not useful for the definition of a cycle. If in a time series a point is located on a straight line connecting two subsequent peaks, it does not define any cycle, thus it will be eliminated. On the other hand the simple elimination of such points might lead to the omission of signal components in conjunction with a stress state deriving from a peak into another signal. Since it is important to consider the components of all the signals for a given peak event, all the values of the other signal components will be taken as well for that specific time-location.

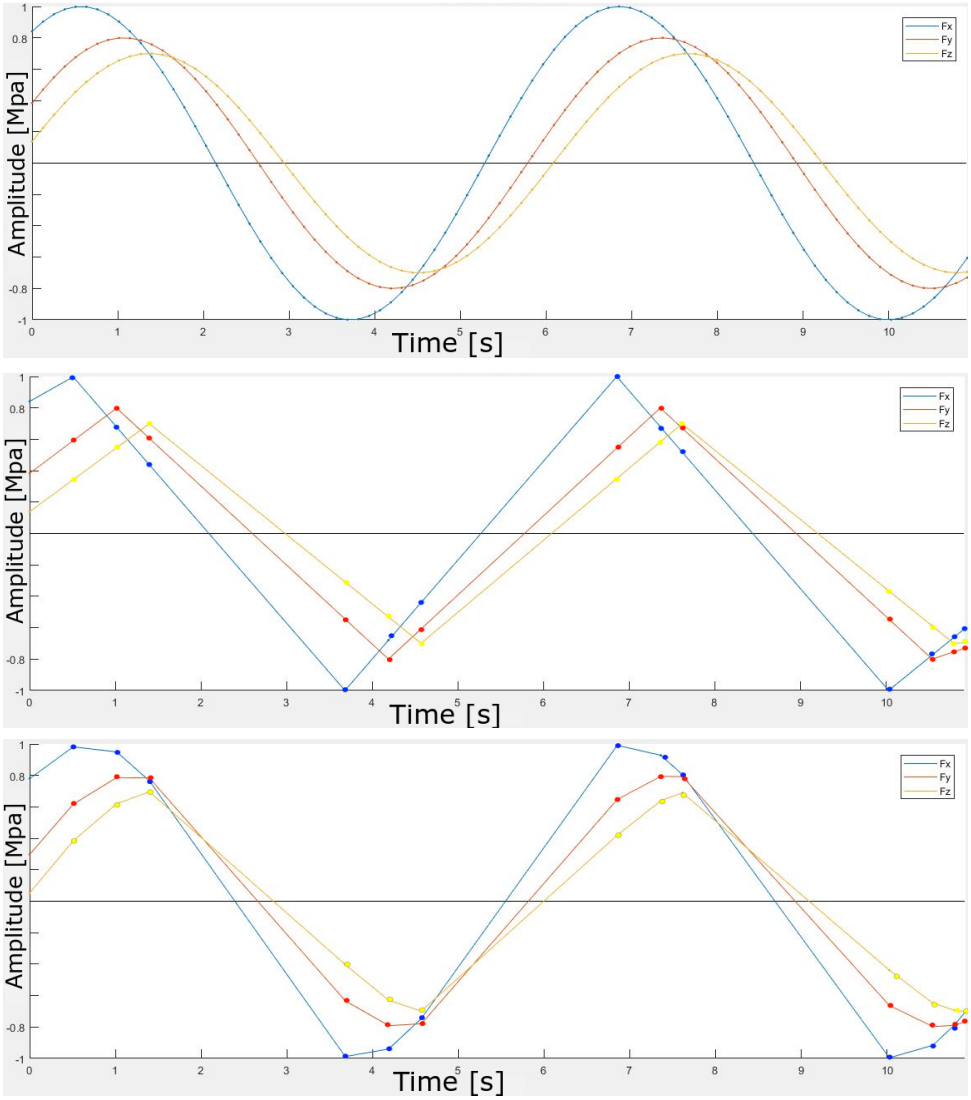

Figure 50: Original signal and signal after extremization process has taken place. The data point are indicated with small circle. Please note the presence of data at the same time instant on all the signal when a peak or valley event happen in any of them.

If the input signal is not represented by a triangular signal, (like the sinusoidal in fig:50) a method has to be used in parallel with the extremization process in order to take into account the real value of the components of the signal at a certain time. As a matter of fact the signal extremized in fig:50, second image, shows how the pure extremization process has some issued in determining the signal values for the corresponding peak. As a matter of fact the extremization process involves a linearization of the signals into a triangular signal. In order to avoid such dicrepancies between extremized and original signal, a method has been deployed that collects the true value state of all the signal components for any extreme event using the original signal value. This leads to the third image in fig:50 that presents the correct values as in the first image of fig:50.

The technique adopted in this work consist in the interpolation of stress states deriving from a maximum of three external signals. A space defined by different values of the signal interferences must be calculated. Every point corresponds to a tern of signal values, for winch an associated stress state is calculated via the FEM analyser.

11 Method implementation

The whole analysis procedure is composed of different parts that by working in concert allow to a fatigue estimation of the model analysed as well as providing useful information for the crack location and direction of crack propagation.(fig: 51). There are four main sections: model definition, stress calculation, signal analysis and stress interpolation, damage calculation.

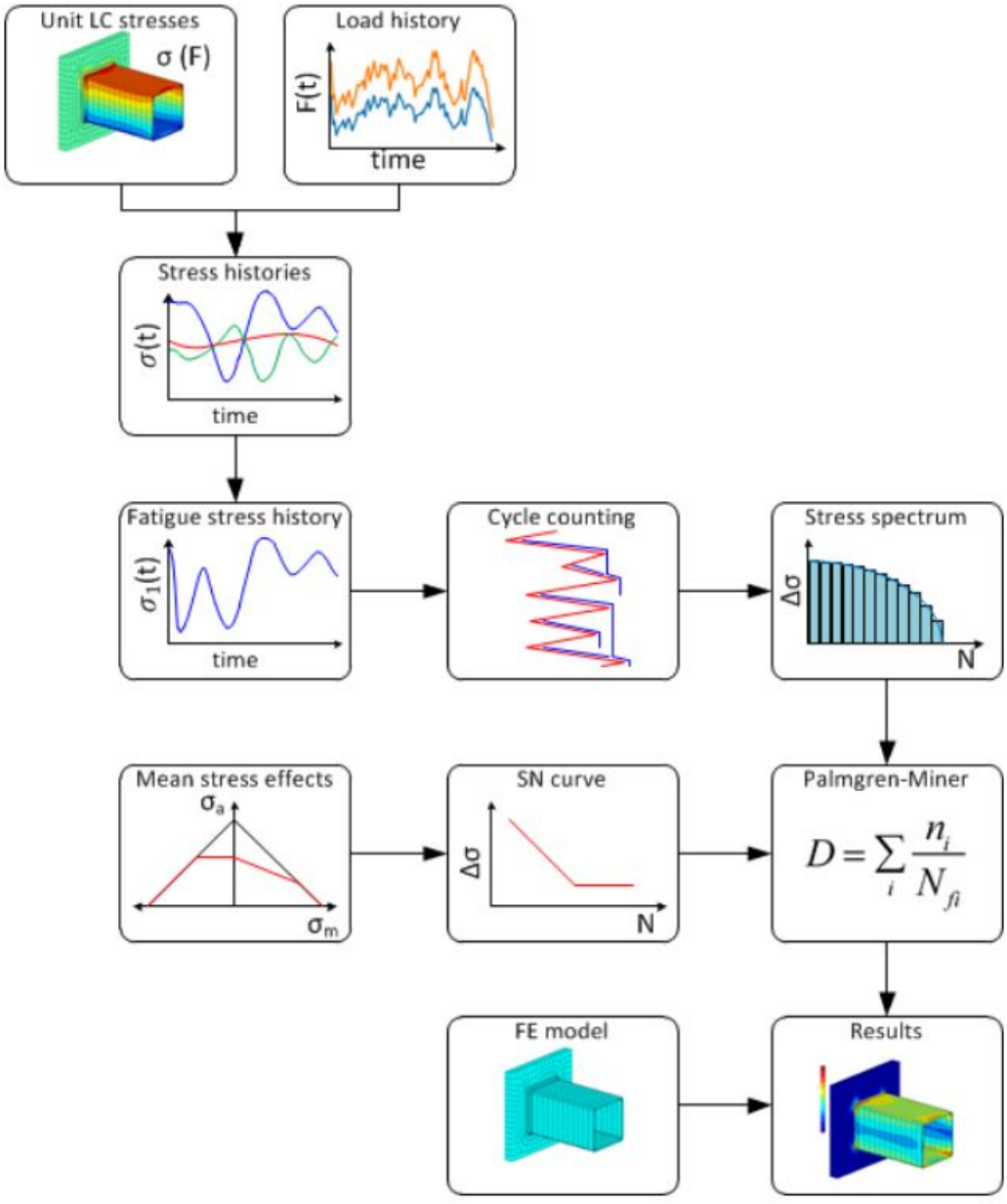

Figure 51: Procedure schematic. Source [27]

The process begins with the calculation of the stress state for a series of steps of a load signal. For every signal component, a certain amount of stress states associated with a finite quantity of signal levels is calculated. In this way there is a direct relation between the external signal and the stress state associated with it. If the input signal has more then one component, a more complicated process has to be implemented in order to account for interference of stress states due to combination of external loads. In facts the load boundaries are set and some load intervals are defined on these boundaries. Based on a discrete amount of load configuration for each signal, the procedure calculates the stress state corresponding to the combination of the external load.(fig: 52)

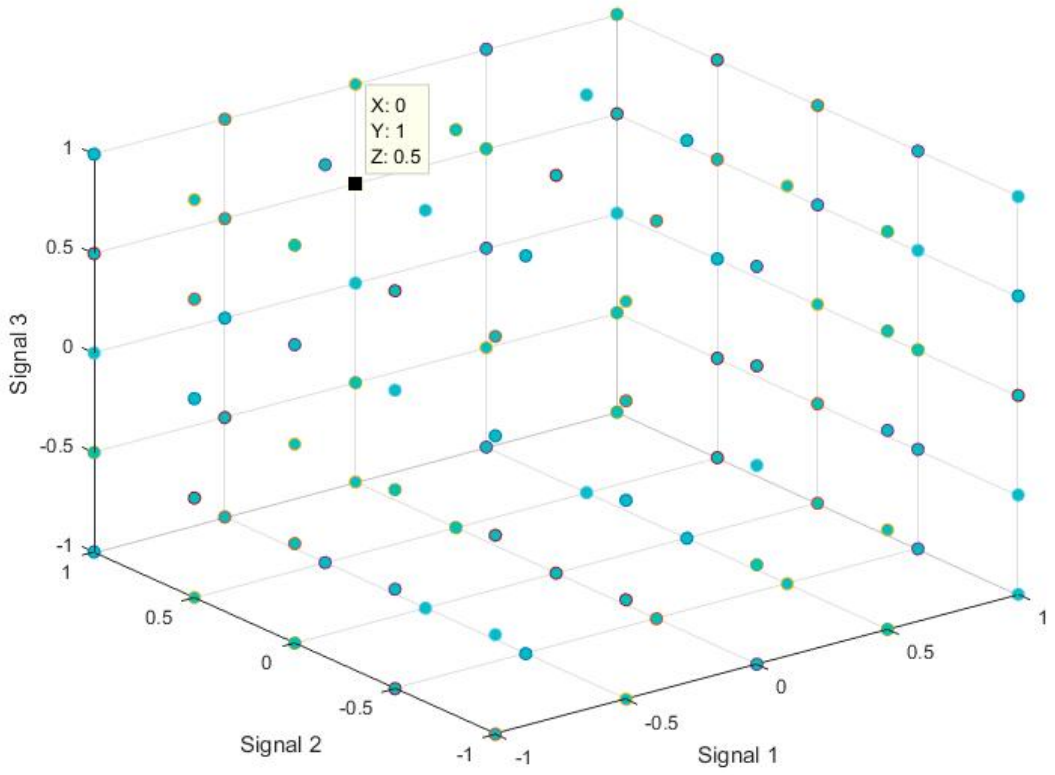

Figure 52: Points of stress state calculation via FEM method. The highlighted point correspond to the combination of 0 value of the first signal, 1 of the second signal and 0.5 of the third signal.

The cube of fig: 52 represents the concept expressed before. For each of the point in the space, corresponding to a load combination, a stress tensor has been calculated. This stress derives from FEM model. After all the stress states corresponding to the the signal couples or triplets are calculated, a linear interpolation method is used in order to determine the values on the whole domain. In this way, for every signal superposition corresponds a defined stress state.

Using the interpolated stresses derived from the procedure before and the external load history, a stress fatigue history is created. Following this step, through and an appropriate cycle counting method (rain-flow or range pair method), the stress load history is analysed. If using the critical plane method described in section 8, the higher stresses direction for each cycle is stored. The stress spectrum is then created in order to effectively store the fatigue history in a compact way. The stress-life curve has to be given as an input to the procedure, and it will not be modified during following calculations. Using the Haigh correction method for mean stress sensitivity , described in section7, the information deriving from the amplitude and mean stress is converted into an equivalent stress quantity with zero mean stress. (it is also possible to change the procedure to give as output the stresses referred to any value of R, since the values of the Wöhler curves for any R value can be extracted from the Haigh diagram). The equivalent damages are then calculated and the equivalent life is calculated. In case of critical plane method, the damages will be accumulated over distinct planes. Failure in this case will occur when the total damage accumulated on a plane will pass a damage threshold. Once identified the location of the failure, it is also possible to identify the direction of the crack propagation. Due to the use of the co-rotated Cauchy stresses, obtained with the aid of the rotational component of the deformation gradient, the direction of the crack will be referred to the underformed configuration.

The whole procedure is based upon MSC Marc software for the non linear FEM analysis and a Matlab script. The Matlab code takes as input the model and the loads and feeds them to the solver in order to obtain data regarding Cauchy stresses and deformation gradient. In order to adapt the existing script written for Metallic material to Rubber materials a series of procedures described in section:10 have been incorporated. The Haigh correction is also fully automatized and needs as an input only the text file contain experimental data.

In order to implement the fatigue concepts described before, a series of methods had to be developed in order to tackle with the following tasks:

- Creation an automated procedure for writing the Input file for the FEM solver. A input file is created for every combination of external load.
- Creation of an automated execution procedure for the running of all simulations.
- Creation of an automated gatherer of nodal Cauchy Stresses as well as the information regarding the Deformation Gradient.
- Creation of an automated procedure for calculating the polar decomposition of each Deformation gradient and calculating the co-rotated Cauchy stresses for each point of every simulation.
- Modification of the existing Matlab script [27], in order to accept three dimensional load signals.

- Creation of a script able to cope with the peculiar Haigh diagram of the Rubber.
- Creation of a signal creator able to take as input means and amplitude data with corresponding cycle count, that gives as output a complete signal in time.

12 Model Validation

In order to verify the correct implementation of the procedure developed, different sample were studied. In particular some models have been custom created in order to verify the correct implementation of the rotation for the stresses and for the correct interpolation of the stress states based upon the FEM data.

Furthermore examples of real tested components from the work of [21] as well as from the work of [33] have been used. The testing has been made using increasingly complexes models, in order to verify step by step the correct implementation of the created procedures.

For this reason the following models have been studied:

- A single element cube (fig:53) subjected to cyclic axial loading and a solid body rotation. This has been performed in order to verify that the pull-back process on the Cauchy stress tensor was correct.
- A eight element cube (fig:60) subjected to triaxial loading. This has been used in order to verify the correct three dimensional stress interpolation, as well as the correct functioning of the stress calculation procedure.
- A diabolo specimen from [33] used in order to assess the correct direction and location of the most critical element and the critical plane direction associated.
- A diabolo specimen from [21] coupled with three different load signal in order to determine the predicted fatigue life of the specimen and to compare the quality of the results.

12.1 Single-Element Cube

The aim of this particular model was to verify the correct calculation of the rotated Cauchy stresses (co-rotated Cauchy stress tensor). In order to verify the procedure, a simple element made out of a rubber material has been modelled.(fig: 53) A series of mono-axial loads (fig: 54 and fig reffig:loady) have been applied throughout the simulation with application point always on the same face. The opposite face has been locked. After 5 peaks the whole element has been subjected to a rigid body motion consisting in a rotation of 90 degrees around the z reference axis. After the body rotation, the Cauchy stresses along the principal X direction are zeros. (fig 59) Through the use of the mposition was possible to deformation gradient polar decocalculate the rotational matrix associated with the change in the reference system between the material and the reference system. The rotated Cauchy stresses assumed the correct value as seen in chapter 6.

The following material parameters have been used:

C10	C01	C11	C20	C30
0.284	0.105	0.106E-2	0.237E-2	0.104

Table 2: Material Parameters for the cube

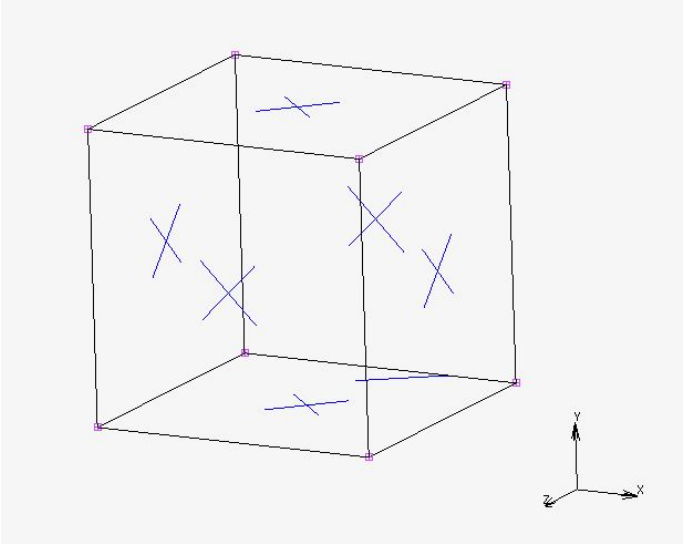

Figure 53: The simple cube element used to verify the correct implementation of the rotation of the Cauchy stresses. The initial orientation of the stress is outbound on the right face. Once the 90 degree rotation is enacted, the stress will continue to be exerted on the same face, thus pulling 'down' the initial stresses face.

The stress load used is a simple displacement controlled one. The amplitude and frequency of the peaks before and after the rotation are the same.

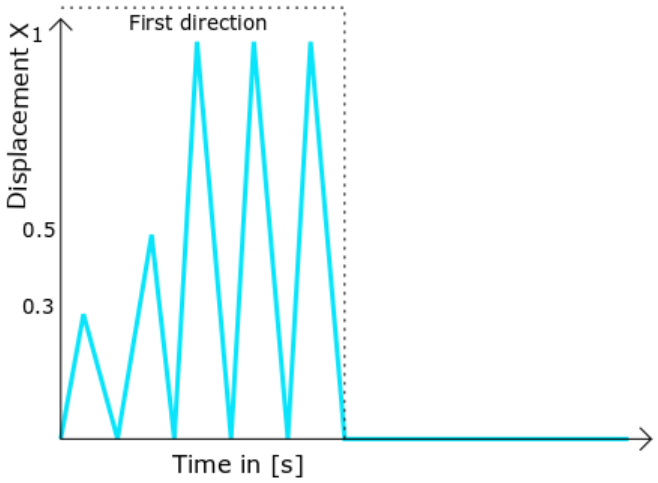

Figure 54: Load in the X direction over time.

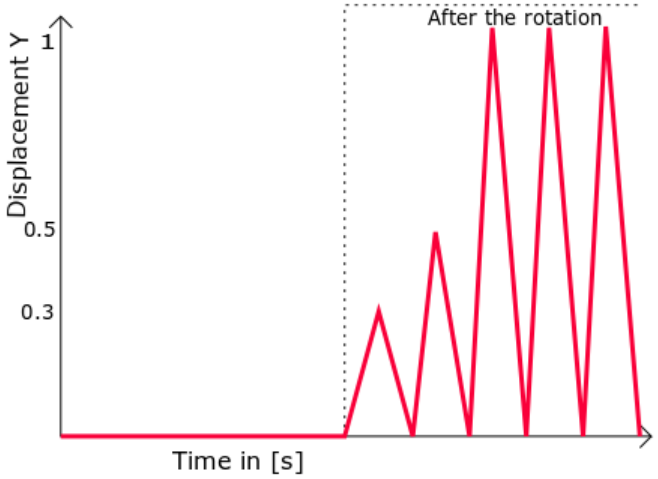

Figure 55: Load in the Y direction over time.

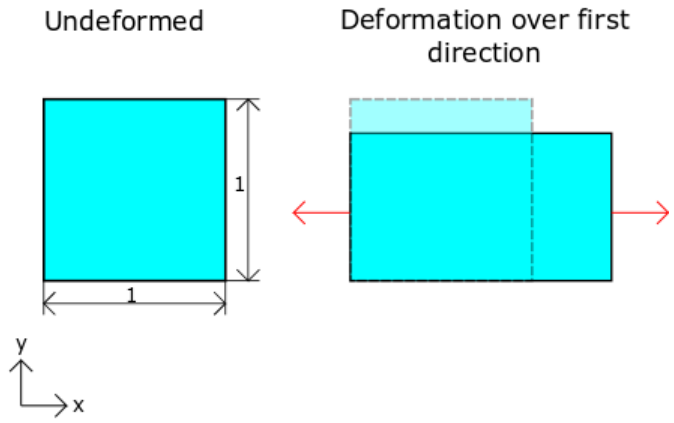

Figure 56: The simple cube element used to verify the correct implementation of the rotation of the Cauchy stresses. The initial orientation of the stress is outbound on.

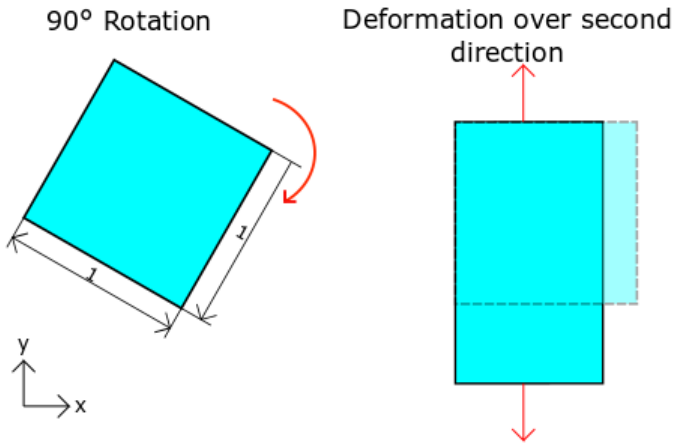

Figure 57: The simple cube element used to verify the correct implementation of the rotation of the Cauchy stresses. The initial orientation of the stress is outbound on.

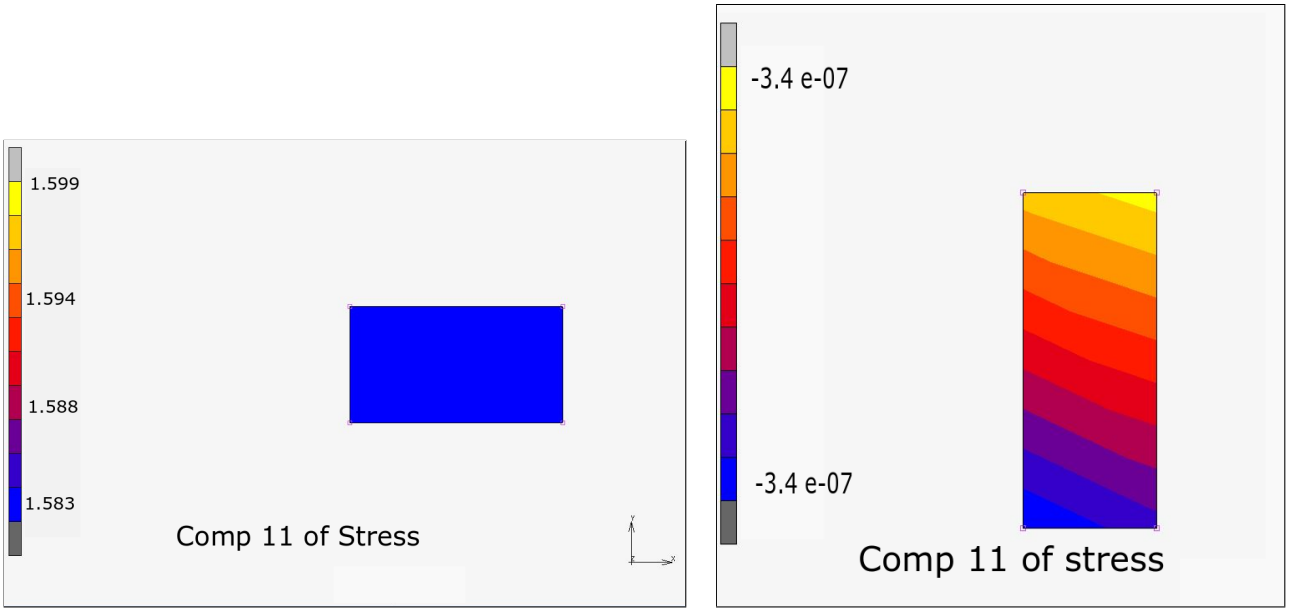

Figure 58: Deformation of the element referring to the initial spacial configuration and the rotated one. Note that in the rotated configuration , the stresses are almost zero (3.4 e-7 Mpa)

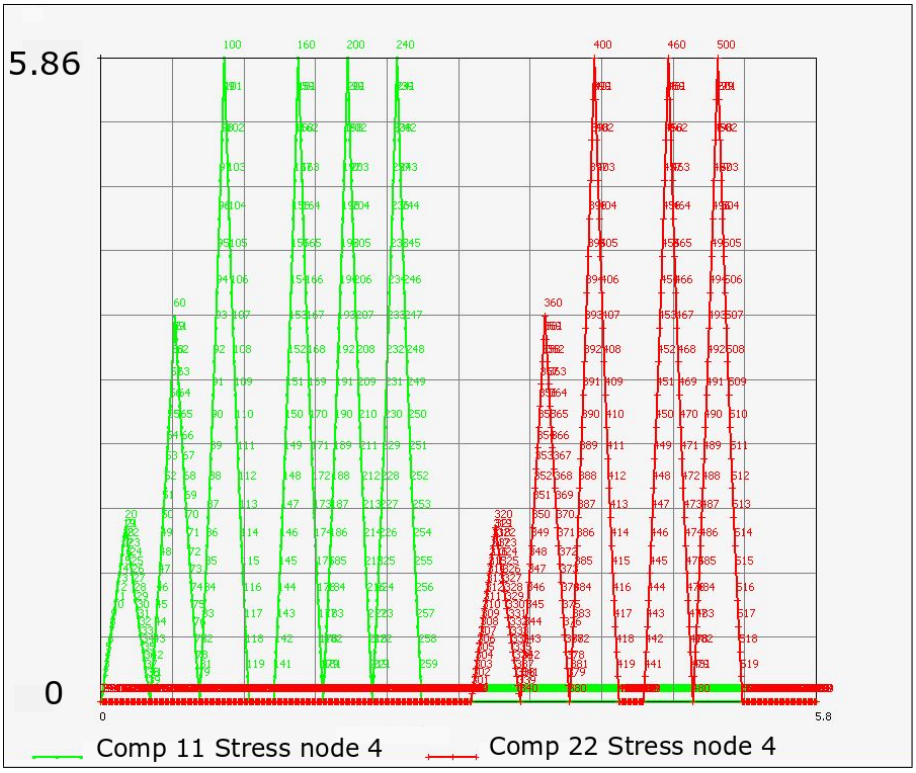

Figure 59: The peaks in the signal correspond to the peaks in stress. In green is represented the Cauchy stress along the xx component. The peaks in red are the one referring to the direction yy. It is clearly shown how the Cauchy stresses depend from the spacial orientation of the specimen.

Cauchy Stress xx inc 100	Cauchy Stress xx inc 400	Corotated Stess in X inc 100	Corotated Stess in X inc 400
5.846039772034	-117 E-06	5.846039772034	5.846039772034

Table 3: Stresses level at peaks 100 (horizontal orientation) and peak 400 (vertical orientation). The procedure works as expected, modifying the stresses only when the rigid body motion takes place.

The Cauchy stresses show a dependency from the spatial orientation of the body, wherase the Co-Rotated ones are seen as independent as seen in table 3

12.2 Eight Block Cube

This model (fig:60) was tested in order to assess the correct implementation of the 3 load signal interpolation. A simple geometry consisting of a cube made by eight elements was created. A series of progressive displacement loads were imposed on the model. An axial displacement along x direction, a displacement on the y direction and a rotation along the x direction were performed.

The following material parameters have been used:

C10	C01	C11	C20	C30
0.284	0.105	0.106E-2	0.237E-2	0.104

Table 4: Material Parameters

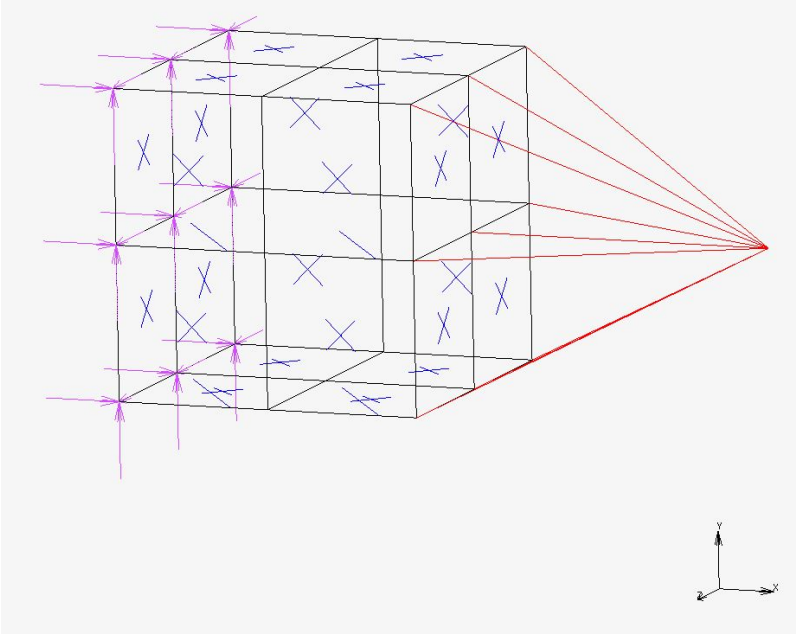

Figure 60: The eight block cube used to verify the correct 3D interpolation of the stress state. The boundary conditions are a fixed back face and a slave and leader boundary condition on the right face. The lead node on the right is the one used to impose a displacement along x and y axis as well as a rotation along the z axe.

The choice of this peculiar load condition is to assess the ability of the procedure to tackle with extremely complicated load cases. As a matter of fact in real world scenario is highly unlikely to have a pure mono-axial load case, and the ability to calculate stress states deriving from the interference of multiple loads might result in a more accurate fatigue life prediction.

A third order, five parameter, non linear constitutive model was used to describe the rubber material.

In order to take into account the non linearity of the model, the loads spanned from a negative value to the equivalent positive one. All the different combination of loads were performed with three values possible for each load signal. A total of 27 combination of load signal were tested. For every load combination Cauchy stresses and deformation gradient were requested as output. For each load combination the rotated Cauchy stresses were calculated. Once all the 27 stress states were calculated, their values have been fed as input for the interpolation process.

Stresses values derived from the interpolation have been checked against the ones deriving from the FEM solver and a satisfactory agreement has been found between the two.

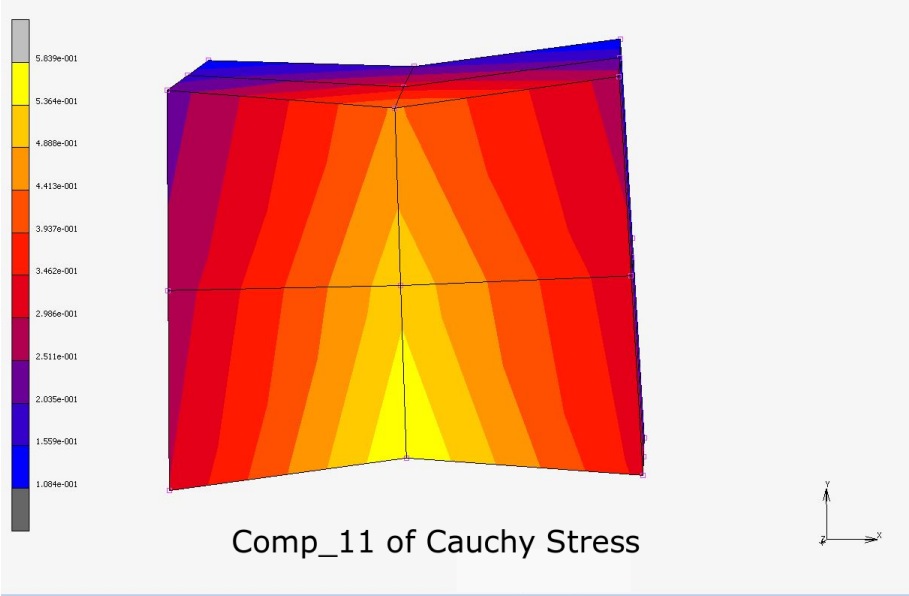

Figure 61: Stress level obtained through Marc FEM. The first component of the Cauchy stresses is shown. External loads are 1 for X and Y displacement and 0.1 radiant in the rotation.

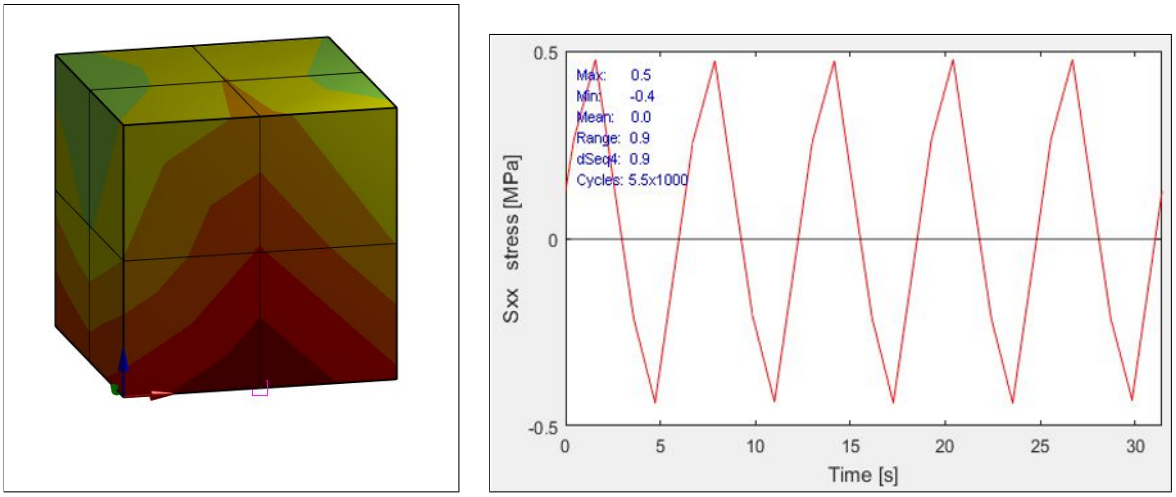

Figure 62: Stress levels due to interpolation process through the procedure. Data from three different signals are merged into the model. A sinusoidal external signal is used only to obtain data. The peaks in the right graph refers to the first component of the Cauchy stresses. External loads are 0.9 for X and Y displacement and 0.09 radiant in the rotation. This slightly smaller values are needed in order to avoid the extreme values of the interpolation method. The stress levels reached are in accordance with the FEM solver.

12.3 Diabolo Test n.1

Model description

This test has been performed in order to verify the correct location and direction of the crack onto a diabolo shaped specimen. In order to verify the tecnique developed, data from [32] diabolo specimen have been used.The geometry is shown in fig:63 with material data defined in tab:6

The following material parameters have been used:

C10	C01	C11	C20	C30
0.284	0.105	0.106E-2	0.237E-2	0.104

Table 5: Material Parameters of the specimen

In order to reduce calculation time, the axial-symmetry of the specimen has been used. Only a slice of the diabolo has been tested, using the Marc possibility of performing axial-symmetric analysis.(fig: 63, fig : 67) The rotation imposed was of 15 degrees around the symmetry axis.
Mesh structure and location of boundary can be seen in fig:64.

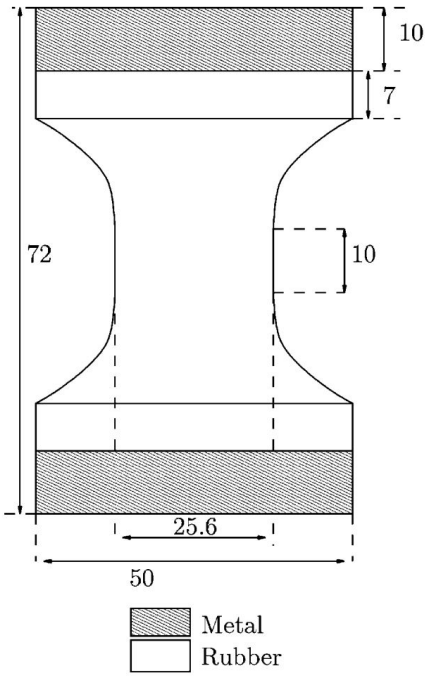

Figure 63: Diabolo Geometry. Source [32]

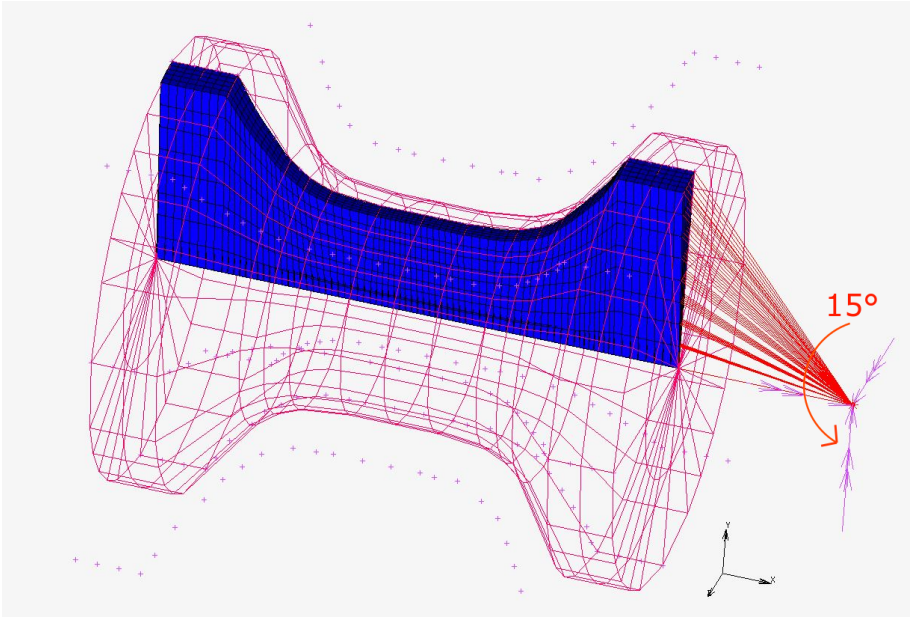

Figure 64: Mesh and boundary conditions of the Diabolo specimen. In order to simulate the torsional load, the axisimmetry is exploited to generate only three elements along the circumference of the specimen. Each element occupies 5 degrees along the circumference.

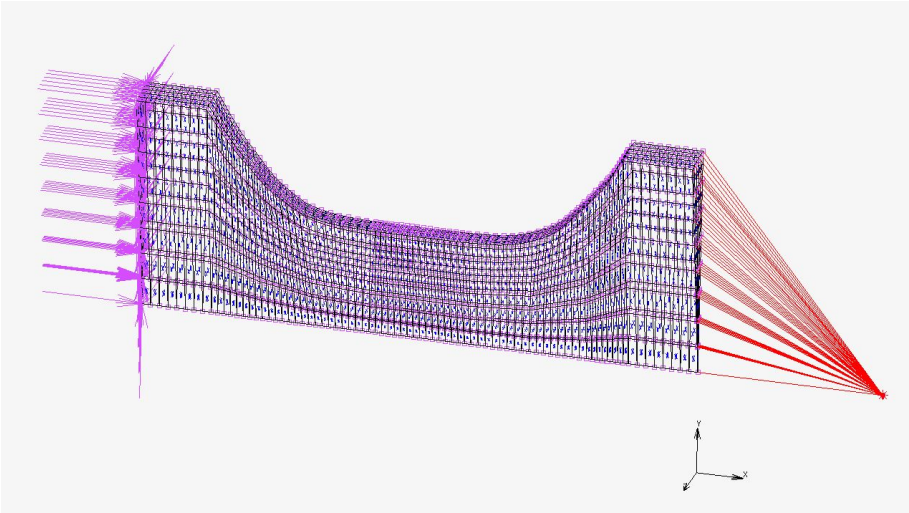

Figure 65: Boundary conditions are set on the left face as fixed and a slave and master on the right. The master node is used in order to impose the rotation

The nature of the loading induced a multi-axial stress state into the material. Displacement along the symmetry axis (x) has been created as shown in fig:67

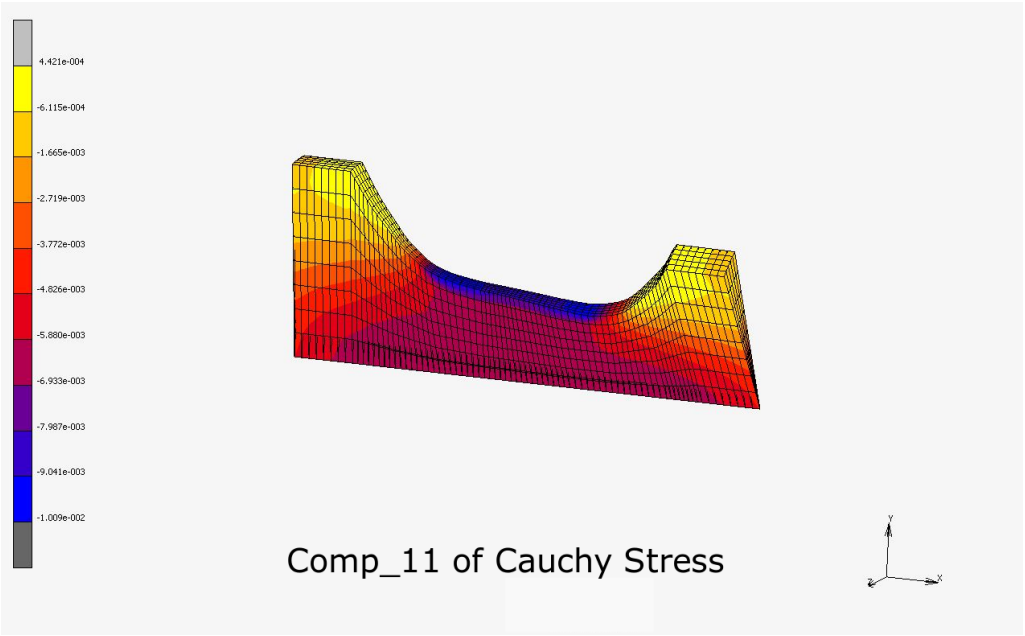

Figure 66: Deformed view of the specimen. The color scale represents the Cauchy stresses along first principal direction. (Cauchy 11)

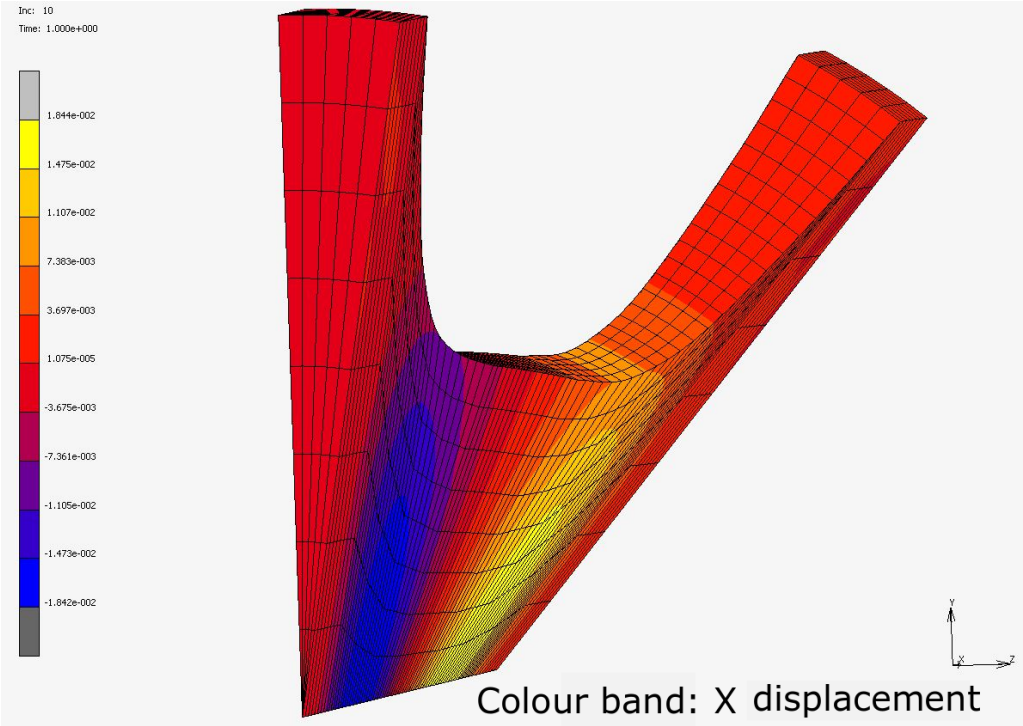

Figure 67: Deformed view of the specimen. The colour map indicates the axial (x) displacement resulting from the torsion. It is possible to see how a monoaxial load induces a multiaxial stress state inside the specimen. The prospective also shows the size and disposition of the model's elements.

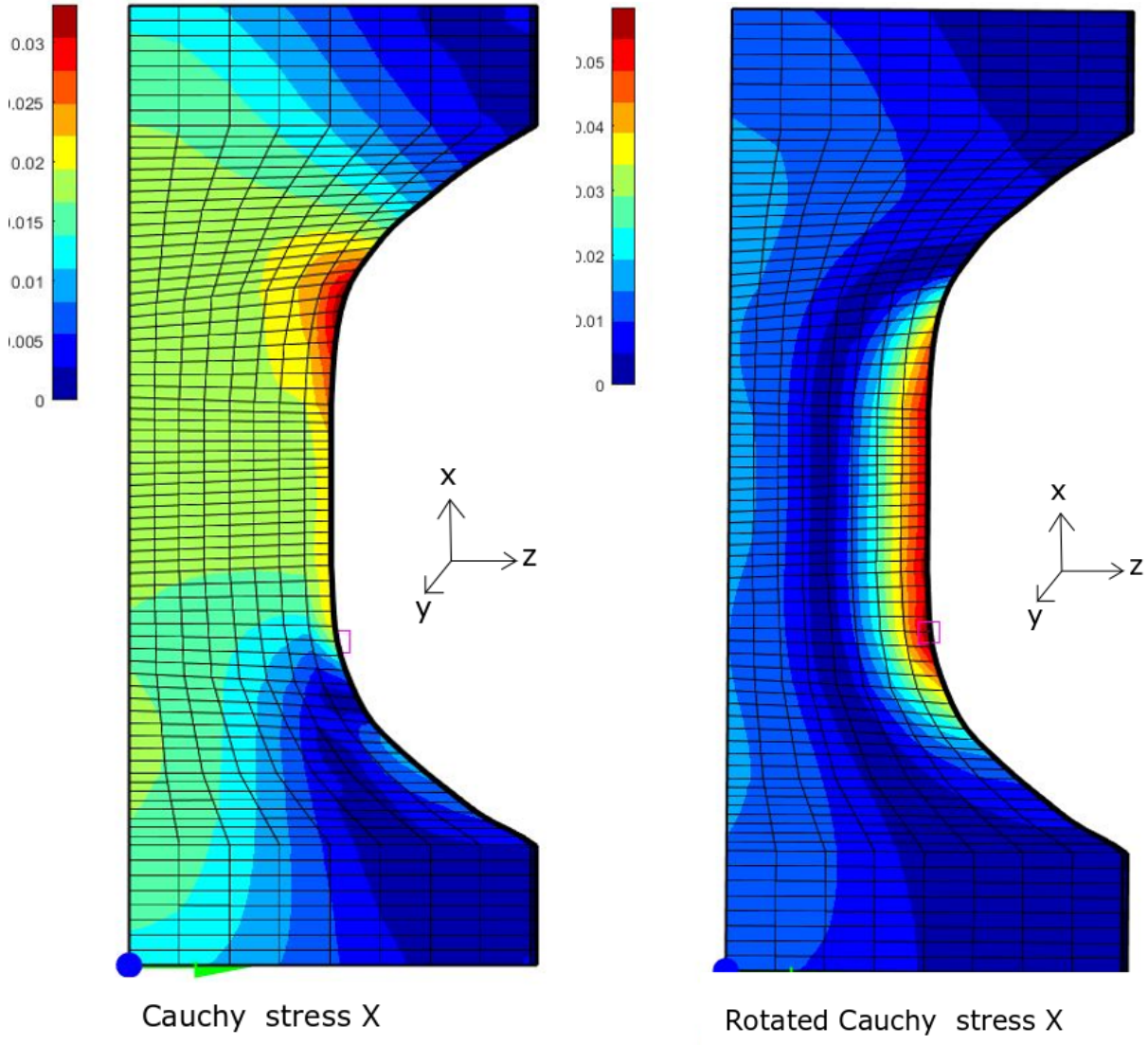

Figure 68: Comparison between stresses distribution using simple Cauchy stresses and Co-rotated Cauchy. The left image depicts stress distribution of Cauchy stresses. The on on the right depicts the Cauchy rotated stresses. The rotation value imposed to the model is of 15 degrees

The difference between the Cauchy stresses and the rotated ones has been found to be remarkable. As possible to be seen in fig: 68, the stress distribution is different when the rotation is performed.The Cauchy stresses do not correctly predict the location of the crack location, whereas after the rotation, they most critical area is correctly located.

The data from the FEM solver were imported into the Fatigue tool, and the zone of maximum stresses were correctly predicted as being located on the skin of the specimen. The highest stresses corresponding with the preferred crack location, are situated on the

center of the specimen.(fig: 69)

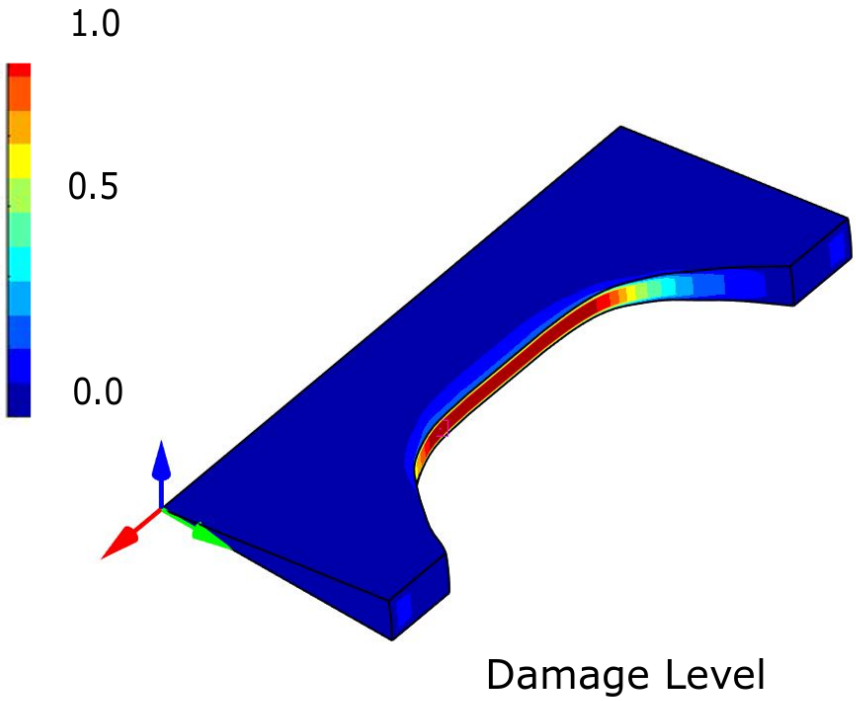

Figure 69: Colour Map of the most damaged area. This has been found to be in accordance with literature. [33] The critical plane angle is dependent of the torsion imposed.

Through the use of the critical plane method was possible to determine the direction of the crack direction referred to every single elelment. As possible to see in the figure 70 the orientation of the cracks are diagonal in respect with the simmetry axis. The orientation of the crack is in relation with the torsional level. This has been found to be in accordance with the results of [32].

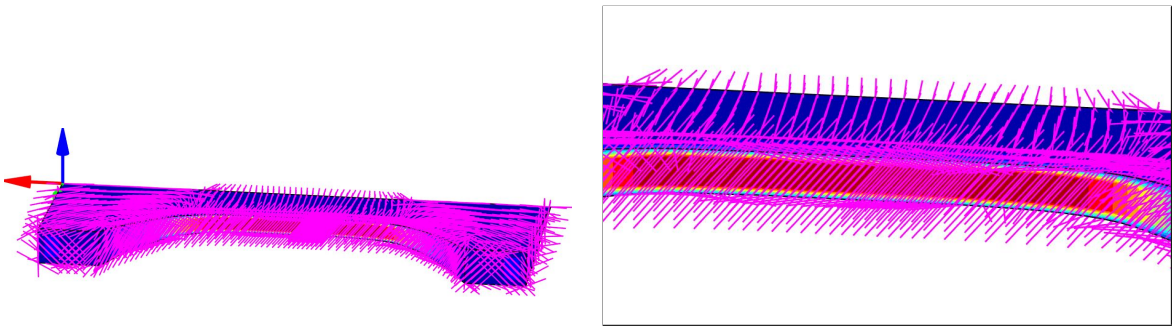

Figure 70: Direction of all the critical planes and detail of the most stressed area.

12.4 Diabolo Test n. 2

This model has been simulated using the data deriving from the work of [24]. A diabolo specimen was modelled using a third order, five parameter, phenomenological model. The loading conditions consists in a mono-axial displacement over the symmetry axe. The mono-axial load case and the symmetry of the model, allowed the exploitation of a axial simulation.

12.4.1 Material properties

C10	C01	C11	C20	C30
0.506237	0.023480	0.004979	-0.112556	0.031628

Table 6: Material Parameters of the specimen

12.4.2 Element type

Elements used in the simulation are a Marc Type 82 (Hermann formulation), corresponding to a four-node, isoparametric quadrilateral element, purposely written for axy-simmetric incompressible materials . This element uses bi-linear interpolation functions, and thus the strains tend to be constant thought the element. [10]

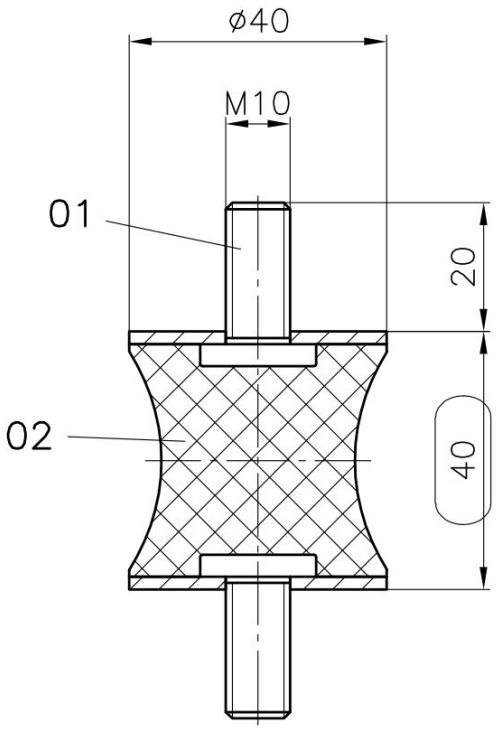

Figure 71: Geometry of the Diabolo specimen. Source [24]

Here shown the mesh created for the model (fig:72a) and an example of a deformed configuration deriving from a mono-axial tension.(fig:72b)

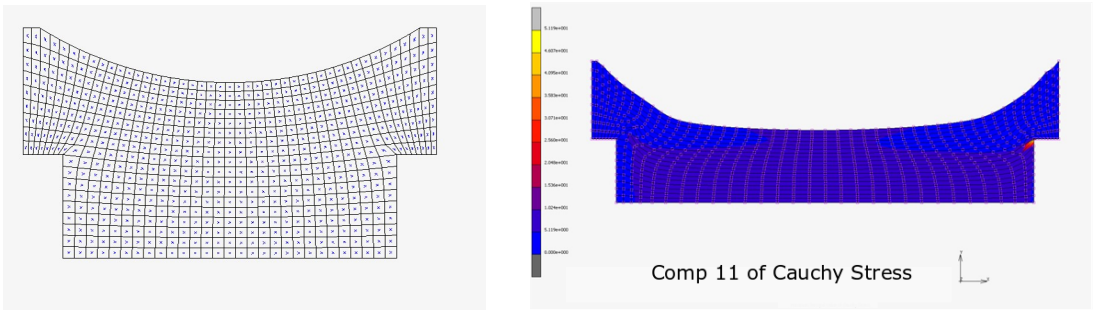

(a) Mesh of the diabolo specimen

(b) Deformed view due to axial loading

Figure 72

In order to test the accuracy of the material model used, a series of data from compression and extension have been retrieved. (fig: 73) In particular the model tested has been used to simulate the force-elongation and stress-elongation and the data have been compared to the ones from [24]. The model results were found to be in accordance with the ones from literature as seen in the following figure.

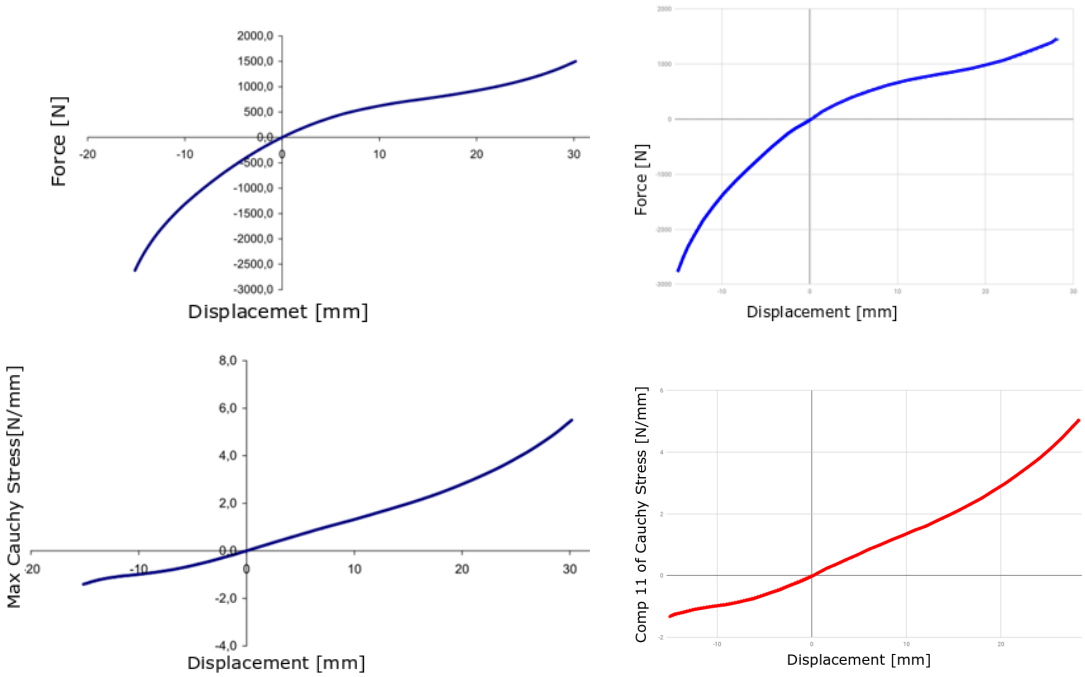

Figure 73: First row: Comparison of Force-Displacement between literature [24] model and simulated model.
Second row: Comparison between Cauchy 1st component stress and displacement between literature [24] model and simulated model.

Stresses have been calculated using an automated procedure that calculated the values at various steps using the FEM solver as a source. The correct interpolation of the stresses obtained through the FEM solver has been checked (fig: 74). Good accordance between the FEM solver and the interpolation procedure has been found.

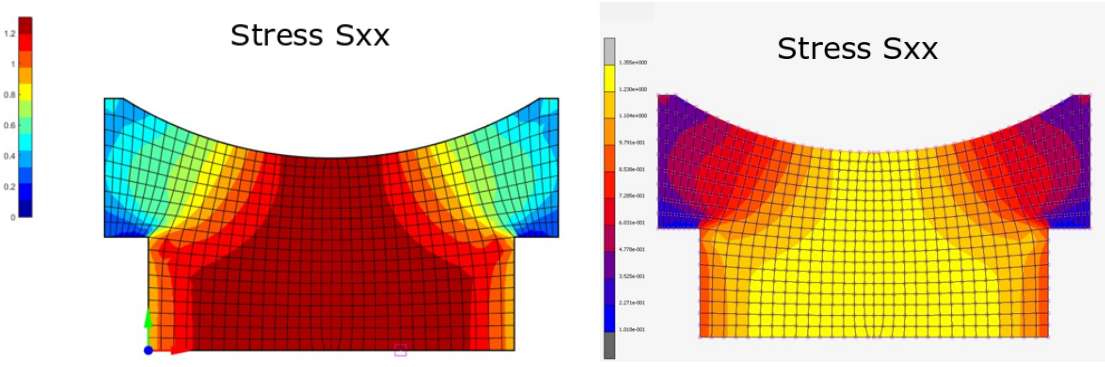

Figure 74: Test for verification of quality of interpolation method for the stresses in the FATLAB environment

The rotated Cauchy stresses and the Cauchy ones have been compared for this model (fig:75). Neverhteless the loading condition resulted in a cauchy stress very close to the rotated one as possible to be seen in the image below.

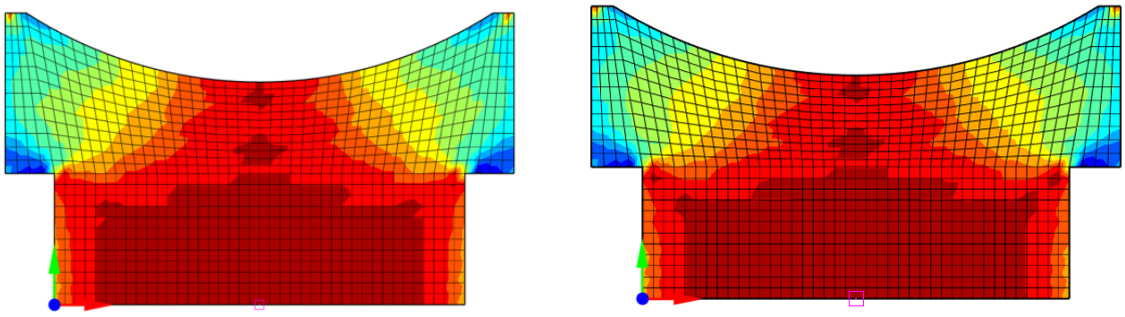

Figure 75: Comparison between Cauchy stresses along first principal direction and the Co-rotated ones. For this load configuration no great difference is seen.

12.4.3 Signal for diabolo test

Since no original data signal were available, three test signals have been recreated using the amplitude, mean and number of occurrence given in the table 7. The signals have been created using a saw-tooth signal of constant frequency.

Block nr	Amplitude	Mean Load	R	Repetitions
1	8	8	0	20
2	10	0	-1	70
3	7	0	-1	150
4	4.5	4.5	0	80
5	6	0	-1	220
6	7	7	0	30
7	8	0	-1	120
8	6	6	0	50

Table 7: Data for signal n.1 Source [24]

The first signal created (n.1, fig:76) looks like the following.

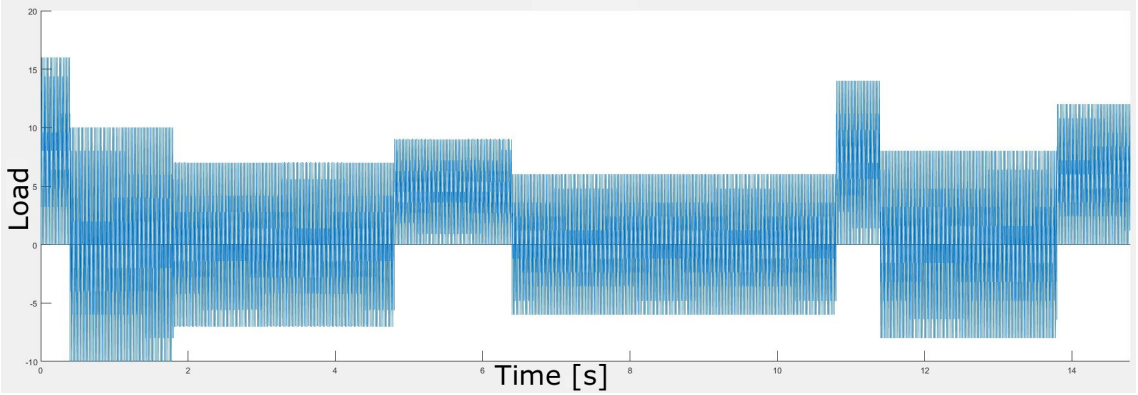

Figure 76: Signal n. 1. The eight blocks are then repeated during the fatigue simulation.

For creating the signal n. 2 (fig:77) the data from tab n 8 have been used.

Block nr	Amplitude	Mean Load	R	Repetitions
1	9.9	1.2	1276	129
2	5.9	1.2	1511	1545
3	9.9	-0.6	0.886	21
4	5.9	-0.6	0.814	678
5	5.9	4.7	8834	102
6	9.9	4.7	2808	3
7	5.9	3	3069	498
8	9.9	3	1.87	9

Table 8: Data for signal n. 2. Source [24]

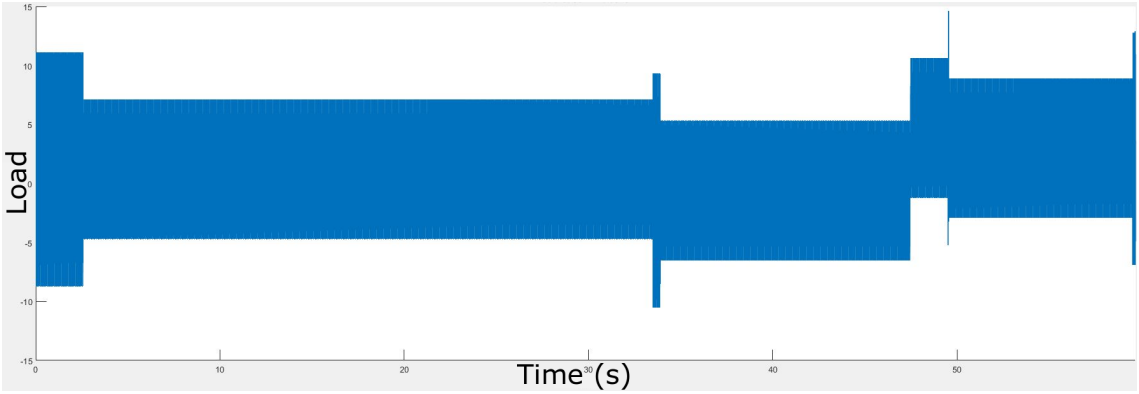

Figure 77: Signal n. 2. The eight blocks are then repeated during the fatigue simulation.

12.4.4 Life estimation

Signal ID	Experimental	Literature Life[24]	Estimated Life (literature/estimated)	Relative Difference
1	1434	1610	478	3.36
2	838	539	155	3.47

Table 9: Life estimation differences between literature and Estimated ones

The procedure consisting of performing the stress analysis, the interpolation of the stress states and the load simulation produced three different life estimation. The model correctly predicted the location of the most stresses area on the surface of the specimen. The implementation of the whole procedure proven to be stable and requiring a moderate amount of time (approx 5 minutes for each signal case)

Nevertheless the results obtained (tab:9) have been significantly different from the one in [24]. As a matter of fact they were off by a factor 3. The method nevertheless produced a result that was precise although not accurate. The relative difference between Estimated life and Literature life has attested to a constant value. This results might be attributed to a difference in the Haigh data used by [24] and the ones used in this work.

13 Discussion and Conclusions

This work considered many aspect of fatigue life, such as material parameters, working conditions, loads, and production processes. The aim of this work was to develop a procedure that could be used by designers to estimate and improve fatigue life of components. After an overview on the possible life indicators Stresses have been selected as the most fit to the purpose of predicting fatigue life as well as crack location and crack direction. Furthermore the use of a conventional Stress tensor such as the Cauchy one, allows for the use of the stress-life data that are already present in literature. A damage accumulation method has been selected having in mind the possibility of implementing it on long time history, without requiring the need of excessively time and calculation consuming simulation, as well as the need of having a very limited amount of parameters. Since the components are usually designed and inspected into a un-deformed configuration, a procedure to rotate the stresses from the deformed to the un-deformed configuration has been implemented. This allows for the correct orientation of the crack direction referred to the undeformed configuration. Such procedure allows also the calculation of any stress tensor that might be needed for future works (1st Piola-Kirchhoff, 2nd Piola-Kirkhhoff,...). Rubber material exhibit a peculiar mean stress sensitivity, and for this reason a procedure has been developed in order to modify the loads based on the mean stresses and the original amplitude. The outcome of such process is an equivalent stress load that takes account the peculiar mean stress sensitivity deriving from phenomena such Strain induced crystallization. This procedure is based on experimental data in order to have a very adaptable procedure that could closely describe the real fatigue behaviour of rubber.

The whole procedure has been validated with a series of models: The rotation procedure used for obtaining alternative stress measures has proven to be successful, and its correct implementation has been tested on three separate specimen. The ability to create Haigh diagrams with a highly flexible interpolating procedure has been tested and validated. The capability of the method to generate equivalent stresses based on amplitude and mean stress of the signal has been tested, and the results have proven to be good. The stress distribution resulting from the interpolation of calculated stress have been verified with three different tests, and the values have proven to be excellent. Location and direction of the cracks has proven to be in accordance with literature data. The rotation of the stresses into the deformed configuration has proven to successfully determine the crack direction in the un-deformed configuration. The fatigue life of real components have been estimated using different load signals. A relative difference in fatigue life estimation has been found, and its value has attested on estimation 3 times bigger then the ones from experimental data. These discrepancies between fatigue might be attributed to different Whöler data between the literature case and the one of this work. The relative difference of a constant factor of 3 between literature and simulated fatigue life has given a good insight on the consistency of the model developed in this work.

Most of the rubber design implemented in the industrial world are based on simple trial and error design processes. Despite the presence in Literature of extremely complex models for the description of fatigue life of rubber components,[4, 5, 6, 13, 37] most of them focus on laboratory samples whose nature is highly tunable and controllable. Such control level over material properties is usually not possible during Industrial application, and most of the parameter needed are highly dependent from the composition of the rubber mixture.[34, 18, 17]

The method created in this work aims at bridging the gap between the laboratory and the industrial world. This procedure is able to use accurate fatigue life estimators coped with calculation efficient damage-accumulation tecniques, being able to handle the peculiarities deriving from the nature of the Natural rubber. At the same time the procedure is able to automatically gather and analyse data from FEM solver, Haigh data and external laod signals, thus comprising of all the aspect of fatigue life. The flexibility in the interpolation process of the Haigh diagrams allows for the use of this procedure on rubber material presenting fatigue properties also very different from the ones studied in this thesis. The high parametrization level of the procedure developed during this work, makes its implementation fast and effective. The complete automation of the interpolation of multi-axial stress states deriving from up to three external loads allows for an efficient calculation of the stress states with a time efficiency not possible using existing approaches [4, 6, 13, 37, 25].

For the reasons described above this procedure could be adopted in the estimation of fatigue life of rubber components and its implementation into industrial world might bring a great advantage in terms of fatigue design of rubber. In particular it presents the capability of correctly estimate fatigue life and crack location while at the same time retaining a highly automated nature and a simple enough structure for being used in an industrial environment.

Future work

A possible extension of this work is the extension of the interpolation process to the full 6 external signal dimensions. This option would on the other hand be extremely computational heavy on a program that, being written in Matlab, was not written with the calculation efficiency in mind. Further testing on some different specimen data would allow also to tweak the Haigh diagram creation procedure in order to narrow the gap between predicted and real fatigue life. Testing on components subjected to real life conditions would also allow for testing the accuracy of the model for industrial application. Future work could also include in the model a description of the crack growth dynamic, in particular for analysis of failed components, since during nucleation phase the mechanical propertied usually degrade beyond acceptable levels. An extension of the procedure might also include phenomena such as like Mullins effect (cyclic softening) or great changes in the mechanical properties. Load sequence effect simulation might be further investigated if shorter fatigue life would become of interest.

List of Figures

1 cis-1,4 Polyisopropene, the monomer at the base of the structure of the Natural rubber polymeric chain in fig:2 source [39] . . . 4
2 Polymerization principle and final polymer structure. source [39] . . . 5
3 Havea Brasilianis. source [39] . . . 6
4 Figure 4: Injection Molding (a), Compression Molding (b) and Transfer Molding (c) . . . 7
5 Example of measured stress strain curve. . . . 8
6 Comparison of constituive models. . . . 9
7 Example of different constitutive models . . . 9
8 Depiction of temperature increase due to straining of rubber. Source [39] . 10
9 Hysteresis behaviour during a loading-unloading cycle. Source [24] . . . 11
10 mullins effect during showed for different strain level. Source [21] . . . 12
11 Effect of the strain induced crystallization on the Polymeric chains. Source [29] . . . 13
12 Comparison between measured data and Model prediction on Stress-Strain relation. . . . 16
13 TEM micrographs of composites: (a) NR-0; (b) CB-10.7; (c) CNTs-1.2; (d) GO-1.6. Source: [12] . . . 18
14 Images of cracks due to decohesion processes in a specimen deformed state Source: [32] . . . 19
15 Images of cracks in a specimen deformed state Source: [32] . . . 20
16 Images of Micro and Macroscopic craks inside a specimen Source: [9] . . . 20
17 Images of cracks in a specimen deformed state Source: [9] . . . 21
18 A generic Wöhler line, where **W** is a generic fatigue life indicator . . . 23
19 Wöhler curves created using the maximum principal stretch. They clearly show a disagreement in the life estimation, thus defining the principal stretch as not a suitable fatigue life indicator. **a** and **b** refer to different experimental setups. Source[6] . . . 24
20 Wöhler curves created using the maximum principal Cauchy stress. **a** and **b** refer to different experimental setups. Source[6] . . . 25
21 Wöhler curves created using the continuum damage mechanics. **a** and **b** refer to different experimental setups. Source[6] . . . 27
22 Wöhler curves created using strain energy density indicator. **a** and **b** refer to different experimental setups. Source[6] . . . 28
23 Wöhler curves created using continuum damage model. Note that the prediction not able to unify all experimental data. **a** and **b** refer to different experimental setups.Source[6] . . . 29
24 Wöhler curves created using continuum damage mechanics, where the introduction of a threshold value for the effective stress S_{eff} allows the model to successfully predict fatigue life. **a** and **b** refer to different experimental setups Source[6] . . . 30

25 Wöhler curves created using configurational mechanics. Such technique does not allow a satisfactory fatigue life prediction. **a** and **b** refer to different experimental setups. Source[6] 31
26 Comparison of predicted life vs measured fatigue life using continuum mechanics tecniques. **a** and **b** refer to different experimental setups. Source[6] 33
27 Stresses S and corresponding fatigue life N. Source [29] 34
28 Comparison of predicted life vs measured fatigue life using Palgrem-Miner linear accumulation damage. **a** and **b** refer to different experimental setups.Source[6] 34
29 Comparison of predicted life vs measured fatigue life using Palgrem-Miner modified accumulation damage. **a** and **b** refer to different experimental setups. Source[6] 35
30 Haigh Diagram for Natural Rubber with Shore Hardness 60A. Source[21] . 36
31 Data points used to determine the Haigh Diagram, view from side. The height of the point is in accordance with life value. 37
32 Critical plane method. In the fist image is possible to see the plane directions and the normal axe of the plane sheaf. Second picture shows the parameters defining plane directions and components. Picture to the right shows how a stress tensor has different components along a path into space. Source [27] 38
33 Example of a Load signal 41
34 Example of signal block that can be repeated through time. Source [29] . . 42
35 Example of signal block with random block sequence. Source [29] 42
36 Examples of different sequences of the same load. Depending on the material properties they might influence the fatigue life of the component . Source [29] 43
37 Left Top: load stress signal. Right Top: rainflow counting illustration. Left Bottom: Resulting count. Source [29] 44
38 Result of the previous Rain-Flow counting .Source [29] 44
39 Result of the previous Rain-Flow counting .Source [29] 45
40 Range pair counting. In step (a) the smaller cycles are counted and eliminated from the signal. Increasing with cycle size as in (b). In (c) there is the last cycle left by the method.Source [29] 46
41 Level Crossing Method.Source [29] 47
42 peak counting method. Source [29] 47
43 Racetrack filtering. This technique allows smoothing of the signal in order to exclude small amplitude cycles, whose effect is negligible. Source [29] . . 48
44 Original signal and signal filtered with a 40% racetrack filter. It is possible to see how in the filtered signal all the small cycle components have been eliminated. 49
45 Deformation process of a body. The un-deformed configuration (*Reference* or *Material*)is represented with Capital letters. The deformed configuration (*Spatial* or *Current*) is represented by small letters. Source [39] 50

46 Interpolation made using a surface interpolation. In order to achieve a sufficient surface smoothness a very high number of data points are needed. Most of the times it is unlikely to dispose of such data quantity. 52
47 Data points used to determine the Haigh Diagram.Top view. Different points colour refers to different interpolation section. X axis contains the mean stress, y axis the amplitude stress. 53
48 Representation of the interpolation planes. 55
49 In in this image is shown how the parameters can be changed to manually modify slope and height of interpolating surfaces 56
50 Original signal and signal after extremization process has taken place. The data point are indicated with small circle. Please note the presence of data at the same time instant on all the signal when a peak or valley event happen in any of them. 58
51 Procedure schematic. Source [27] 60
52 Points of stress state calculation via FEM method. The highlighted point correspond to the combination of 0 value of the first signal, 1 of the second signal and 0.5 of the third signal. 61
53 The simple cube element used to verify the correct implementation of the rotation of the Cauchy stresses. The initial orientation of the stress is outbound on the right face. Once the 90 degree rotation is enacted, the stress will continue to be exerted on the same face, thus pulling 'down' the initial stresses face. 65
54 Load in the X direction over time. 66
55 Load in the Y direction over time. 66
56 The simple cube element used to verify the correct implementation of the rotation of the Cauchy stresses. The initial orientation of the stress is outbound on. 67
57 The simple cube element used to verify the correct implementation of the rotation of the Cauchy stresses. The initial orientation of the stress is outbound on. 67
58 Deformation of the element referring to the initial spacial configuration and the rotated one. Note that in the rotated configuration , the stresses are almost zero (3.4 e-7 Mpa) 68
59 The peaks in the signal correspond to the peaks in stress. In green is represented the Cauchy stress along the xx component. The peaks in red are the one referring to the direction yy. It is clearly shown how the Cauchy stresses depend from the spacial orientation of the specimen. 69
60 The eight block cube used to verify the correct 3D interpolation of the stress state. The boundary conditions are a fixed back face and a slave and leader boundary condition on the right face. The lead node on the right is the one used to impose a displacement along x and y axis as well as a rotation along the z axe. 70

61 Stress level obtained through Marc FEM. The first component of the Cauchy stresses is shown. External loads are 1 for X and Y displacement and 0.1 radiant in the rotation. 71
62 Stress levels due to interpolation process through the procedure. Data from three different signals are merged into the model. A sinusoidal external signal is used only to obtain data. The peaks in the right graph refers to the first component of the Cauchy stresses. External loads are 0.9 for X and Y displacement and 0.09 radiant in the rotation. This slightly smaller values are needed in order to avoid the extreme values of the interpolation method. The stress levels reached are in accordance with the FEM solver. 72
63 Diabolo Geometry. Source [32] 73
64 Mesh and boundary conditions of the Diabolo specimen. In order to simulate the torsional load, the axisimmetry is exploited to generate only three elements along the circumference of the specimen. Each element occupies 5 degrees along the circumference. 73
65 Boundary conditions are set on the left face as fixed and a slave and master on the right. The master node is used in order to impose the rotation . . . 74
66 Deformed view of the specimen. The color scale represents the Cauchy stresses along first principal direction. (Cauchy 11) 74
67 Deformed view of the specimen. The colour map indicates the axial (x) displacement resulting from the torsion. It is possible to see how a monoaxial load induces a multiaxial stress state inside the specimen. The prospective also shows the size and disposition of the model's elements. 75
68 Comparison between stresses distribution using simple Cauchy stresses and Co-rotated Cauchy. The left image depicts stress distribution of Cauchy stresses. The on on the right depicts the Cauchy rotated stresses. The rotation value imposed to the model is of 15 degrees 76
69 Colour Map of the most damaged area. This has been found to be in accordance with literature. [33] The critical plane angle is dependent of the torsion imposed. 77
70 Direction of all the critical planes and detail of the most stressed area. . . . 77
71 Geometry of the Diabolo specimen. Source [24] 78
72 79
73 First row: Comparison of Force-Displacement between literature [24] model and simulated model. Second row: Comparison between Cauchy 1st component stress and displacement between literature [24] model and simulated model. 80
74 Test for verification of quality of interpolation method for the stresses in the FATLAB environment 80
75 Comparison between Cauchy stresses along first principal direction and the Co-rotated ones. For this load configuration no great difference is seen. . . . 81
76 Signal n. 1. The eight blocks are then repeated during the fatigue simulation. 82
77 Signal n. 2. The eight blocks are then repeated during the fatigue simulation. 83

Bibliography

[1] *http://femfat.magna.com/FEMFAT-software.2881.0.html*. 2017.

[2] *http://www.mscsoftware.com/product/msc-fatigue*. 2017.

[3] S. Ata, S. Tomonoh, T. Yamda, and K. Hata. Improvement in thermal durability of fluorinated rubber by the addition of single-walled carbon nanotubes as a thermally table radical scavenger. *Polymer*, 119:112–117, jun 2017. doi: 10.1016/j.polymer.2017.05.025. URL https://doi.org/10.1016/j.polymer.2017.05.025.

[4] G. Ayoub, M. Naït-abdelaziz, F. Zaïri, and J. Gloaguen. Multiaxial fatigue life prediction of rubber-like materials using the continuum damage mechanics approach. *Procedia Engineering*, 2(1):985–993, apr 2010. doi: 10.1016/j.proeng.2010.03.107. URL https://doi.org/10.1016/j.proeng.2010.03.107.

[5] G. Ayoub, M. Naït-Abdelaziz, F. Zaïri, J. Gloaguen, and P. Charrier. A continuum damage model for the high-cycle fatigue life prediction of styrene-butadiene rubber under multiaxial loading. *International Journal of Solids and Structures*, 48(18):2458–2466, sep 2011. doi: 10.1016/j.ijsolstr.2011.04.003. URL https://doi.org/10.1016/j.ijsolstr.2011.04.003.

[6] G. Ayoub, M. Naït-Abdelaziz, and F. Zaïri. Multiaxial fatigue life predictors for rubbers: Application of recent developments to a carbon-filled SBR. *International Journal of Fatigue*, 66:168–176, sep 2014. doi: 10.1016/j.ijfatigue.2014.03.026. URL https://doi.org/10.1016/j.ijfatigue.2014.03.026.

[7] J.-B. Brunac, O. Gérardin, and J.-B. Leblond. On the heuristic extension of haigh's diagram for the fatigue of elastomers to arbitrary loadings. *International Journal of Fatigue*, 31(5):859–867, may 2009. doi: 10.1016/j.ijfatigue.2008.11.008. URL https://doi.org/10.1016/j.ijfatigue.2008.11.008.

[8] S. C. Y. F. Cadwell SM, Merrill RA. Dynamic fatigue life of rubber. 1940.

[9] J.-B. L. Cam, B. Huneau, and E. Verron. Fatigue damage in carbon black filled natural rubber under uni- and multiaxial loading conditions. *International Journal of Fatigue*, 52:82–94, jul 2013. doi: 10.1016/j.ijfatigue.2013.02.022. URL https://doi.org/10.1016/j.ijfatigue.2013.02.022.

[10] M. S. Corporation. User guide. may 2017.

[11] J. Diani, B. Fayolle, and P. Gilormini. A review on the mullins effect. *European Polymer Journal*, 45(3):601–612, mar 2009. doi: 10.1016/j.eurpolymj.2008.11.017. URL https://doi.org/10.1016/j.eurpolymj.2008.11.017.

[12] B. Dong, L. Zhang, and Y. Wu. Influences of different dimensional carbon-based nanofillers on fracture and fatigue resistance of natural rubber composites. *Polymer Testing*, 63:281–288, oct 2017. doi: 10.1016/j.polymertesting.2017.08.035. URL https://doi.org/10.1016/j.polymertesting.2017.08.035.

[13] A. Fatemi and N. Shamsaei. Multiaxial fatigue: An overview and some approximation models for life estimation. *International Journal of Fatigue*, 33(8):948–958, aug 2011. doi: 10.1016/j.ijfatigue.2011.01.003. URL https://doi.org/10.1016/j.ijfatigue.2011.01.003.

[14] O. K. Garishin, V. V. Shadrin, A. L. Svistkov, A. K. Sokolov, and W. K. Stöckelhuber. Visco-elastic-plastic properties of natural rubber filled with carbon black and layered clay nanoparticles. experiment and simulation. *Polymer Testing*, 63:133–140, oct 2017. doi: 10.1016/j.polymertesting.2017.08.002. URL https://doi.org/10.1016/j.polymertesting.2017.08.002.

[15] A. Griffith. *The phenomena of rupture and flow in solids Philosophical Transactions*, volume 221 of *pp. 163-198*. Royal Society of London A,, 1921.

[16] D. Guyomar, Y. Li, G. Sebald, P.-J. Cottinet, B. Ducharne, and J.-F. Capsal. Elastocaloric modeling of natural rubber. *Applied Thermal Engineering*, 57(1-2):33–38, aug 2013. doi: 10.1016/j.applthermaleng.2013.03.032. URL https://doi.org/10.1016/j.applthermaleng.2013.03.032.

[17] G. Heinrich, editor. *Advanced Rubber Composites*. Springer Berlin Heidelberg, 2011. doi: 10.1007/978-3-642-19504-4. URL https://doi.org/10.1007/978-3-642-19504-4.

[18] N. Huntink. *Durability of rubber products - Development of new antidegradants for long-term protection*. PhD thesis, Netherlands, 11 2003.

[19] W. Irwing. Catch-22. *Paperback*, 1961.

[20] F. JH. Flex life and crystallization of syntetic rubber. *Ind En Chem*, 1943.

[21] S. Kaindl. *Simulation der Schwingfestigkeit von Elastomerbauteilen*. PhD thesis, Martin Luther Universität Halle Wittenberg, 2014.

[22] J. KIM and H. JEONG. A study on the material properties and fatigue life of natural rubber with different carbon blacks. *International Journal of Fatigue*, 27(3):263–272, mar 2005. doi: 10.1016/j.ijfatigue.2004.07.002. URL https://doi.org/10.1016/j.ijfatigue.2004.07.002.

[23] F. Li, J. Liu, W. Mars, T. W. Chan, Y. Lu, H. Yang, and L. Zhang. Crack precursor size for natural rubber inferred from relaxing and non-relaxing fatigue experiments. *International Journal of Fatigue*, 80:50–57, nov 2015. doi: 10.1016/j.ijfatigue.2015.05.011. URL https://doi.org/10.1016/j.ijfatigue.2015.05.011.

[24] C. Madritsch. Ein konzept zur lebensdauerberechnung von elastomerbauteilen für fahrwerke von schienenfahrzeugen unter mehrachsiger dynamischer belastung. Master's thesis, Tu Graz, 2009.

[25] Y. Marco, B. Huneau, I. Masquelier, V. L. Saux, and P. Charrier. Prediction of fatigue properties of natural rubber based on the descriptions of the cracks population

and of the dissipated energy. *Polymer Testing*, 59:67–74, may 2017. doi: 10.1016/j.polymertesting.2017.01.015. URL https://doi.org/10.1016/j.polymertesting.2017.01.015.

[26] I. A. Morozov, L. A. Komar, and B. Lauke. Structural–mechanical model of filled rubber: Influence of filler arrangement. *International Journal of Mechanical Sciences*, 107:160–169, mar 2016. doi: 10.1016/j.ijmecsci.2016.01.013. URL https://doi.org/10.1016/j.ijmecsci.2016.01.013.

[27] M. M. Pedersen. *https://www.fatiguetoolbox.org/*. 2017.

[28] G. Previati and M. Kaliske. Crack propagation in pneumatic tires: Continuum mechanics and fracture mechanics approaches. *International Journal of Fatigue*, 37:69–78, apr 2012. doi: 10.1016/j.ijfatigue.2011.10.002. URL https://doi.org/10.1016/j.ijfatigue.2011.10.002.

[29] R. R. Ralph I. Stephens, Ali Fatemi. *Metal Fatigue in Engineering*. Wiley-Interscience, 2000.

[30] S. Rolere, S. Liengprayoon, L. Vaysse, J. Sainte-Beuve, and rédéric Bonfils. Investigating natural rubber composition with fourier transform infrared (FT-IR) spectroscopy: A rapid and non-destructive method to determine both protein and lipid contents simultaneously. *Polymer Testing*, 43:83–93, may 2015. doi: 10.1016/j.polymertesting.2015.02.011. URL https://doi.org/10.1016/j.polymertesting.2015.02.011.

[31] M. D. Romero-Sánchez, M. M. Pastor-Blas, J. M. Martín-Martínez, and M. Walzak. Addition of ozone in the UV radiation treatment of a synthetic styrene-butadiene-styrene (SBS) rubber. *International Journal of Adhesion and Adhesives*, 25(4):358–370, aug 2005. doi: 10.1016/j.ijadhadh.2004.12.001. URL https://doi.org/10.1016/j.ijadhadh.2004.12.001.

[32] N. SAINTIER, G. CAILLETAUD, and R. PIQUES. Crack initiation and propagation under multiaxial fatigue in a natural rubber. *International Journal of Fatigue*, 28(1):61–72, jan 2006. doi: 10.1016/j.ijfatigue.2005.03.006. URL https://doi.org/10.1016/j.ijfatigue.2005.03.006.

[33] N. SAINTIER, G. CAILLETAUD, and R. PIQUES. Multiaxial fatigue life prediction for a natural rubber. *International Journal of Fatigue*, 28(5-6):530–539, may 2006. doi: 10.1016/j.ijfatigue.2005.05.011. URL https://doi.org/10.1016/j.ijfatigue.2005.05.011.

[34] S. Seichter, V.-M. Archodoulaki, T. Koch, A. Holzner, and A. Wondracek. Investigation of different influences on the fatigue behaviour of industrial rubbers. *Polymer Testing*, 59:99–106, may 2017. doi: 10.1016/j.polymertesting.2017.01.018. URL https://doi.org/10.1016/j.polymertesting.2017.01.018.

[35] timco. *https://www.timcorubber.com/rubber-resources/rubber-molding-process/*. 2017.

[36] S. Toki, T. Fujimaki, and M. Okuyama. Strain-induced crystallization of natural rubber as detected real-time by wide-angle x-ray diffraction technique. *Polymer*, 41(14):5423–5429, jun 2000. doi: 10.1016/s0032-3861(99)00724-7. URL https://doi.org/10.1016/s0032-3861(99)00724-7.

[37] S. Vantadori, A. Carpinteri, G. Fortese, C. Ronchei, D. Scorza, and A. Zanichelli. Fatigue lifetime evaluation of notched components: Implementation of the control volume concept in a strain-based LCF criterion. *Theoretical and Applied Fracture Mechanics*, jul 2017. doi: 10.1016/j.tafmec.2017.07.001. URL https://doi.org/10.1016/j.tafmec.2017.07.001.

[38] E. VERRON and A. ANDRIYANA. Definition of a new predictor for multiaxial fatigue crack nucleation in rubber. *Journal of the Mechanics and Physics of Solids*, 56(2):417–443, feb 2008. doi: 10.1016/j.jmps.2007.05.019. URL https://doi.org/10.1016/j.jmps.2007.05.019.

[39] Wikipedia. *https://en.wikipedia.org/wiki/Isoprene*. 2017.

[40] A. Zine, N. Benseddiq, and M. N. Abdelaziz. Rubber fatigue life under multiaxial loading: Numerical and experimental investigations. *International Journal of Fatigue*, 33(10):1360–1368, oct 2011. doi: 10.1016/j.ijfatigue.2011.05.005. URL https://doi.org/10.1016/j.ijfatigue.2011.05.005.